

**PETROGRAPHY AND GEOCHEMISTRY OF  
THE ANYABONI FORMATION OF KWAHU  
GROUP, VOLTAIAN SUPERGROUP,  
GHANA: IMPLICATIONS FOR  
PROVENANCE AND URANIUM  
EXPLORATION**

The crest of the University of Ghana is a shield-shaped emblem. It features three golden, stylized, flame-like or leaf-like symbols arranged horizontally at the top. Below these, there is a central golden decorative motif consisting of a horizontal line with a central dot, from which two curved lines spiral downwards and outwards, resembling a stylized flower or a traditional Ghanaian symbol.

**FLORENCE AMOAKOHENE AKONTOH**  
**(10274165)**

**THIS THESIS IS SUBMITTED TO THE UNIVERSITY OF  
GHANA, LEGON IN PARTIAL FULFILMENT OF THE  
REQUIREMENT FOR THE AWARD OF MASTER OF  
PHILOSOPHY DEGREE IN GEOLOGY**

**LEGON**

**JULY, 2015**

## DECLARATION

I, Florence Amoakohene Akontoh declare that this thesis work is my own work as part of the requirements for the award of a Master of Philosophy degree, and that it contains no material previously published by another person or material which has been accepted for the award of any other degree by the university, except where due acknowledgement has been made in the text.

Florence A. Akontoh (10274165) ..... [Date]

[Signature]

Prof. Daniel K. Asiedu ..... [Date]

[Principal Supervisor's signature]

Prof. Samuel B. Dampare ..... [Date]

[Co-Supervisor's Signature]

## ABSTRACT

An integrated petrographic and geochemical study of the Anyaboni Formation, Kwahu Group, Voltaian Supergroup in Ghana was carried out to infer the provenance, tectonic setting, paleoweathering and paleoclimate conditions and uranium mineralisation potential of the basin. Twenty representative rock samples were collected from the Anyaboni Formation in Aseewa and its surrounding areas for petrographic and whole rock geochemical studies. The major elements were analysed by ICP-OES and the trace elements/REEs by ICP-MS. Two main rock types were identified in the area based on field observations; feldspathic sandstones and quartz sandstones. The petrographic studies indicated that the sandstone type was quartz arenite with texturally and compositionally matured minerals. On the basis of petrography the provenance was defined as metamorphic source and the tectonic setting was revealed as that of craton interior (predominantly) and recycled orogen. The sedimentation also occurred in a low-relief and tropical (humid) climatic conditions. The geochemical studies indicated that the sandstone types are mainly subarkose with contributions of arkose, sublitharenite and quartz arenite. The parent lithology is a quartzose sedimentary igneous source with contributions from felsic source. The CIA and PIA values range from 66.05 to 80.77 and 66.67 to 98.34 respectively. These values indicate that the paleoweathering condition is moderate to high, leading to alteration of unstable minerals to stable, oxide/hydroxide and clay minerals. Tectonic setting discrimination diagrams based on the geochemistry confirmed a passive continental margin setting. Uranium concentration studied alongside with Th, Zr and V in the study area indicates generally low levels. However, there is a strong positive correlation between U and Th, Zr and V concentrations and can serve as pathfinders for U in the area.

## DEDICATION

This work is dedicated to my siblings; Rosemond, Esther, Christopher, Samuel, David, Marshall and Peace for their immense support and encouragement throughout the period of study.



## ACKNOWLEDGEMENTS

I thank the Lord Almighty for His grace and mercy that has always been sufficient for me especially throughout this period of study. I could not have made it without God.

I thank my siblings for being a backbone to me in this period of study and their many words of encouragement and financial support. God richly bless you all.

I am very much grateful to Professor Daniel K. Asiedu and Professor Samuel B. Dampare for their tremendous help and supervision throughout this period of study. Thank you for making this thesis a reality.

Thanks to Prof. P.M. Nude, Head of Department of Earth Science, all my lecturers, teaching assistants, laboratory technicians, colleagues and friends from the department who were of great help to me during the study.

I am very much grateful to Felix Aidoo and John Kobina Hanson for their immense support and hard work towards the realization of this thesis. I also appreciate my facilitator, Professor Michel Cuney (Nancy Université, France) for the materials provided to enhance this work. God bless you all.

I appreciate my friends, Edwinfred Owusu Ansah, Nana Ama Owusuaa Afriyie Kankam, Nancy Darko, Marian Amofa, Melchizedek Ntim, Regina Tetteh, Peter Addo and Victor O. Agyemang for their regular encouragement. Thank you to all the individuals who assisted me in this work especially Benjamin and Sarah (GAEC).

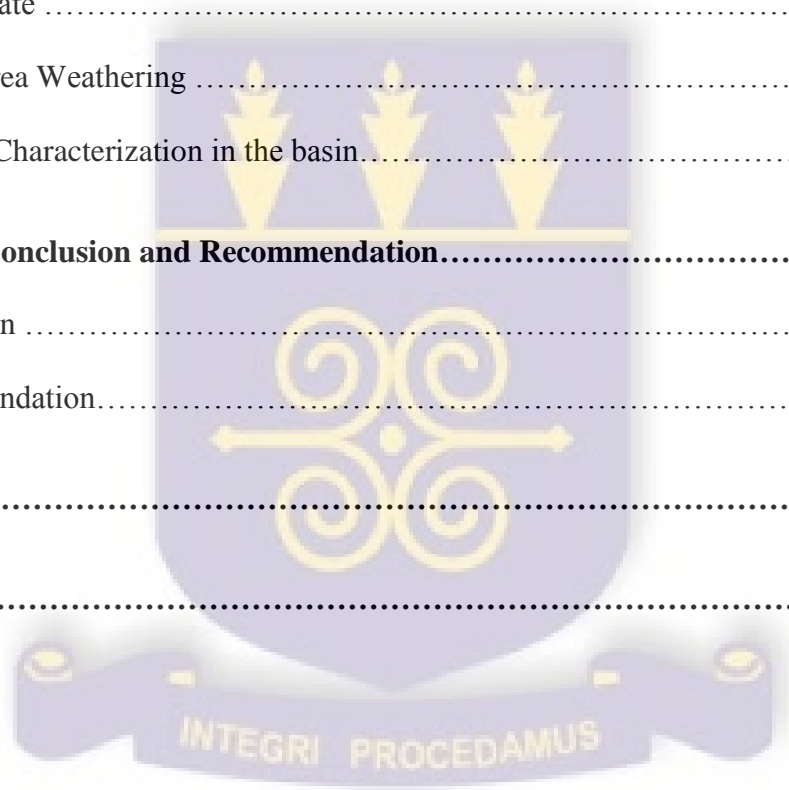
## TABLE OF CONTENTS

Declaration.....	I
Abstract.....	II
Dedication.....	III
Acknowledgement.....	IV
List of Figures.....	IX
List of Tables.....	XIV
<b>Chapter 1: Introduction.....</b>	<b>1</b>
1.1 Background.....	1
1.2 Problem Statement.....	2
1.3 Justification.....	3
1.4 Research Objectives.....	4
1.5 Location, Physiography and Geology of study area.....	5
1.5.1 Geographic location.....	5
1.5.2 Accessibility.....	5
1.5.3 Drainage and relief.....	5
1.5.4 Climate.....	6
1.5.5 Vegetation and soil.....	6
<b>Chapter 2: Literature Review.....</b>	<b>8</b>
2.1 Geology of Ghana.....	8
2.2 Geology of the Voltaian Supergroup.....	8

2.3 Geology of the Kwahu Group.....	10
2.4 Geology of the Anyaboni Formation.....	11
2.4.1 Petrographic and geochemical characteristics of the Anyaboni Formation.....	12
2.4.2 Provenance and Tectonic Setting of the Anyaboni Formation.....	13
2.5 Uranium Deposit Types.....	14
2.5.1 Intrusive Deposits.....	15
2.5.2 Granite-Related Deposits.....	15
2.5.3 Polymetallic Iron-Oxide Breccia Complex (IOCG) Deposits.....	15
2.5.4 Metasomatite Deposits.....	16
2.5.5 Metamorphite Deposits.....	16
2.5.6 Unconformity Related Deposits.....	16
2.5.7 Collapse-Breccia Pipe Deposits.....	17
2.5.8 Sandstone Deposits.....	17
2.5.9 Quartz-Pebble Conglomerate Deposits.....	18
2.5.10 Surficial Deposits.....	18
2.5.11 Lignite-Coal Deposits.....	19
2.5.12 Carbonate Deposits.....	19
2.5.13 Phosphate Deposits.....	19
2.5.14 Volcanic-Related Deposits.....	20
2.5.15 Black Shale Deposits.....	20
2.6 History of Uranium Exploration in Ghana.....	21
2.7 Uranium Minerals.....	24

<b>Chapter 3: Materials and Methods.....</b>	<b>26</b>
3.1 Sampling.....	26
3.2 Sample Preparation.....	28
3.3 Analytical Methods.....	28
3.4 Data Treatment.....	29
3.4.1 Geochemical Approach.....	29
3.4.2 Statistical and Geostatistical Approach.....	29
<b>Chapter 4: Results .....</b>	<b>30</b>
4.1 Field Observations.....	30
4.1.1 Reddish Brown to Chocolate feldspathic Sandstone.....	30
4.1.2 Gray to white (and pinkish) feldspathic Sandstone.....	30
4.1.3 Quartz sandstone.....	30
4.1.4 Structures.....	30
4.2 Petrography.....	33
4.2.1 Feldspathic Sandstone.....	33
4.2.2 Quartz sandstone.....	36
4.2.3 Modal composition.....	37
4.3 Geochemistry.....	37
4.3.1 Major Element.....	37
4.3.2 Trace Element.....	41
4.3.3 Rare Earth Element.....	43
4.4 Statistical and Geostatistical Analysis.....	46
4.4.1 Statistical Summaries.....	46

4.4.2	Experimental Semivariogram for U, Th, Zr and V Concentrations.....	51
4.4.3	Geochemical Map for U, Th, Zr and V Concentrations.....	54
<b>Chapter 5: Discussion.....</b>		<b>58</b>
5.1	Sandstone classification.....	58
5.2	Parent Rock Lithology.....	59
5.3	Tectonic Setting.....	67
5.4	Paleoclimate .....	70
5.5	Source Area Weathering .....	71
5.6	Uranium Characterization in the basin.....	74
<b>Chapter 6: Conclusion and Recommendation.....</b>		<b>75</b>
6.1	Conclusion .....	75
6.2	Recommendation.....	76
<b>References.....</b>		<b>77</b>
<b>Appendix.....</b>		<b>86</b>



**LIST OF FIGURES**

Figure 1.1: A location map of Asesewa and its surrounding area (modified after Duodo 2009).....7

Figure 2.1: Geological map of the Anyaboni Formation (modified after Duodo, 2009).....12

Figure 3.1: A sample location map of Asesewa and its surrounding areas (modified after Doudo, 2009).....27

Figure 4.1: (a) Feldspathic sandstones with clast of feldspathic rock material observed in the Anyaboni Formation, SE (b) Feldspathic sandstones characterized by colour differentiation due to weathering, SE.....31

Figure 4.2: (a) Gray coloured feldspathic sandstone sampled from Anyaboni locality, SE (b) White and pinkish coloured feldspathic sandstone sampled from Anyaboni locality, SE.....31

Figure 4.3: (A) Jointed quartz sandstone of the Anyaboni Formation observed at Asesewa, E(B) Laminated quartz sandstones of the Anyaboni Formation observed at Asesewa, E.....32

Figure 4.4: Some sedimentary features observed in the Anyaboni Formation: (a) Bedding, SE (B) quartz veins, SE (c) Raindrop structures, SE (e) Ripple marks, E.....32

Figure 4.5: Photomicrograph of feldspathic sandstones from Bisa locality under cross polarized light. Qtz: Quartz, Qm: monocrystalline quartz, Qp: Polycrystalline quartz, Plg: plagioclase, Mic: microcline and Op: Opaque mineral.....34

Figure 4.6: Photomicrograph of feldspathic sandstones from Anyaboni locality under cross polarized light Q: Quartz, Plg: plagioclase and Op: Opaque mineral.....34

Figure 4.7: Photomicrograph of feldspathic sandstones from Apimsu locality under cross polarized light. Q: Quartz, Plg: plagioclase, Mic: microcline, I: Isotropic mineral and Op: Opaque mineral.....35

Figure 4.8: Photomicrograph of feldspathic sandstones from Bisa locality under (a) cross polarized light (b) plane polarized light.....35

Figure 4.9: Photomicrograph of quartz sandstones from Asesewa locality under (a) cross polarized light (b) plane polarized light (Q: Quartz and Rf: Rock fragment.....36

Figure 4.10: Harker variation diagram of major elements for the Anyaboni Formation sandstones.....40

Figure 4.11: Histogram representation indicating the frequency distribution of U, Th, Zr and V concentrations in the Anyaboni Formation sandstones.....49

Figure 4.12: Scatter diagram for Th, Zr and V against U concentration of the Anyaboni Formation sandstones.....50

Figure 4.13: Experimental semivariogram fitted with a spherical model for U concentration in the Anyaboni Formation sandstones.....52

Figure 4.14: Experimental semivariogram fitted with a spherical model for Th concentration in the Anyaboni Formation sandstones area.....52

Figure 4.15: Experimental semivariogram fitted with a spherical model for Zr concentration in the Anyaboni Formation sandstones.....53

Figure 4.16: Experimental semivariogram fitted with a spherical model for V concentration in the Anyaboni Formation sandstones.....53

Figure 4.17: Geochemical map for U concentration in the Anyaboni Formation sandstones using Kriging.....55

Figure 4.18: Geochemical map for Th concentration in the Anyaboni Formation sandstones using Kriging.....56

Figure 4.19: Geochemical map for Zr concentration in Anyaboni Formation sandstones using Kriging.....56

Figure 4.20: Geochemical map for V concentration in the Anyaboni Formation sandstones using Kriging.....57

Figure 5.1: QFL diagram for sandstone classification of the samples from the study area modified after Folk, 1974.....58

Figure 5.2: Chemical classification of sandstones from the study area based on Log (SiO<sub>2</sub>/Al<sub>2</sub>O<sub>3</sub>) versus Log (Fe<sub>2</sub>O<sub>3</sub>/K<sub>2</sub>O) diagram of Pettijohn et al. (1972).....59

Figure 5.3: The effect of source rock on the composition of the sandstones using Suttner et al., 1981.....62

Figure 5.4: Provenance discriminant function diagram using major elements in sandstones from Anyaboni and surrounding areas after Roser and Korsch (1986).....62

Figure 5.5: Source rock La/Th-Hf discrimination diagram for the sandstone samples from the study area; modified after Floyd and Leveridge, 1987.....63

Figure 5.6: Provenance discrimination diagram using TiO<sub>2</sub> (wt %) versus Zr (ppm) with fields from Hayashi et al., 1997.....63

Figure 5.7: (A) Chondrite-normalized trace element diagram (B) Upper Continental Crust-normalized patterns for Anyaboni Formation sandstone samples. Normalization factors from Sun and McDonough 1989 (for A); Taylor and McLennan, 1985 (for B).....64

Figure 5.8: Upper Continental Crust-normalized patterns for Anyaboni Formation sandstone samples. Normalization factors from Taylor and McLennan, 1985.....65

Figure 5.9: (a) Chondrite-normalized REE diagram (b) Upper continental crust-normalized REE diagram Normalization factors from Sun and McDonough 1989(for a) and Taylor and McLennan, 1985 (for b) .....66

Figure 5.10: QFL ternary diagram showing the provenance and plate tectonic setting of the samples from the study area: using the petrography of the sandstones (after Dickson et al., 1983).....68

Figure 5.11: Log (K<sub>2</sub>O/Na<sub>2</sub>O) versus SiO<sub>2</sub> tectonic setting discrimination diagram of Roser and Korsch (1986) showing the location of the studied samples.....68

Figure 5.12: Bivariate plots of Al<sub>2</sub>O<sub>3</sub>/SiO<sub>2</sub> versus Fe<sub>2</sub>O<sub>3</sub>+MgO after Bhatia, 1983.....69

Figure 5.13: Bivariate plots TiO<sub>2</sub> versus Fe<sub>2</sub>O<sub>3</sub>+MgO after Bhatia, 1983.....69

Figure 5.14: Log-ratio plot after Weltje et al. (1998). Q; Quartz, F; Feldspar, RF; Rock fragment Fields 1–4 refer to the semi-quantitative weathering indices defined on the basis of relief and climate as indicated in the table 5.1.....70

Figure 5.15: Source area weathering characteristics represented on  $Al_2O_3$ -( $CaO^*+Na_2O$ )- $K_2O$  diagram. The diagrams represent the field of idealized minerals: Pl; Plagioclase, Ks; K-feldspars, Il; Illite, Mu; Muscovite, Sm; Smectite, Ka; Kaolinite, Gi; Gibbsite, Ch; Chlorite.....72

Figure 5.16: Source area weathering characteristics represented on  $(Al_2O_3-K_2O)$ - $CaO$ - $Na_2O$  ternary diagram (Modified after Nesbitt and Young, 1984). The diagrams represent the field of idealized minerals: An; Anortite, Ab; Albite.....73

Figure 5.17: Source area weathering characteristics represented on  $Al_2O_3$ -( $CaO^*+Na_2O+K_2O$ )-(Fe<sub>2</sub>O<sub>3</sub>+MgO) ternary diagram (Modified after Nesbitt and Young, 1984). The diagrams represent the field of idealized minerals: Il; Illite, Mu; Muscovite, Sm; Smectite, Ka; Kaolinite, Gi; Gibbsite, Ch; Chlorite, Fs; Feldspars, Pyx; Pyroxene, Am; Amphibole and Bi; Biotite.....73

Figure A: Airborne geophysical survey of the Volta River Basin and Keta Basin, Ghana (Jordan et al., 2008).....86

**LIST OF TABLES**

Table 2.1: Some common uranium minerals (Kesse 1985; Gupta and Singh, 2003).....25

Table 3.1: Log sheet format for recording rock sample data.....26

Table 4.1: Measured variables for Q-F-L ternary diagram and Log-plot.....37

Table 4.2: Major element concentration (in wt %) of the Anyaboni Formation sandstones.....39

Table 4.3: Measured Variables for CIA and PIA ternary diagram presentation.....41

Table 4.4: Trace element concentrations in ppm for Anyaboni Formation sandstones Trace elements data determined by ICP-OES (ALS Mineral, South Africa).....42

Table 4.5: Ranges and averages of elemental ratios of the Anyaboni Formation Sandstones.....43

Table 4.6: Rare Earth Elements (REEs in ppm) of the Anyaboni Formation sandstones.....45

Table 4.7: Ranges and averages of elemental ratios of the Anyaboni Formation Sandstones.....45

Table 4.8: Trace element concentrations (in ppm) for U, Th, Zr and V of the Anyaboni Formation.....48

Table 4.9: Summary statistics of the variables studied.....48

Table 4.10: Summary statistics of log transformed data for U, Th, Zr and V concentrations from the Anyaboni Formation sandstones.....49

Table 4.11: Summary correlations and regression analysis of Th, Zr and V.....	50
Table 4.12: Fitted semivariograms of models with their parameters.....	54
Table 5.1: Semi-quantitative weathering indices defined on the basis of relief and climate (after Weltje et al., 1998).....	71

## **CHAPTER ONE**

### **INTRODUCTION**

#### **1.1 BACKGROUND**

Petrographic and geochemical studies of sedimentary rocks can reveal the nature of the source regions, provenance and tectonic setting of sedimentary basins, paleoweathering and paleoclimate conditions (Dickson and Suzeck, 1979; Bhatia 1983; Bhatia and Crook, 1986). The mineral chemistry of clastic sedimentary rocks is the result of the nature of the source rocks, source area weathering and diagenesis (Dickson and Suzeck, 1979; Roser and Korsch 1986; McLennan et al., 1993). The primary control of the chemical composition or mineral chemistry is the plate tectonic setting (Dickson, 1985). The formation of sedimentary basins and the nature of the sediments they contain are also important in the economic mineralisation of uranium (IAEA, 2015). Understanding basin tectonics in an integrated manner can throw more light on the factors and their contributions to uranium accumulation in the surficial and deep continental settings (IAEA, 2015).

The Neoproterozoic Voltaian Supergroup covers about 115,000km<sup>2</sup> in the Volta Basin, covering approximately 40% of Ghana (Carney et al., 2010). It is characterised by flat-lying sedimentary rocks mainly sandstones (Kalsbeek et al., 2008). The Voltaian Supergroup unconformably overlies the crystalline basement rocks of the West African Craton (Kalsbeek and Frei, 2010). The sediments from which the sedimentary rocks are formed varied in ages ranging from ~1000 Ma to 635 Ma (Kalsbeek and Frei, 2010; Kalsbeek et al., 2008; Carney et al., 2010). The chemical composition of sedimentary rocks relates to their source regions and can be used to decipher their tectonic setting (Fralick and Kronberg, 1997). Hence, this research seeks to describe the nature of the source regions, tectonic setting

of the sedimentary basin, paleoweathering, and paleoclimate conditions through petrographic and geochemical studies. It also aims at evaluating the significance of the basin to uranium mineralisation in the study area.

## **1.2 PROBLEM STATEMENT**

Previous studies reveal that the sediment characteristics vary in the western, eastern and southern portions of the Voltaian Supergroup (Affaton et al., 1980; Kalsbeek et al., 2008; Kalsbeek and Frei, 2010; Anani et al., 2013). Although the sandstone composition, provenance and tectonic setting of the Voltaian Supergroup have been studied by other workers, different arguments have been raised concerning the provenance of the Voltaian Supergroup. On the basis of geochronological studies carried out by Kalsbeek et al. (2008), the Kwahu-Morago (Bombouka) Group of the Voltaian Supergroup from which the Anyaboni Formation forms a part has the Amazonian Craton as a plausible source alongside with contributions from the Birimian and Archaean rocks of the West African craton. Conversely, Anani et al. (2013) suggest the Birimian Supergroup with possible contribution from the Pan-African rocks as the likely source of the Anyaboni Formation. The use of major oxide geochemistry revealed that the sandstones of the Voltaian Supergroup are associated with a passive continental margin tectonic setting (Anani et al., 2013). Much study has not been carried out on the Anyaboni Formation to constrain its paleoweathering and paleoclimate conditions.

According to Guelpa and Vogel (1982), the Voltaian Supergroup is likely to be associated with sandstone type uranium deposit due to its similarities with the Taoudeni basin in Guinea which hosts uranium deposits. Airborne geophysical survey carried by FUGRO Airborne survey limited in 2008 revealed that the Anyaboni Formation is moderately enriched in

uranium (Jordan et al., 2008; 2009). Preliminary studies carried out in the Voltaian Supergroup using Track Etch technique indicated that the uranium concentration was low in the area studied. However, the use of other technique in determining uranium in the area may help improve the knowledge base towards effective uranium exploration and evaluation in the area. This research seeks to describe the nature of the source regions, tectonic setting of the sedimentary basin, paleoweathering, and paleoclimate conditions of the Anyaboni Formation through petrographic and geochemical studies. REEs analysis gives better signatures of the source region and is included in this study to help ascertain the likely provenance of the study area. It is also aimed at evaluating the sandstone types in the study area with respect to uranium mineralisation potential using geostatistical applications.

### **1.3 JUSTIFICATION**

Bhatia (1983), Taylor and McLennan (1985) and Bhatia and Crook (1986) indicate that provenance discrimination diagrams based solely on major elements are unreliable because major elements are mobile during weathering and alteration. On the other hand, certain trace elements and REEs are most suitable for provenance and tectonic setting studies because of their relatively low mobility during sedimentary processes and low residence time in seawater (Taylor and McLennan, 1985). These elements are quantitatively transported into clastic sedimentary rocks after weathering. Hence they reflect the signature of the parent rock (Anani et al., 2013). The present work seeks to propose the basin characteristics with respect to source, tectonic setting and paleoweathering and paleoclimate conditions using petrography and whole rock geochemistry (considering major oxides, trace elements and REEs).

Formation of the sedimentary basins and the nature of the sediments and of the organic matter they contain are important points to consider in the economic mineralization of uranium (IAEA, 2015). About 85% of the world's production of uranium comes from deposits associated with sedimentary and supergene processes (Obaje, 2009). Basin tectonics, understood in an integrated manner, can throw more light on the complex set of factors and their interplay that led to the origin of coal, petroleum and uranium accumulation in these surficial and deep continental settings, thus creating some of the well-known 'energy basins (IAEA, 2015). Based on the airborne geophysical survey carried out in the Volta basin, preliminary study is necessary to be carried on the ground to investigate the likely concentration of uranium in the Anyaboni Formation. Hence, the study is relevant in examining the possibility of exploring the rocks of the Anyaboni Formation for uranium deposits. This study also presents for the first time the paleoweathering and paleoclimate conditions of the Anyaboni Formation of the Voltaian Supergroup.

#### **1.4 RESEARCH OBJECTIVES**

1. To determine the petrographic and geochemical characteristics of the rocks from the Anyaboni Formation.
2. To infer the rock classification provenance and tectonic setting, paleoweathering and paleoclimate conditions of the sandstones from the Anyaboni Formation.
3. To determine the distribution of uranium and its associated pathfinder elements in the study area.
4. To evaluate and estimate the concentration of uranium at unsampled areas in the study area.

5. To generate a geochemical map and spatial model for the variation of uranium in the study area.

## **1.5 LOCATION AND PHYSIOGRAPHY OF THE STUDY AREA**

### **1.5.1 Geographic Location**

The Anyaboni Formation of the Kwacha Group outcrops in Asesewa and its environs. Asesewa is located in the southeastern part of Ghana (Anani, 1999). It is also found in the Manya Krobo district of the Eastern Region. Asesewa is the district capital and it is surrounded by towns such as Abuasa, Asaasehene, Ogome-Atowa, Abetima, Apimsu, Anyaboni, Bisa and Yiti ([www.ghanadistricts.com](http://www.ghanadistricts.com)). Asesewa is approximately 133km away from Accra. Asesewa lies between the geographic coordinates, Latitude 6°18' South and 6° 24' North and Longitude 0° 0' East and 0° 09' West on Field Sheet 0601D2 (Figure 1.1).

### **1.5.2 Accessibility**

Asesewa and its surrounding environments are characterized by relatively good roads (Figure 1.1). This creates easy access to the study area. However, the roads of the study area are predominantly untarred with some major routes tarred and motorable (Duodu, 2009). At places where footpaths are used, it requires walking on relatively sloping lands with great care. Basically, the means of transport of the natives are by buses and on foot.

### **1.5.3 Drainage and Relief**

Asesewa and its environs are mainly drained by the Volta River and its tributaries. The general pattern of drainage in the study area is dendritic (Figure 1.1). The relief of the study area is associated with rocks with heights between 180 meters and 300 meters (Dickson and Benneh, 1992).

#### **1.5.4 Climate**

Asesewa falls within the wet-semi equatorial climatic region of Ghana (Dickson and Benneh, 1992). The mean annual rainfall is between 125 and 200 centimeters. There are two high rainy seasons in this area (Dickson and Benneh, 1992). The first rainy season is from May to June, with the heaviest rainfall in June. The second rainy season is from September to October. The dry seasons in the study area are quite sharp and pronounced (Dickson and Benneh, 1992). In Asesewa, the mean monthly temperature ranges from 26 °C to 30 °C (Dickson and Benneh, 1992). Average monthly relative humidity in Asesewa is highest (75% - 80%) during the two rainy seasons and lowest (70% - 80%) during the rest of the year (Dickson and Benneh, 1992).

#### **1.5.5 Vegetation and Soil**

The vegetation type of Asesewa and its environments is the Moist-semi deciduous forest (Dickson and Benneh, 1992). With this type of vegetation, the trees do not all shed their leaves at the same time. The predominant soil types in Asesewa and its environs are the forest ochrosols (Dickson and Benneh, 1992). Forest ochrosols are formed from the same kind of highly weathered parent materials (Dickson and Benneh, 1992).

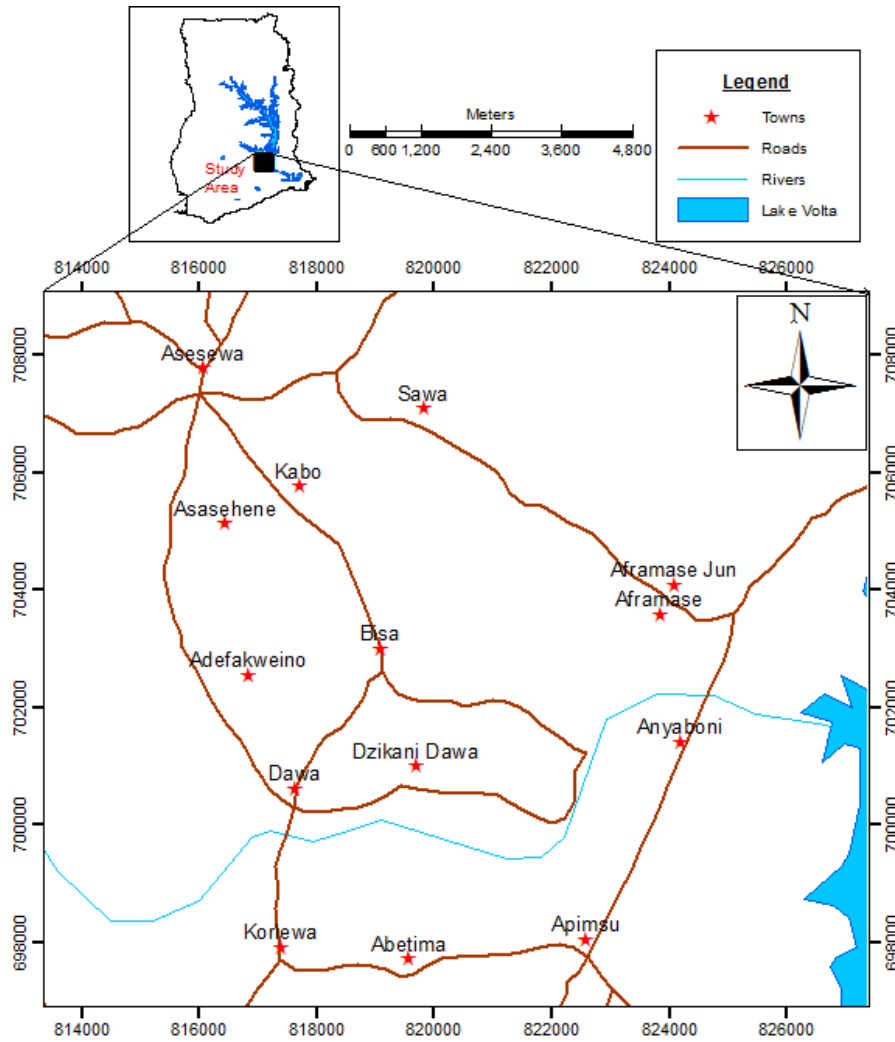


Figure 1.1: A location map of Aseseva and its surrounding area (modified after Duodo, 2009)

## **CHAPTER TWO**

### **LITERATURE REVIEW**

#### **2.1 GEOLOGY OF GHANA**

Ghana forms a part of the Leo-Man Shield of the West African Craton (Affaton, 1990). Ghana is made up of five geologic terranes base on their age data, tectonics and lithology; Birimian Supergroup, Tarkwaian Supergroup, Voltaian Supergroup, Dahomeyides and Coastal Sedimentary basins (Kesse, 1985).The Paleoproterozoic Birimian and Tarkwaian Supergroup form the basement rocks of the Voltaian Supergroup (Abouchami et al., 1990). The Voltaian Supergroup is bounded by the Pan-African Orogenic belt (Dahomeyides) on the eastern margin (Kalsbeek et al., 2008). The Phanerozoic crustal evolution of Ghana is characterised by the development of a series of spatially restricted, shallow, mostly marine coastal basin (Duodu, 2009).

#### **2.2 GEOLOGY OF THE VOLTAIAN SUPERGROUP IN GHANA**

The Neoproterozoic Voltaian Supergroup outcrops in the Volta Basin which is located in the eastern portion of the Leo-Man shield of the West African Craton (Carney et al., 2010). The Voltaian Supergroup covers an area of approximately 115,000 km<sup>2</sup>, almost one-third of the total area of Ghana (Kalsbeek et al., 2008; Carney et al., 2010). The thickness of the Voltaian Supergroup ranges between 5000m against the basement rocks (Annan-Yorke, 1971) and 6000m near the Dahomeyide orogenic front (Ako and Wellman, 1985).

The eastern margin of the Voltaian Supergroup has been affected by the Pan-African (600Ma) deformation (Kalsbeek et al., 2008; Carney et al., 2010) and is overthrust by metasedimentary rocks of the Buem and Togo Structural Units of the Dahomeyide orogen (Kalsbeek et al., 2008; Kalsbeek and Frei, 2010). The Voltaian Supergroup is generally flat

lying and unmetamorphosed, except at their eastern margin (Carney et al., 2010). The Voltaian Supergroup is subdivided into three Groups; the Lower Voltaian (Kwahu-Morago) Group, the Middle Voltaian (Oti/Pendjari) Group and the Upper Voltaian (Obosum) Group, each separated by an unconformity marked by a tillite (Carney et al., 2010; Coueffe and Vecoli, 2011; Anani et al., 2013).

The Lower Voltaian Kwahu-Morago (Bombouaka) Group unconformably overlies the strongly deformed Paleoproterozoic Birimian Supergroup rocks and Tarkwaian sedimentary rocks (Kalsbeek and Frei, 2010; Abouchami et al., 1990; Boher et al., 1992). The Lower Voltaian Kwahu-Morago Group is made up of mainly medium to coarse grained quartzitic and feldspathic sandstones (Kalsbeek and Frei, 2010). The Lower Voltaian is characterized by massive to cross-bedded sequence. The estimated thickness of the Lower Voltaian is approximately 1000 m (Kalsbeek and Frei, 2010). A radiometric age of  $993 \pm 62$  Ma from the lower part of the Bombouaka Group gives the approximate period for the beginning of sedimentation of the Group (Clauer, 1976; Bohzo et al., 1971). The depositional environment for the Bombouaka Group is considered to be shallow marine or fluviatile (Carney et al., 2010). The Bombouaka Group is characterized by a fairly stable tectonic setting throughout the depositional area (Carney et al., 2010).

The Middle Voltaian Oti/Pendjari Group overlies the Bombouaka Group with a slight angular unconformity and has thickness of about 3000 m (Kalsbeek and Frei, 2010). It consists of shales, siltstones and sandstones, glauconitic in part. The Middle Voltaian Group consists of a flyschoid sequence (Kalsbeek and Frei, 2010). The basal part is characterized by conglomeratic beds which are interpreted as tillites (Affaton 1990; Porter et al., 2004). K–Ar

dating of glauconite from a borehole core at Tibagona yielded a Vendian age of  $600 \pm 20$  Ma (Barfod et al., 2004).

The Upper Voltaian (Obusom) Group overlies the Oti/Pendjari unconformably and has an estimated thickness of 1000 m (Kalsbeek and Frei, 2010). The Obusom Group largely composed of quartzitic and feldspathic sandstones of variable grain sizes (Kalsbeek and Frei, 2010; Anani et al., 2013). The age of deposition of the Obosum Group is suggested to be approximately 620 Ma (Clauer, 1976; Bohzo et al., 1971; Kalsbeek et al., 2008). The Obusom Group constitutes the molasse deposits formed in the Cambro–Ordovician period by the erosion of some horizons in the Pan-African mobile belt (Affaton 1990; Trompette, 1994; Kalsbeek and Frei, 2010).

### **2.3 GEOLOGY OF THE KWAHU GROUP**

The sedimentary rocks of the Kwahu Group of the Voltaian Supergroup is associated with the Kwahu Plateau and is about 1000m thick (Kalsbeek and Frei, 2010). The Kwahu Group is divided into three main formations; Mpraeso Formation, Abetifi Formation and Anyaboni Formation and each formation is subdivided into two different units (Coueffe and Vecoli, 2011). The lower unit comprising shales and siltstone and the upper unit compose of sandstones (Coueffe and Vecoli, 2011). The Mpraeso Formation corresponds to the lower division of the Kwahu Group (Saunders, 1970; Carney et al., 2010). The Mpraeso Formation is mainly composed of white to pink, fine to medium grained quartzitic sandstones with thickness of about 250-300m (Coueffe and Vecoli, 2011). Overlying the Mpraeso Formation is the Abetifi Formation which is characterized by predominantly medium to coarse grained sandstones with quartz pebbles and shales with thin intercalations of siltstones and fine grained sandstones (Coueffe and Vecoli, 2011). The Abetifi Formation has thickness of

about 500m (Carney et al., 2010). The Anyaboni Formation comprise of micaceous shales with one fine grained sandstone intercalation in the lower unit and medium grained feldspathic sandstones with conglomeratic lenses in the upper unit (Coueffe and Vecoli, 2011). The Anyaboni Sandstone Formation has thickness s of approximately 400 m (Anani, 1999).

#### **2.4 GEOLOGY OF THE ANYABONI FORMATION**

The Anyaboni Formation of the Lower Voltaian Kwahu-Morago Group is exposed at Anyaboni, Apimsu, Bisa, Asesewa and Anyilesu localities and predominant in and around the Anyaboni locality (Anani, 1999). The Anyaboni Formation is subdivided into two units, a lower unit dominated by beds ranging from 1 to 5 m in thickness, and an upper unit of thick sandstone beds, about 10 m on average (Coueffe and Vecoli, 2011; Anani et al., 2013). Both units consist of feldspathic sandstone (Carney et al., 2010). The lower unit is dominated by relatively high mica contents and less frequent feldspar but mica is rare or absent in the upper unit (Anani, 1999; Coueffe and Vecoli, 2011). The boundary between the two units is either gradational or poorly defined. The pink colour of the rocks in both units is due to the feldspar present (Coueffe and Vecoli, 2011). The sandstones are mostly chocolate or reddish brown (probably hematite) in colour (Anani et al., 2013). A few localities are associated with gray or white sandstones. Both units contain cross-bedding and/or parallel laminations, with other sedimentary structures such as poorly developed graded-bedding at some localities (Anani, 1999).

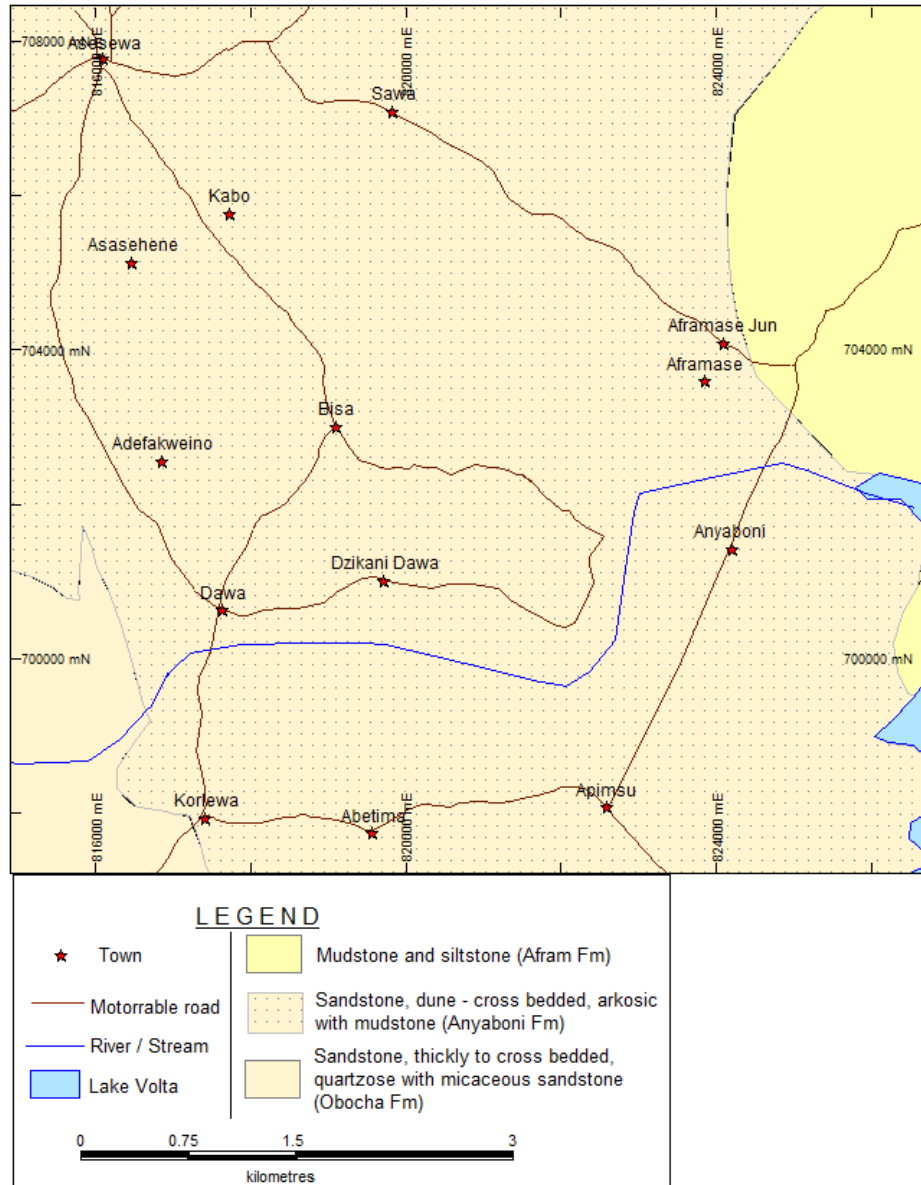


Figure 2.1: Geological map of the Anyaboni Formation (modified after Duodo, 2009)

#### 2.4.1 Petrographic and geochemical characteristics of the Anyaboni Formation

The Petrographic characteristics of the Anyaboni Formation sandstones as studied by Anani (1999), shows the framework grains compose of monocrystalline quartz, polycrystalline quartz, feldspar, aphanitic lithic fragments (volcanics, meta-volcanics, sediments, meta-sediments and cherts), heavy minerals, monocrystalline phyllosilicates (sericites, chlorites, kaolinites, etc), and miscellaneous and unidentified framework grains. Anani (1999)

recognized some pore-filling quartz as well as significant amounts of hematite infilling pore spaces in the petrographic studies carried out. Opaque oxide pigments, probably mainly hematite, which result from the oxidation of ferromagnesian minerals, were observed by Anani (1999). Geochemical studies done by Anani et al. (2013) revealed the Anyaboni Formation sandstones to be characterised by major oxides high in  $\text{SiO}_2$  and low in  $\text{Al}_2\text{O}_3$  with a limit range in  $\text{K}_2\text{O}$  and low contents in  $\text{TiO}_2$ ,  $\text{MnO}$ ,  $\text{CaO}$ ,  $\text{Na}_2\text{O}$ ,  $\text{Fe}_2\text{O}_3$  and  $\text{MgO}$ . On the basis of trace element characteristics, the Anyaboni Formation sandstones possess generally high concentration of LILE and HFSE, and high concentrations of ferromagnesian trace elements such as Co, Cr and V (Anani et al., 2013).

#### **2.4.2 Provenance and Tectonic Setting of the Anyaboni Formation**

The relationship between the Anyaboni Formation sandstone composition and provenance and tectonic setting was recognized through the work of Anani (1999), Kalsbeek et al. (2008) and Anani et al. (2013). Anani (1999) showed that plotting the detritus framework modes of the Anyaboni Formation sandstones on QFL and QmFLt ternary diagrams resulted in information about the tectonic setting of the Anyaboni Formation sandstones and their associated provenance. According to Anani (1999), the QFL diagram which plots quartz (Q), feldspar (F) and lithics (L) and QmFLt diagram and is similar to the QFL diagram except plotting exclusively monocrystalline quartz (Qm) and total polycrystalline lithics (Lt) plotted the Anyaboni sandstones in transitional continental and Craton interior fields when compared with those of Dickson et al. (1983). Anani et al. (2013) revealed that on the basis of major element geochemistry, the sediments were derived from recycled sedimentary rocks and deposited in a passive continental margin compared with those of Roser and Korsch (1986).

Kalsbeek et al. (2008) on the basis of zircon geochronology suggested that the Bombouka (Kwahu-Morago) group from which the Anyaboni Formation sandstones are part may be derived from the surrounding Birimian Supergroup (crystalline basement rocks), Archaean rocks of the West African Craton and Grenvillian orogenic belts of the Amazonian Craton.

## **2.5 URANIUM DEPOSIT TYPES**

Uranium is highly incompatible in silicate magmas due to its large ionic radius and high valence (Langmuir, 1978). According to Cuney (2009), this behavior of uranium during partial melting and fractional crystallization has brought about its enrichment from the primitive mantle (21 ppb) to the continental crust (1.3ppm in the whole crust and 2.7ppm in the upper crust). Uranium enrichment occurs simultaneously with large highly charged cations such as  $\text{Th}^{4+}$ ,  $\text{Zr}^{4+}$ , and  $\text{REE}^{3+}$  (Cuney, 2009). Uranium precipitates under oxidizing conditions.  $\text{H}_2\text{S}$ , magnetite, ilmenite, and sulfides also serve as other potential reductants for the precipitation of uranium (Cuney, 2009).

Uranium deposit types are formed under a variety of geological conditions and range in age from Archaean to recent, but none is expected to exist before about 3.1 Ga (Nininger, 1956; World Nuclear Association, 2010). The classification of uranium deposit types are either based on the host rock or the morphology of the ore deposit (Dahlkamp, 1993). According to the International Atomic Energy Agency (2013), uranium deposits world-wide can be grouped into 15 major categories of deposit types based on the geological setting of the deposits. These categories are as follows; intrusive, granite-related, polymetallic iron-oxide breccia complex (IOCG), metasomatite, metamorphite, Proterozoic unconformity related, collapse-breccia pipe, sandstone, quartz-pebble conglomerate, surficial, lignite-coal, carbonate, phosphate, volcanic-related, and black shale.

### **2.5.1 Intrusive Uranium Deposits**

Intrusive uranium deposits are contained in intrusive rocks of many different petrochemical compositions (Blaise, 2014). The intrusive rocks includes; granite, pegmatite, monzonite, peralkaline syenite and carbonatite. Intrusive uranium deposit types occur in Namibia, Greenland, USA, Cameroon, Brazil and Australia (World Nuclear Association, 2010).

### **2.5.2 Granite-Related Deposits**

Granite-related deposits have uranium mineralization occurs within, at the contact or peripheral to the intrusion (Blaise, 2014). The deposits related to the granite include; veins or disseminated mineralization (World Nuclear Association, 2010). The veins may compose of ore and gangue minerals in granite or adjacent (meta-) sedimentary rocks whiles the disseminated mineralization in granite as episyenite bodies. These deposit types are found in France, China and Czech Republic (Blaise, 2014).

### **2.5.3 Polymetallic Iron-Oxide Breccia Complex Deposits**

Polymetallic iron-oxide breccia complex deposits are associated with iron, copper, uranium, gold, silver, rare earth elements (mainly lanthanum and cerium) and fluorine (Blaise, 2014). The Olympic Dam in Australia is the only representative of this type of deposit and uranium is mined as a by-product of gold (World Nuclear Association, 2010). It also accounts for one of the world's largest deposits of uranium. The uranium occurs in hematite-rich granite breccia complex (World Nuclear Association, 2010). Uranium grades average from 0.08 to 0.04%  $U_3O_8$ , the higher-grade mineralisation being pitchblende (World Nuclear Association, 2010; Blaise, 2014).

#### **2.5.4 Metasomatite Deposits**

Metasomatite deposits consist of unevenly disseminated uranium in structurally deformed rocks that were affected by sodium (or potassium or calcium) metasomatism (Blaise, 2014). The alteration may result from a variety of processes. Uranium mineralized skarn deposits are also associated with metasomatic processes (World Nuclear Association, 2010). They are generally confined to Precambrian shields in orogenic belts. Examples of metasomatite deposits occur in Australia, Brazil, Canada, Namibia, Russian Federation, Madagascar and Ukraine (Blaise, 2014).

#### **2.5.5 Metamorphite Deposits**

Metamorphic uranium deposits are formed during the circulation of metamorphic fluids in association with folding, faulting and/or thrusting of the rocks (Cuney 2009). These deposits consist of disseminations, impregnations, veins and shear zones within metamorphic rocks of various ages with no relation to granitic intrusions (Blaise, 2014; Bruneton, 2014). Metamorphite deposits occur in Austria, Brazil, Czech Republic, Democratic Republic of Congo and USA (Blaise, 2014).

#### **2.5.6 Unconformity-Related Deposits**

Unconformity-related uranium deposits are the most typical diagenetic-hydrothermal uranium deposits (Blaise, 2014). These deposits arise from geological changes occurring close to major unconformities (Cuney, 2009). Below the unconformity, the host rock is usually faulted and brecciated. They occur between a Paleo- to Meso-Proterozoic sandstone cover and an Archaean to Paleoproterozoic crystallized basement rock (Cuney, 2009). They constitute the world's largest and richest high grade (20-22% wt) uranium deposits (World Nuclear Association, 2010). According to Blaise (2014), unconformity related uranium

mineralization occur in Canada (the Athabasca Basin, Saskatchewan and Thelon Basin, Northwest Territories); and Australia (the Alligator Rivers region in the Pine Creek Geosyncline, NT and Rudall River area, WA).

### **2.5.7 Collapse-Breccia Pipe Uranium Deposits**

Collapse-Breccia pipe uranium deposits occur in sedimentary basins within cylindrical, vertical pipes filled with down-dropped fragments from overlying lithological units filling karst dissolution cavities developed in the underlying, thick carbonate layers (Blaise, 2014). Uranium mineralisation is mostly within permeable sandstone breccias within the pipe (World Nuclear Association, 2010). The mineralization is also associated with low temperature (80–173°C), saline oxidized solutions of diagenetic origin, derived from deeper parts of the basin (World Nuclear Association, 2010). The best-known example is the Arizona Strip, USA (Blaise, 2014).

### **2.5.8 Sandstone Uranium Deposits**

Sandstone uranium deposits occur in medium to coarse-grained sandstones deposited in a continental fluvial or marginal marine sedimentary environment (Blaise, 2014). Uranium is precipitated under reducing conditions caused by a variety of reducing agents within the sandstone including: carbonaceous material, sulphides, hydrocarbons, and interbedded basic volcanics with abundant ferromagnesian minerals (Kesse, 1985). Uranium deposits related to sandstones units have the largest resources. They constitute about 18% of world uranium resources (Blaise, 2014). World Nuclear Association (2010) indicates that ore bodies of this type are commonly low to medium grade (0.05 - 0.4%  $U_3O_8$ ) and individual ore bodies are small to medium in size (ranging up to a maximum of 50 000 t  $U_3O_8$ ). Large resources in sandstone deposits occur in countries such as USA, Niger, Kazakhstan, Uzbekistan, Gabon

(Franksville Basin), and South Africa (Karoo Basin). Other resources of sandstone type can be found in Australia, France and Argentina (World Nuclear Association, 2010; Blaise, 2014).

### **2.5.9 Quartz-Pebble Conglomerate Deposits**

Quartz-pebble conglomerate deposits form as basal units or intra-formational conglomerates in fluvial to lacustrine braided stream systems (Blaise, 2014). Fluvial transport of detrital uraninite was possible at the time because of the prevailing anoxic atmosphere. They occur in Proterozoic beds unconformably situated above granitic and metamorphic Archaean basement rocks (World Nuclear Association, 2010). These deposit types forms about 13% of the world's uranium resource. The grade and size may vary from 0.01%-0.15%  $U_3O_8$  and 6000-17000t respectively (World Nuclear Association, 2010). Major examples are the Elliot Lake deposits in Canada and the Witwatersrand gold-uranium deposits in South Africa (Kesse, 1985; Blaise, 2014).

### **2.5.10 Surficial Uranium Deposits**

Surficial uranium deposits are uraniferous sediments or soils; usually of Tertiary to Recent age (Kesse, 1985). These types of deposits have not been subjected to deep burial and usually have secondary cementing minerals including calcite, gypsum, dolomite, ferric oxide, and halite (Kesse, 1985; Cuney, 2009). Detrital uraninites are accumulated in fluvial to fluvio-deltaic environments with less intense remobilization of the detrital uraninite (Cuney, 2009). The largest of the surficial uranium deposits are found in calcrete (calcium and magnesium carbonates). Deposits associated with calcretes are formed by evapotranspiration processes in fluvial to playa systems in arid to semi-arid climatic conditions (Cuney, 2009). Surficial deposits comprise about 4% of world uranium resources (World Nuclear

Association, 2010). They are mined in countries such as USA, Australia, Namibia and Bulgaria (Blaise, 2014).

#### **2.5.11 Lignite-Coal Deposits**

Uranium mineralization occurs in lignite or coal mixed with mineral detritus (silt, clay), and in immediately adjacent carbonaceous mud and silt/sandstone beds (Blaise, 2014). This type of deposit is associated with surficial accumulation of uranium where it is deposited by adsorption on organic material and/or by anaerobic bacteria activity (Cuney, 2009). According to Cuney (2009), this produces gases such as  $H_2S$ ,  $CH_4$ , etc which are capable of reducing ( $UO_2^{2+}$ ). Lignite-coal uranium deposits occur in Australia, Germany, Greece, Kazakhstan and USA (World Nuclear Association, 2010; Blaise, 2014)

#### **2.5.12 Carbonate Deposits**

Carbonate uranium deposits are hosted in carbonate rocks such as limestone and dolostone (Blaise, 2014). Mineralization can be syngenetic and strata bound or more commonly structure-related within karsts, fractures, faults and folds. Examples of carbonate uranium deposits occur in China, India, and Kyrgyzstan (Blaise, 2014).

#### **2.5.13 Phosphate Deposits**

Phosphate deposits are principally represented by marine phosphorite of continental-shelf origin containing syn-sedimentary, stratiform, disseminated uranium in fine-grained apatite (Cuney, 2009).  $U^{4+}$  is a proxy for  $Ca^{2+}$  in the apatite structure, but biologic activity may create reducing environments where U may precipitate outside of the apatite structure (Cuney, 2009). The largest episode of phosphate deposition occurred during the late Cretaceous to Eocene (Blaise, 2014). Phosphate deposits contain many million tonnes of uranium (World Nuclear Association, 2010). However, uranium concentrations are very low,

ranging from 0.01-0.015%  $U_3O_8$ . Phosphate uranium deposits are mined in Central African Republic, Kazakhstan, Morocco and Tanzania (Blaise, 2014).

#### **2.5.14 Volcanic Related Deposits**

Volcanic related deposits are located within and near volcanic calderas filled with mafic to felsic volcanic lavas or more commonly pyroclastic rocks and intercalated clastic sediments (Blaise, 2014). Rhyolitic pyroclastic tuffs represent the largest proportion of the extruded magmas. Peralkaline magmatism provides the most interesting uranium source (Cuney, 2009). The genesis of significant deposits also requires a relatively shallow magma chamber, lasting over several million years, and able to provide the heat flux necessary to promote focused and long lasting convective fluid circulation (World Nuclear Association, 2010). These deposits make up only a small proportion of the world's uranium resources. Significant resources of this type occur in China, Kazakhstan, Russian and Mexico. Minor amounts occur in Australia and Canada (World Nuclear Association, 2010; Blaise, 2014).

#### **2.5.15 Black Shale Deposits**

Black shale deposits form in shallow marine environments (Blaise, 2014). They consist of marine organic-rich shale or coal-rich pyritic shale, containing syngenetic disseminated uranium adsorbed onto organic material and clay minerals (Blaise, 2014). Preferential U enrichment occurs in the vicinity of paleo-shores where clastic input is limited and where vigorous bottom water circulation promotes high rates of mass-transfer across the sediment/water interface (Schovsho, 2002). Examples of such deposits are found in Germany, Sweden and Uzbekistan (World Nuclear Association, 2010; Blaise, 2014).

## **2.6 HISTORY OF URANIUM EXPLORATION IN GHANA**

The search for radioactive elements (U and Th) in Ghana began in 1952 by D. Ostle, P.H. Hale and one geologist from Ghana Geological Survey Department (Kesse, 1985). A reconnaissance survey was carried out using carbon equipment which had sensitive Geiger counters coupled to amplifiers alongside a self recorder and an automatic alarm adjusted to operate above certain intensity of gamma radiation (Kesse, 1985). All the mobile roads (72,270km) in Ghana were surveyed and at the end of the survey, anomalies were observed in the laterites above the gneisses of the Dahomeyan Structural Unit, locations above the Bongo Granite and the laterites above the older Cape Coast granites (Kesse, 1985). Increases in background were observed in certain locations underlain by the Voltaian Supergroup. It was concluded from the survey that the rocks of Ghana had only 1% Th while the U content was not remarkable (Kesse, 1985).

According to Beer and Taylor (1953), a geochemical survey was carried out by Ghana Geological Survey Department. This revealed that some of the samples contained > 0.02% Th and the radioactive minerals observed in them included; monazite, xenotime and zirconium. Beer and Taylor (1953) indicated that the samples from which these minerals were observed were from the border areas of the Cape Coast Granite. From this study, it was concluded that the probability of finding alluvium monazite placer deposits which could be exploited economically in Ghana was very poor. In 1957, Geological Survey carried out a radiometric ground survey mainly over intrusions of syenites in the Dahomeyan Structural Unit (Kesse, 1985). The syenites showed considerable radioactivity in places. The grade was found to be extremely low (Kesse, 1985). Also, portions of the Voltaian Basin were

investigated and areas underlain by syenite and nepheline syenite of the DSU indicated higher radioactivity (Kesse, 1985).

In 1968, uranium prospecting was carried out by Uranerzbergbau GmbH (UEB). The survey employed airborne spectrometric and magnetometric surveys and covered areas of the Tarkwaian Supergroup and the Voltaian Basin (Kesse, 1985). A large number of anomalies were observed to be associated with zircon and monazite rich beach placers (Uranerzbergbau GmbH Co., 1972). An anomaly with uranium mineralization was also observed in the pegmatites (Uranerzbergbau GmbH Co., 1972). According to Kesse (1985), the International Atomic Energy Agency (IAEA) carried out uranium prospecting based on the earlier work carried out by Uranerzbergbau GmbH (UEB) in 1975. This work was associated with the pegmatites. It was concluded that the uranium mobilization was confined to the pegmatites and not the surrounding rocks (IAEA, 1976).

Adamek (1976) reported that the Atomic Energy Organization of Iran commented on the Uranerzbergbau's final report that; Ghana has terranes that are good potential for uranium mineralization. Hence, they suggested that an orientation survey must be carried out to select the most suitable areas before carrying out any expensive exploration survey (Kesse, 1985). According to Adamek (1976), it was recommended that work should be focused on the Voltaian Supergroup which is likely to host easily obtainable uranium deposit type. In 1979, a Track Etch survey was carried out by Ghana Geological Survey Department (GGSD) and Ghana Atomic Energy Commission (GAEC) over the southern part of the Voltaian Supergroup (Kesse, 1985). The study area was underlain by rocks of the Voltaian Supergroup (lower and middle) and the Birimian Supergroup (schist and granites).

According to Guelpa and Vogel (1982), an International Uranium Resource Evaluation Project was carried out to review the current knowledge concerning uranium resource in Ghana. The report summarized its findings of the uranium potential of the major geologic rock units of Ghana as follows; (1) Dahomeyan Structural Unit: High possibility of hosting major uranium potential due to its occurrence in the Pan African-Brazilian Mobile belt. The Mobile belt in Brazil, Algeria and Togo has a high uranium potential (2) Togo and Buem Structural Unit: They are potentially of low interest (3) Voltaian Supergroup: It has a moderate likelihood of hosting uranium deposit due to its similarities with the Taoudeni basin. The Taoudeni basin in Guinea is known to host uranium deposits. (4) Eburnean Granites: They have the potential for further discovery of other uraniferous pegmatites. However, such pegmatites do not represent economic targets. (5) Tarkwaian Supergroup: Likely to host some uranium potential due to its similarities with Witwatersrand basin in South Africa. (6) Coastal basins: The potential for sandstone type uranium is low (7) Accraian and Sekondian Group: they have been partly investigated. However, the anomalous characteristics associated with the Takoradi Shale may be due to uranium mineralization. (8) Keta and Tano basins: They have not revealed surface anomalies. However, the anomalous radioactivity observed in a well drilled in the Keta basin may be related to higher phosphate content in the fossiliferous calcareous bodies. (9) Birimian Supergroup: This shows a low potential for uranium mineralization

In 2008, a uranium content study was carried out by GAEC at Biakpa, Volta Region using Track Etch technique. The mean percentage concentration of uranium content of rocks determined was 0.018 %. This implied that the concentration of Uranium mineralisation in the area was low. Preliminary studies for the determination of uranium mineralization have

been carried out in the geologic terranes in the country. The speculative deposit types in Ghana include the sandstone type of the Voltaian Supergroup and metasomatite type. The sandstone type associated with the Voltaian basin is known to be low. The metasomatite types are Na, K and skarn related. The Na metasomatite can be granite derived, metasediment and metavolcanic derived (Kesse, 1985; Blaise, 2014 and Dampare per comm.).

## **2.8 URANIUM MINERALS**

According to Cuney (2015), uranium in nature may occur as (i) U, Th minerals, (ii) substitute in accessory minerals, (iii) traces in the main rock forming minerals, (iv) adsorbed materials on the surfaces of clay minerals (i.e. at low temperatures U is strongly adsorbed on iron oxide and clay minerals) (v) U associated with organic matter and (vi) dissolved state in geologic fluids such as sea water, rivers and lakes. The major primary ore mineral of uranium is uraninite ( $\text{UO}_2$ ) or pitchblende ( $\text{U}_3\text{O}_8$ ), though a range of other uranium minerals is found in particular deposits (Cuney, 2009). These other minerals include carnotite (uranium potassium vanadate), the davidite-brannerite-absite type, uranium titanates, and the euxenite-fergusonite-samaraskite group (niobates of uranium and rare earths). Uranium is a strongly oxyphile element. It may occur as oxides, hydroxides, oxygen salts and silicates (Kesse, 1985; World Nuclear Association, 2010). The following common uranium minerals occurring in various rocks are shown below as follows;

Table 2.1: Some common uranium minerals (Kesse 1985; Gupta and Singh, 2003)

Type	Name	Chemical Composition
<b>Oxides</b>	Uraninite	UO <sub>2</sub>
	Pitchblende	U <sub>3</sub> O <sub>8</sub>
<b>Multiple Oxides</b>	Brannerite	(U, Ca, Fe, Th, Y) <sub>3</sub> TiO <sub>16</sub>
	Davidite	(Fe, Ce, U) (Ti, Fe, V, Cr) <sub>3</sub> 7H <sub>2</sub> O
<b>Hydrated Oxides</b>	Gummite	UO <sub>2</sub> . nH <sub>2</sub> O
	Becquerelite	2UO <sub>3</sub> .3H <sub>2</sub> O
<b>Simple Silicates</b>	Coffinite	U(SiO <sub>4</sub> ) <sub>1-x</sub> (OH) <sub>4x</sub>
	Uranothorite	Th <sub>(1-x)</sub> U <sub>x</sub> SiO <sub>4</sub>
<b>Phosphate</b>	Autunite	CaO.2UO <sub>3</sub> .P <sub>2</sub> O <sub>5</sub> .8H <sub>2</sub> O
	Torbernite	CuO.2UO <sub>3</sub> .P <sub>2</sub> O <sub>5</sub> .8H <sub>2</sub> O
<b>Vanadates</b>	Carnotite	K <sub>2</sub> O.2UO <sub>3</sub> .V <sub>2</sub> O <sub>5</sub> .3H <sub>2</sub> O
	Tyuyamunite	CaO. 2UO <sub>3</sub> .V <sub>2</sub> O <sub>5</sub> .3H <sub>2</sub> O
<b>Arsenates</b>	Zeunerite	CuO. 2UO <sub>3</sub> .As <sub>2</sub> O <sub>5</sub> .8H <sub>2</sub> O
<b>Hydrated Silicates</b>	Uranophane	CaO. 2UO <sub>3</sub> .2SiO <sub>4</sub> .6H <sub>2</sub> O

\*This research also focuses on understanding the geochemistry towards effective uranium exploration and evaluation in the Anyaboni Formation.

## CHAPTER THREE

### MATERIALS AND METHODS

#### 3.1 SAMPLING

Twenty rock samples were collected from the Anyaboni Formation in Asesewa and its surrounding areas. At the location point of the rock samples, field observations and descriptions were carried out at close and far distances to the outcrops. The observed colour, structure(s) and measurements were read, described and recorded in the field notebook. The outcrops identified in the field were assessed based on weathering condition by using the hammer to strike the outcrop at different places. Fresh outcrops were marked using the marker pen. The direction at which the sample was to be taken was measured using the geological compass. This was then recorded in the field note book. The GPS was used to take the location of the sample and the coordinates were recorded in the field note book. The marked sample was then taken out using a hammer and a chisel.

The samples were labeled using marker pen and were put in sacks. Oriented field photographs of sedimentary structures found in the field were also taken for illustration of the truth in the field. The geological environment from which the samples were collected were observed and described appropriately in the field note book and log sheets. This was to help in the interpretation of the results as to how the environment affected the outcome of the data acquired.

Table 3.1: Log sheet format for recording rock sample data

ID	UTM_E	UTM_N	Colour	Grain size	Lit	Vein	Strike(°)	Dip(°)	Alt	Intensity	Structure	Comment
----	-------	-------	--------	---------------	-----	------	-----------	--------	-----	-----------	-----------	---------

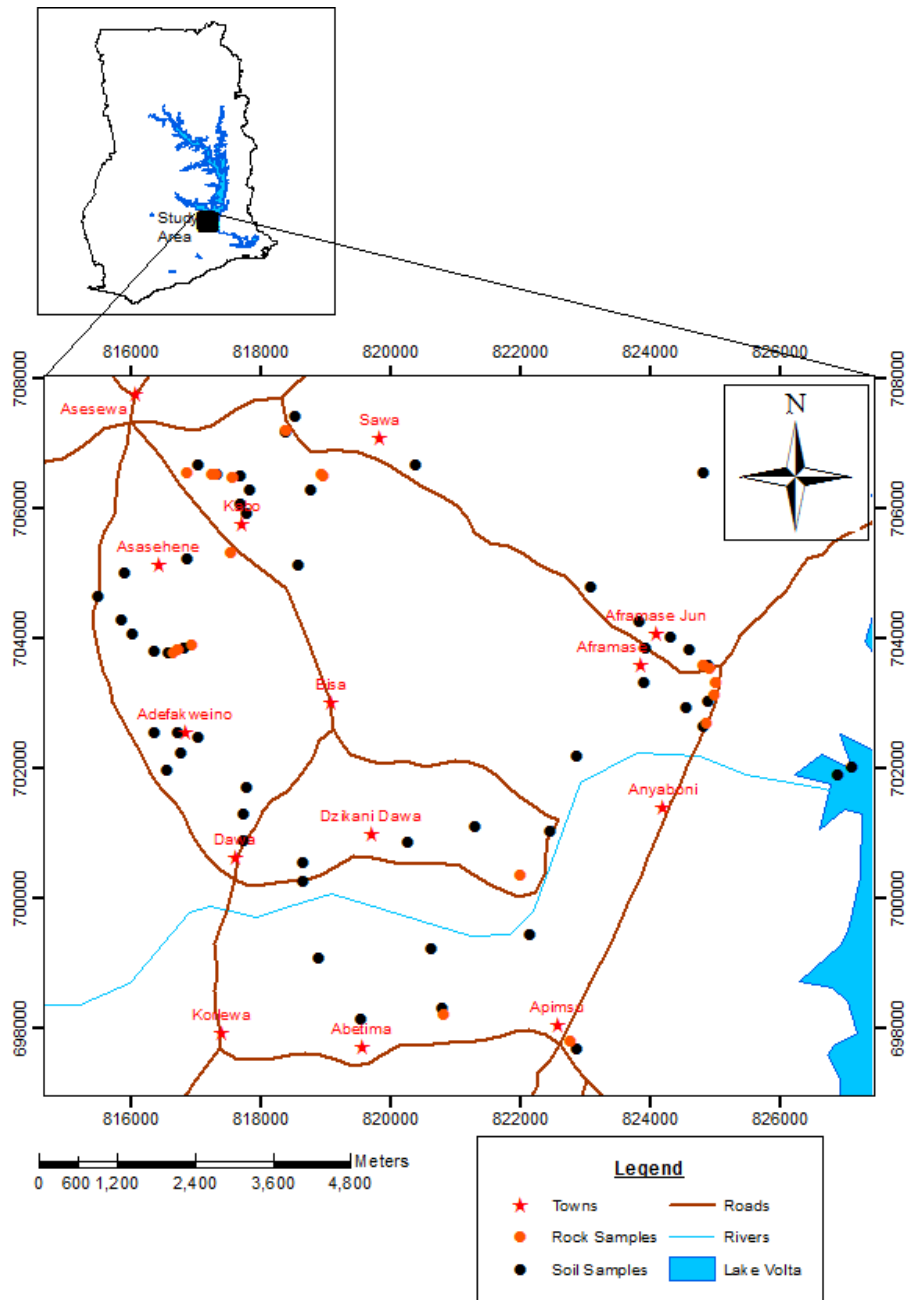


Figure 3.1: A sample location map of Asesewa and its surrounding areas (modified after Doudo, 2009).

### **3.2 SAMPLE PREPARATION**

A thin slice (a few millimeters thick) was cut from the rock sample using a diamond saw. The slice was grounded flat and smooth on one surface using progressively finer abrasive. The smooth surface was cemented to a glass slide (2'' x 1'') using Canada balsam cement. The other surface was then grounded down until the rock section was 0.03mm thick. Progressively finer abrasives were used as the section became thinner, and finishing was done with 600-grade carborundum powder. The thickness was gauged by observing the interference colours of common minerals such as quartz or feldspar. After cleaning excess cement from the section, it was covered with a glass cover-slip cemented on with Canada balsam. Twenty rock samples were also prepared at ALS Minerals in Kumasi, Ghana by first logging the samples into a tracking system and weighing. The samples were then fine crushed to 70% - 2mm. 250g of the crushed samples were split off and pulverized to better than 85% passing 75 microns.

### **3.3 ANALYTICAL TECHNIQUE**

Twenty thin sections of the Anyaboni Formation sandstones from Asesewa and its surrounding areas were examine by petrographic microscope and the modal composition of the sandstones was reviewed. About 300 counts per thin section were made by visual/manual point counting estimation. Twenty sandstone samples were analyzed for major, trace and rare earth elements by ALS minerals in Gauteng, South Africa. Major elements were analyzed by ICP-OES (Inductively Coupled Plasma Optical Emission Spectrometry) and trace element and rare earth element (REE) concentrations were determined by ICP-MS (Inductively Coupled Plasma Mass Spectrometry).

### **3.4 DATA TREATMENT**

#### **3.4.1 Geochemical Approach**

This involved the use of computer software such as Windows Excel, delta plot and CorelDraw X4 to generate variation diagrams and spider diagrams using the element concentrations obtained from the ICP-MS and ICP-OES analyses. The different plots obtained were interpreted according to the different patterns observed. The plots were used to make inference as to the possible rock classification, parent rock lithology, provenance and tectonic setting of the rocks studied. The paleoweathering and paleoclimate conditions were also inferred using the plots.

#### **3.4.2 Statistical and Geostatistical Analysis**

The numeric figures obtained from the geochemical analysis were handled using a computer by organizing data, recording data into tables and plotting maps. The statistical and graphical summaries produced from the data were used in making visual comparison of the different concentration levels of the samples at the different locations. Univariate and multivariate methods were used to uncover hidden trends in the dataset by testing first for the normality and stationary of the dataset. The univariate statistical method of analysis measured the mean, standard deviation (or variance), skewness and kurtosis of the data set. The skewed data was transformed through log transformation to achieve a normal dataset. The multivariate statistical method was used to generate scatter plots and carry out correlation and regression analysis. Semivariogram models were developed using the transformed data obtained from the statistical analysis applied. The semivariogram models were used to model spatial continuity in the dataset for U, Th, Zr and V. Kriging technique was used to estimate the spatial distribution of U, Th, Zr and V in the study area.

## **CHAPTER FOUR**

### **RESULTS**

#### **4.1 FIELD OBSERVATIONS**

##### **4.1.1 Reddish Brown to Chocolate Feldspathic Sandstone**

Presented in figure 4.1a and figure 4.1b are feldspathic (reddish brown to chocolate coloured) sandstones from the Anyaboni Formation. This sandstone type is sampled in and around Asesewa, Bisa and Apimsu localities. The reddish colour of the rocks is imparted by the presence of K-feldspars and iron minerals (due to oxidation of unstable minerals) in the rock.

##### **4.1.2 Gray/White and Pinkish Feldspathic Sandstone**

Presented in figure 4.2a and 4.2b are feldspathic sandstones from the Anyaboni Formation. The sandstones are gray/white and pinkish coloured. The sandstones are medium to coarse grain in size. The feldspathic sandstones were sampled from the Anyaboni locality.

##### **4.1.3 Quartz sandstone**

Presented in figure 4.3a and 4.3b are quartz sandstones from the Anyaboni Formation. The quartz sandstones are associated with joints (figure 4.3a) and laminations (figure 4.3b). The quartz sandstones from the Anyaboni Formation have thickness of about 400m. The sandstones were sampled from the Asesewa locality. The quartz sandstones have medium to coarse grain sizes.

##### **4.1.4 Structures**

Presented in figure 4.4 are some structures associated with the Anyaboni Formation sandstones; bedding, joints, laminations, fractures and ripple marks. Figure 4.1a and 4.2 also show rock fragment inclusions (clast) within the feldspathic sandstones of the Anyaboni

Formation. Quartz veins with preferred orientation (figure 4.4b) are present in the feldspathic sandstones of the Anyaboni Formation

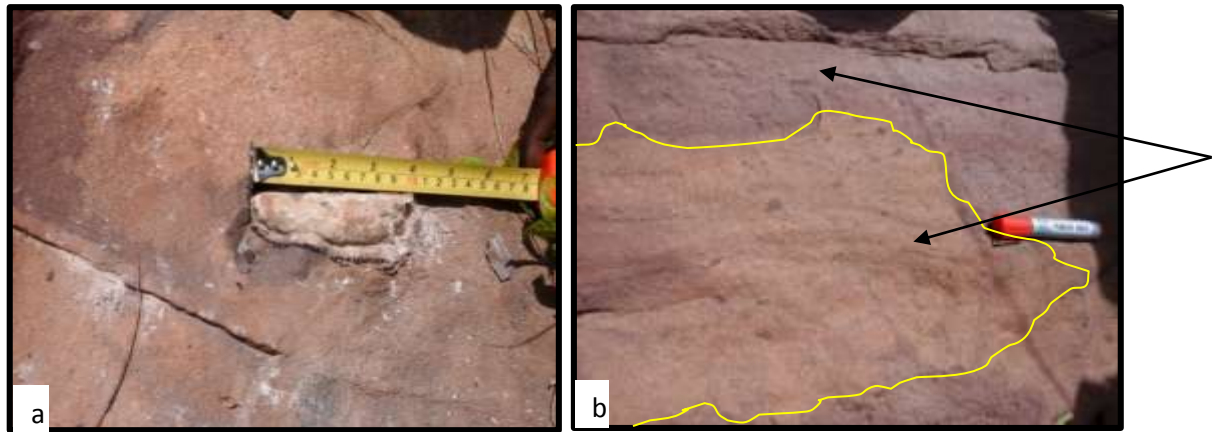


Figure 4.1: (a) Feldspathic sandstones with clast of feldspathic rock material observed in the Anyaboni Formation, SE (b) Feldspathic sandstones characterized by colour differentiation due to weathering, SE

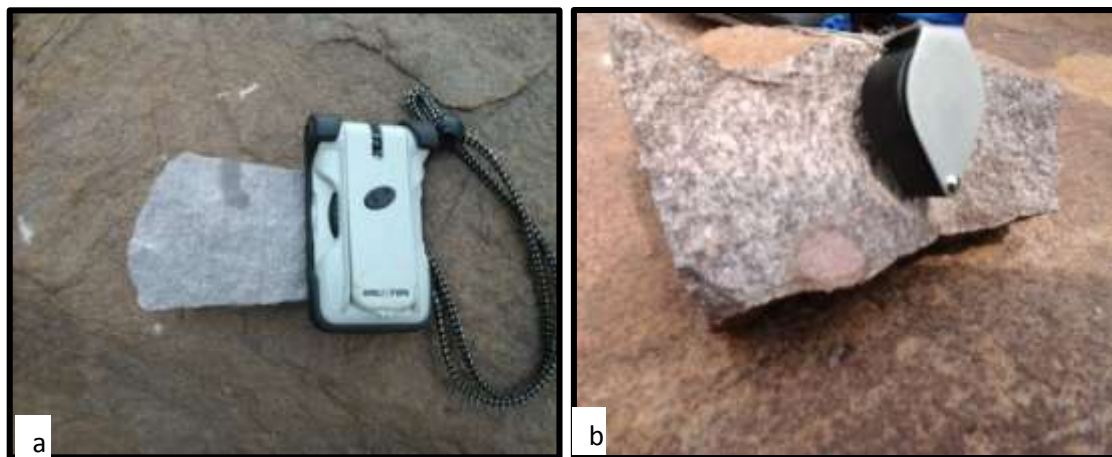


Figure 4.2: (a) Gray coloured feldspathic sandstone sampled from Anyaboni locality, SE (b) White and pinkish coloured feldspathic sandstone sampled from Anyaboni locality, SE



Figure 4.3: (A) Jointed quartz sandstone of the Anyaboni Formation observed at Asesewa, E (B) Laminated quartz sandstones of the Anyaboni Formation observed at Asesewa, E

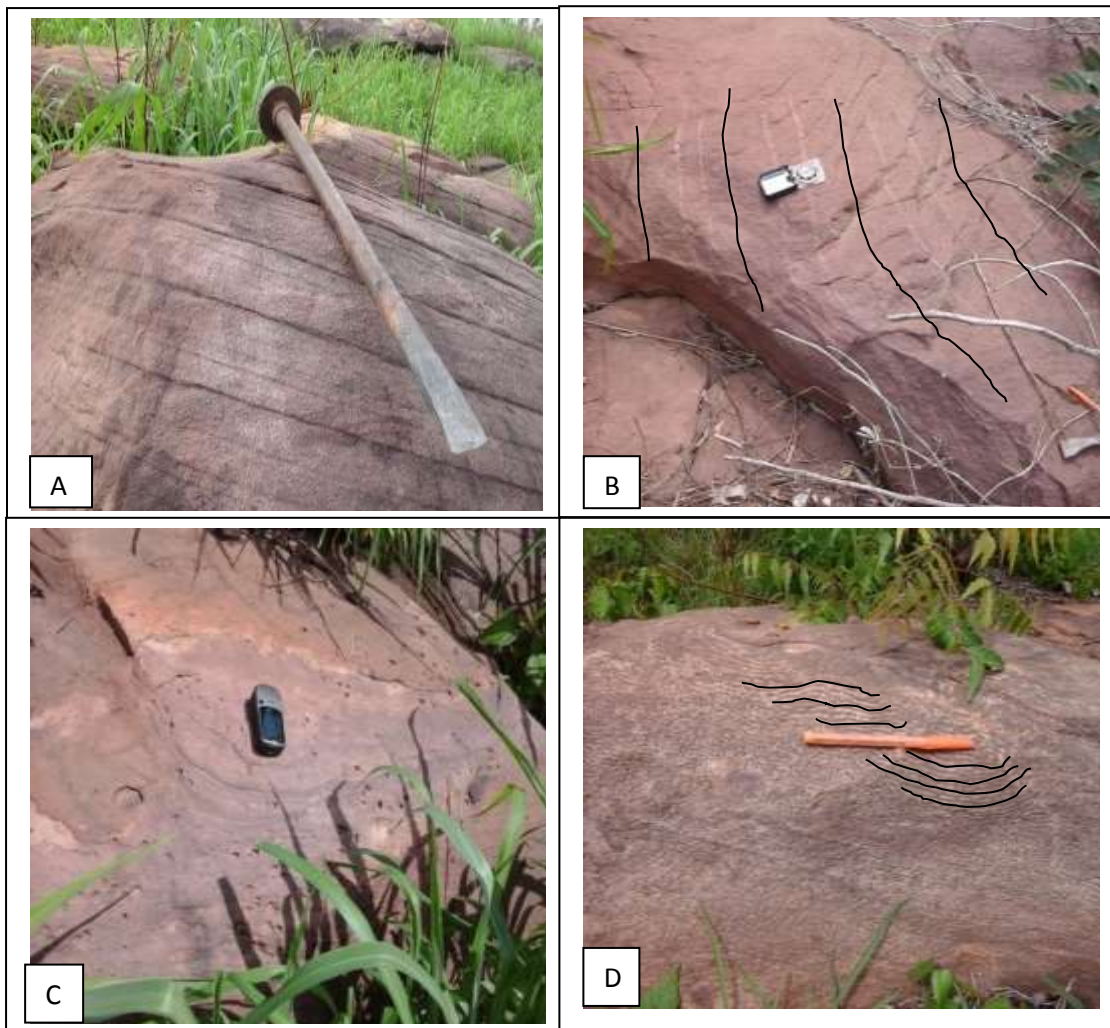


Figure 4.4: Some sedimentary features observed in the Anyaboni Formation: (A) Bedding, SE (B) quartz veins, SE (C) Raindrop structures, SE (D) Ripple marks, E

#### 4.2.1 Feldspathic Sandstone

Presented in figure 4.5, 4.6 and 4.7 are photomicrographs of feldspathic sandstones of the Anyaboni Formation in the Bisa, Anyaboni and Apimsu localities respectively. From figure 4.5, 4.6, 4.7 and 4.8, the sandstones are characterized by grain size variations from medium to fine grained under the petrographic microscope. The framework grains observed under the petrographic microscope are monocrystalline quartz (Qm), polycrystalline quartz (Qp), K-feldspar (microcline), plagioclase, muscovite and opaque minerals (preferably hematite). Iron oxide minerals and quartz overgrowths serve as the main cementing media supporting the sandstones under the petrographic microscope.

Quartz is the most dominant framework grain constituting about 80% of the rock volume, occurring as monocrystalline (most dominant) and polycrystalline grains. From Figure 4.6, the quartz crystals are sub-rounded to round in shape with a few being angular in shape. Figure 4.7 and 4.8 indicate that the quartz grains are mostly stained with iron which is shown in thin section by reddish brown colour under cross polarized light. Feldspars constitute around 10% of total framework grains of the sandstones. From figure 4.6 and 4.8 both K-feldspars (microcline) and plagioclase are present in the thin sections. K-feldspar (average; 9.6%) dominates over plagioclase (average; 0.4%). From figure 4.7, the feldspar grains are partially altered which implies a moderate degree of chemical weathering (Boggs 2009). The feldspar grains appear mostly small in size, sub-rounded to sub-angular and partially weathered (figure 4.7 and 4.8). From figure 4.8, muscovite occurs as a minor accessory grain type within the sample. Muscovite is associated with either the quartz crystals or the iron oxide/mineral (cementing medium) as supporting material in the sandstone. Heavy minerals form a minor constitute of the sandstone. The dominant accessory heavy minerals are

composed mainly of opaque minerals (especially hematite, which has stained the quartz grains in figure 4.6, 4.7, and 4.8 to give a reddish brown colour in cross polarized light).

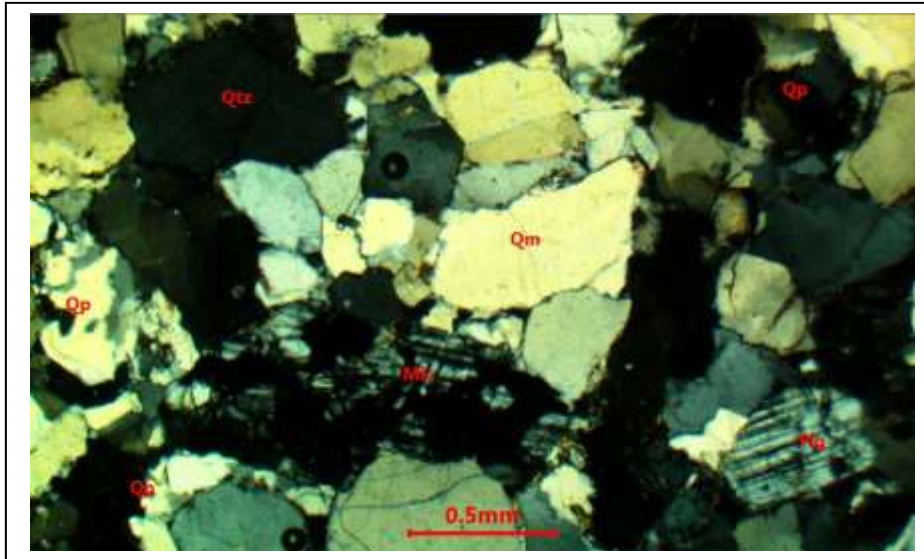


Figure 4.5: Photomicrograph of feldspathic sandstones from Bisa locality under cross polarized light. Qtz: Quartz, Qm: monocrystalline quartz, Qp: Polycrystalline quartz, Plg: plagioclase, Mic: microcline and Op: Opaque mineral

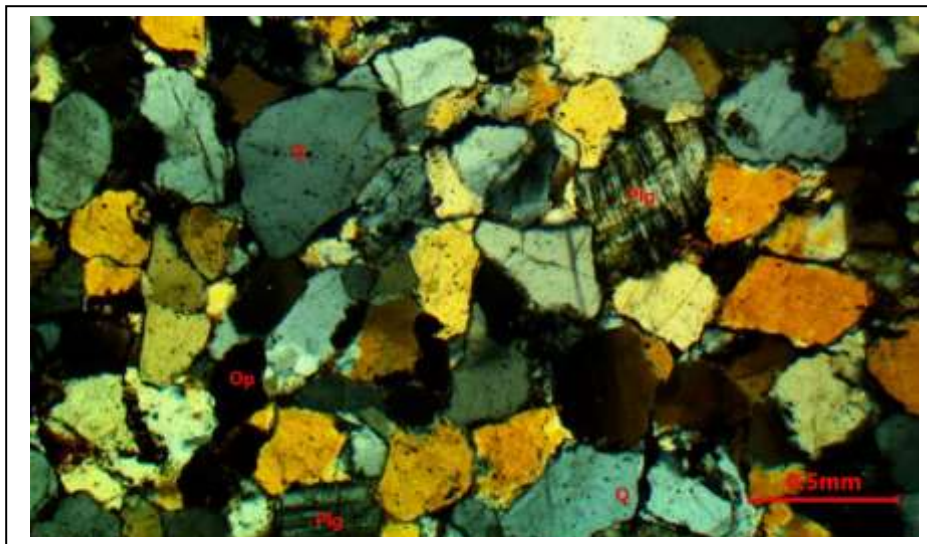


Figure 4.6: Photomicrograph of feldspathic sandstones from Anyaboni locality under cross polarized light Q: Quartz, Plg: plagioclase and Op: Opaque mineral

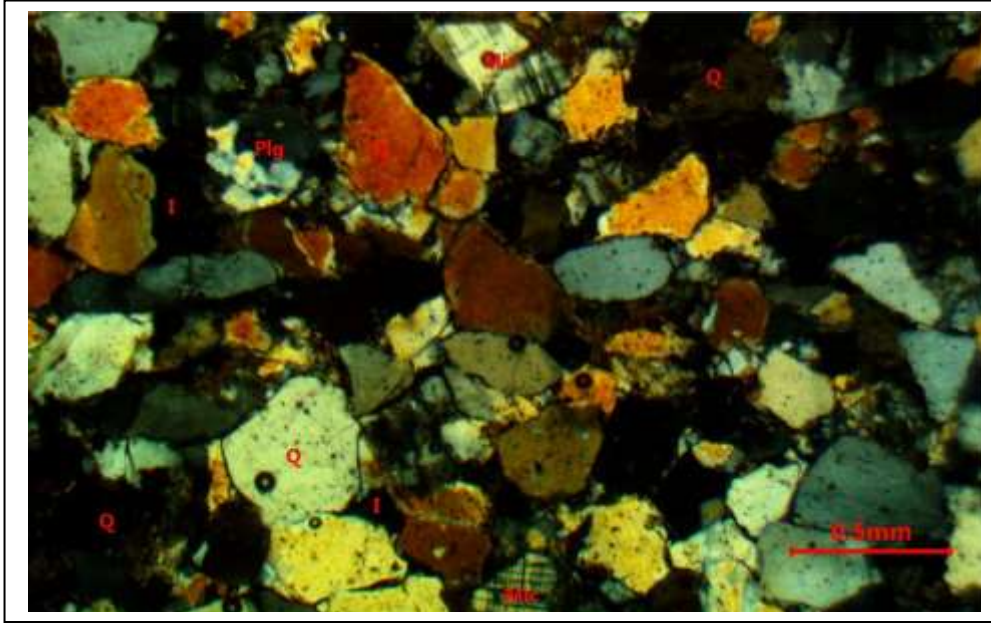


Figure 4.7: Photomicrograph of feldspathic sandstones from Apimsu locality under cross polarized light. Q: Quartz, Plg: plagioclase, Mic: microcline, I: Isotropic mineral and Op: Opaque mineral

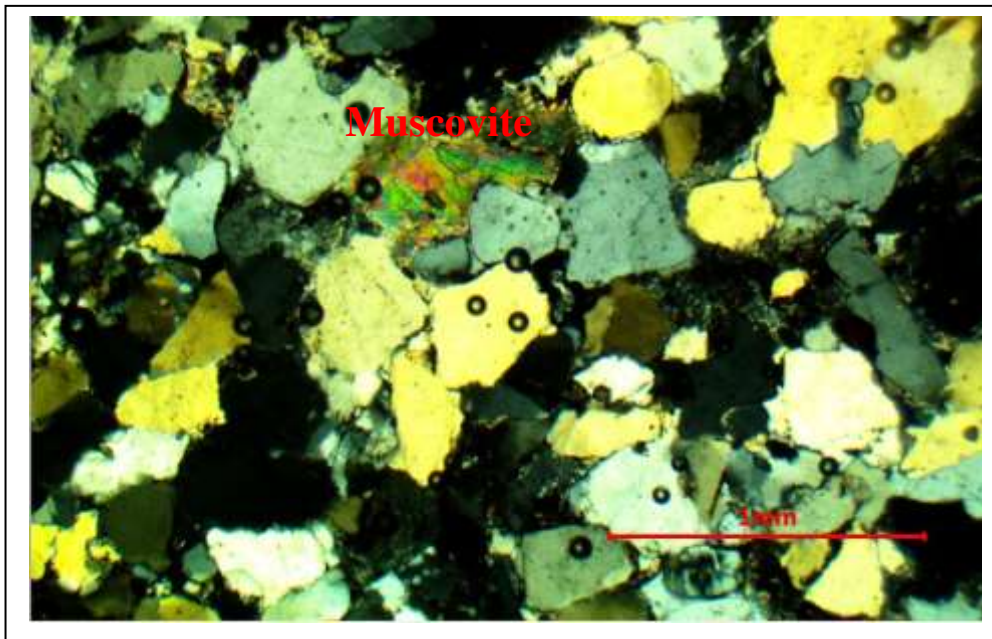


Figure 4.8: Photomicrograph of feldspathic sandstones from Bisa locality under cross polarized light

#### 4.2.2 Quartz Sandstone

Figure 4.9 shows a photomicrograph of quartz sandstones from Asesewa locality. From figure 4.9, the quartz sandstone is made up of about 95% quartz grains and 5% rock (lithic) fragments. The quartz grains are sub-rounded to round in shape and are medium to coarse grained under the petrographic microscope (figure 4.9). From figure 4.9, the quartz grains are predominately monocrystalline with a few polycrystalline quartz grains. Quartz overgrowths serve as the cementing medium in the quartz sandstones from the Anyaboni Formation.

The lithic fragments observed in figure 4.9 are volcanic fragments. The fragments are sub-rounded to round. According to Boggs (2009), the absence of feldspar in the quartz sandstone indicates that the rock is extensively recycled and derived from old sedimentary rocks.

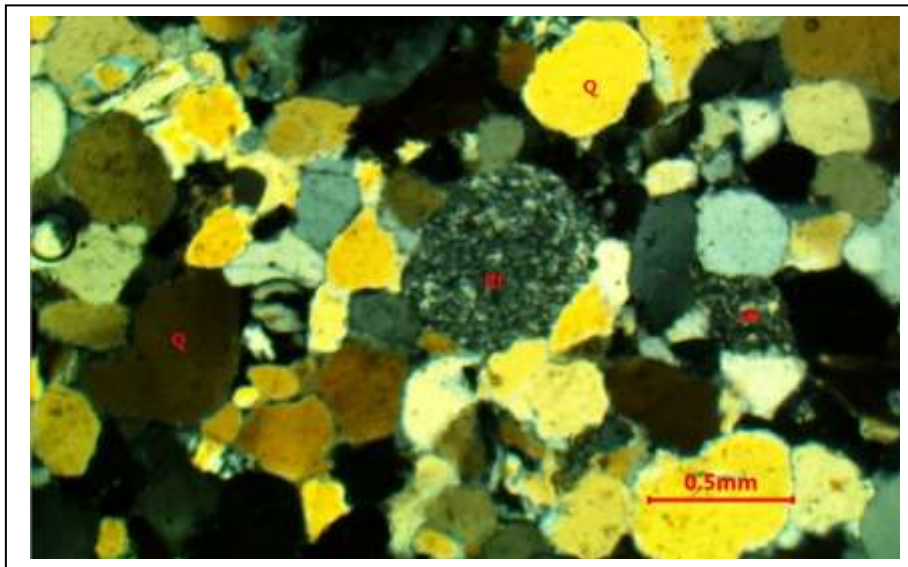


Figure 4.9: Photomicrograph of quartz sandstones from Asesewa locality under cross polarized light  
Q: Quartz and Rf: Rock fragment

### 4.2.3 Modal Composition

Presented in Table 4.1 is the point counting estimation of quartz (Q), Feldspar (F) and rock fragment (L) framework grains of the Anyaboni Formation sandstones. Table 4.1 shows that the sandstones are predominantly made up of quartz grains. Quartz ranges from 91.44% to 100% with average value of 97.19%, feldspar ranges from 0% to 2.83% with average of 1.24% and lithic fragment ranges from 0% to 8.57% with average of 1.57%

Table 4.1: Measured variables for Q-F-L ternary diagram and Log-plot

SAMPLE	Q (%)	F (%)	L (%)	In (Q/F)	In (Q/L)
FBI-101	96.74	1.57	1.70	4.12	4.04
FBI-102	96.34	0.87	2.80	4.71	3.54
FBI-104	93.07	4.22	2.24	3.09	3.73
FBI-105	100.00	0.00	0.00	0.00	0.00
FBI-106A	96.90	0.00	3.11	0.00	3.44
FBI-107	94.75	0.00	5.15	0.00	2.91
FBI-108	91.44	0.00	8.57	0.00	2.37
FAN-201	97.50	2.50	0.00	3.66	0.00
FAN-202	97.02	2.73	0.76	3.57	0.00
FAN-203	98.15	1.85	0.00	3.97	0.00
FAN-204	97.50	2.51	0.00	3.66	0.00
FAN-205	97.17	2.83	0.00	3.54	0.00
FAP-301	99.15	0.43	0.42	5.44	5.46
FAP-302	99.23	0.39	0.39	5.44	5.44
FAP-303	100.00	0.00	0.00	0.00	0.00
FAS-302	100.00	0.00	0.00	0.00	0.00

\*Q-F-L values obtains from visual/manual point counting estimation

## 4.3 GEOCHEMISTRY

### 4.3.1 Major Element Geochemistry

Table 4.2 gives the major element concentration (wt %) of the Anyaboni Formation sandstones from Asesewa and its environs. Table 4.2 shows that the Anyaboni Formation

sandstones have high SiO<sub>2</sub> content (86.2% wt to 100% wt; on average 92.1% wt). The source of silica is mainly quartz and feldspar minerals. The sandstones have a wide range of Al<sub>2</sub>O<sub>3</sub> (0.1 % to 8.32 %). MgO content varies from 0.01%wt to 0.16%wt while the Fe<sub>2</sub>O<sub>3</sub> content varies from 0.5%wt to 3.87%wt. CaO, Na<sub>2</sub>O and K<sub>2</sub>O contents vary from 0.01%wt to 0.24%wt, 0.01% wt to 0.08%wt and 0.02%wt to 2.5%wt respectively. TiO<sub>2</sub>, MnO and P<sub>2</sub>O<sub>3</sub> contents vary from 0.04%wt to 2.84%wt, 0.01%wt to 0.06%wt and 0.01%wt to 0.18%wt respectively.

Al<sub>2</sub>O<sub>3</sub> and the relatively moderate values of K<sub>2</sub>O content reflect a derivation from the K-feldspars (orthoclase and microcline) in the sandstones from the Anyaboni Formation. The small amount of CaO may be related to the presence of clay minerals (alteration of feldspars to clay minerals) present in the sandstones. Na<sub>2</sub>O contents relates to the presence of plagioclase feldspar present in the rocks. The TiO<sub>2</sub> content reflects the presence of Ti-opaque and heavy minerals typically rutile in the sandstones. The samples are characterized by low P<sub>2</sub>O<sub>5</sub> content and the depletion may be due to the lower amount of accessory phases such as apatite and monazite. The substantial Fe<sub>2</sub>O<sub>3</sub> content reflects iron oxide minerals present in grain boundary cement of the rocks. Very low MnO content also reflects low Eu of the depositional basin.

Presented in figure 4.10 is a Harker variation diagram which indicates that Al<sub>2</sub>O<sub>3</sub>, Fe<sub>2</sub>O<sub>3</sub>, K<sub>2</sub>O, MnO, Na<sub>2</sub>O, CaO, MgO and TiO<sub>2</sub>, decrease in concentration as SiO<sub>2</sub> content increases. The negative correlation between SiO<sub>2</sub> and Al<sub>2</sub>O<sub>3</sub> for the studied sandstone samples ( $r = -0.785$ ) indicates that much of the SiO<sub>2</sub> is present as quartz grains. From table 4.3, the samples are characterized by high K<sub>2</sub>O/Na<sub>2</sub>O (1 to 52.25) and SiO<sub>2</sub>/Al<sub>2</sub>O<sub>3</sub> (10.4-1000). McLennan et al. (1990) suggests the sandstones characteristics are derivation of an old

continental crust. According to McLennan et al. (1990), this provenance component constitutes old stable cratons. Presented in Table 4.3 are calculated chemical index of alteration (CIA) and plagioclase index of alteration (PIA) values after Nesbitt and Young (1982). The calculated CIA and PIA values for the Anyaboni Formation sandstones range from 61.05 to 80.77 with an average of 66.51; and 66.67 to 98.34, with average of 93.72 respectively. According to Osae et al. (2006), the CIA and PIA values reflect moderate to high degrees of weathering, either of the source area or during transport before deposition.

Table 4.2: Major element concentration (in wt %) of the Anyaboni Formation sandstones

SAMPLE	SiO <sub>2</sub>	Al <sub>2</sub> O <sub>3</sub>	Fe <sub>2</sub> O <sub>3</sub>	CaO	MgO	Na <sub>2</sub> O	K <sub>2</sub> O	TiO <sub>2</sub>	MnO	P <sub>2</sub> O <sub>5</sub>
FBI-101	92.10	3.57	2.81	0.02	0.04	0.06	1.52	0.11	0.01	0.02
FBI-102	96.30	1.90	0.62	0.01	0.02	0.04	1.04	0.05	0.01	0.02
FBI-103	94.40	3.01	0.71	0.01	0.03	0.06	1.44	0.04	0.01	0.01
FBI-104	92.50	3.59	1.89	0.03	0.04	0.08	1.77	0.24	0.01	0.11
FBI-105	86.50	8.32	1.53	0.04	0.16	0.06	2.39	0.38	0.03	0.09
FBI-106A	91.80	4.76	1.24	0.02	0.06	0.08	2.44	0.14	0.01	0.02
FBI-106B	90.10	4.78	2.44	0.03	0.07	0.07	2.50	0.19	0.01	0.08
FBI-107	98.50	0.84	0.50	0.01	0.03	0.02	0.17	0.05	0.01	0.01
FBI-108	100.00	0.10	0.51	0.02	0.01	0.02	0.02	0.04	0.01	0.14
FBI-109A	93.20	3.31	1.58	0.02	0.04	0.06	1.83	0.29	0.01	0.02
FBI-109B	90.80	3.75	1.69	0.02	0.04	0.06	2.10	0.10	0.01	0.01
FAN-201	93.90	2.35	1.61	0.01	0.04	0.05	1.13	0.17	0.01	0.02
FAN-202	92.90	2.95	1.26	0.01	0.04	0.04	1.77	0.13	0.01	0.01
FAN-203	92.80	2.55	1.16	0.02	0.04	0.04	1.54	0.15	0.01	0.02
FAN-204	91.90	3.59	1.80	0.01	0.04	0.07	2.21	0.10	0.01	0.02
FAN-205	94.10	3.01	1.42	0.01	0.04	0.04	1.68	0.06	0.01	0.02
FAP-301	92.10	3.67	1.62	0.14	0.11	0.07	2.01	0.40	0.06	0.14
FAP-302	86.20	5.13	2.93	0.03	0.08	0.04	2.09	2.84	0.01	0.11
FAP-303	87.60	4.98	2.33	0.24	0.07	0.05	2.47	0.52	0.01	0.18
FAS-302	92.40	1.57	3.87	0.01	0.02	0.01	0.44	0.08	0.01	0.02

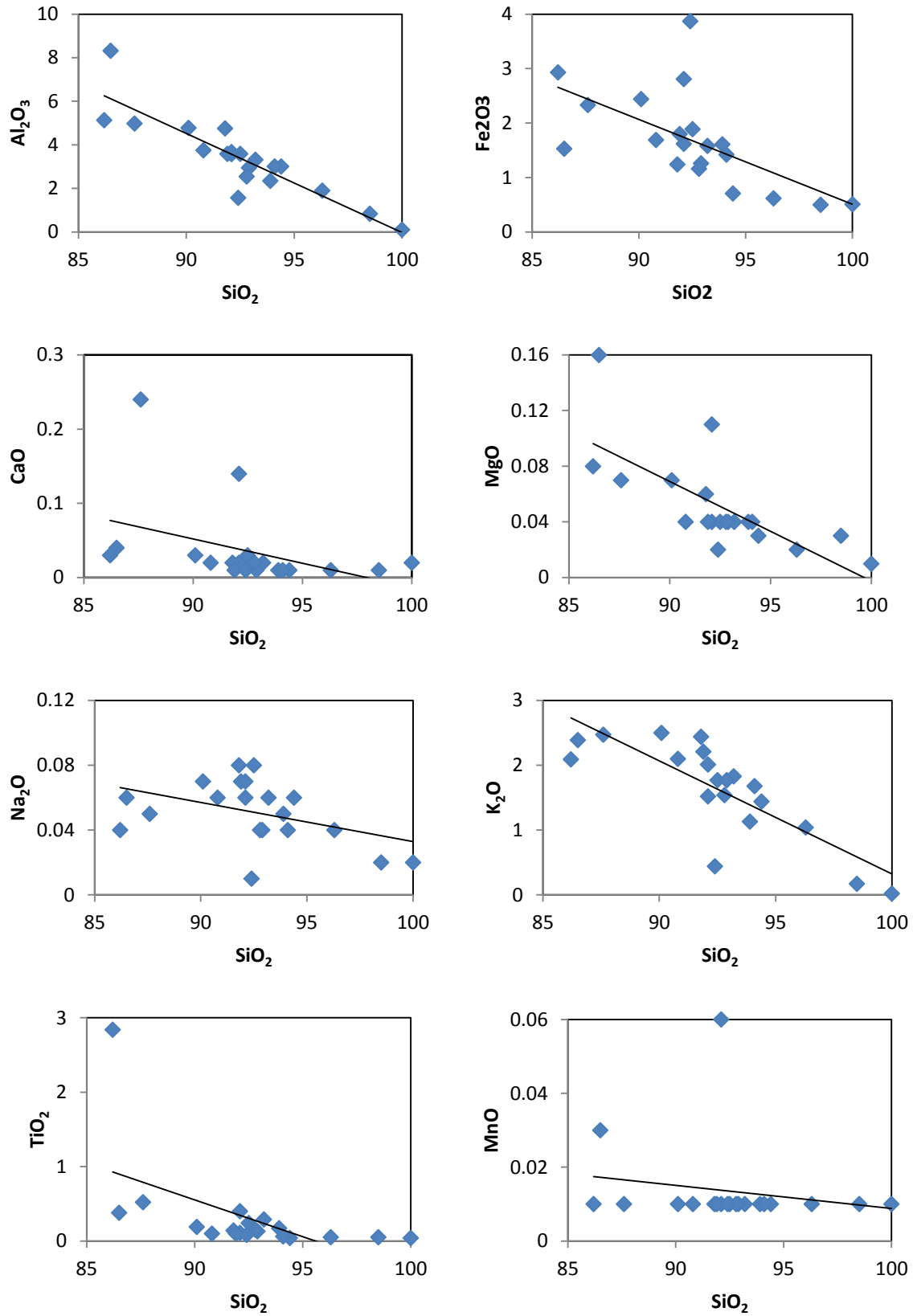


Figure 4.10: Harker variation diagram of major elements for the Anyaboni Formation sandstones

Table 4.3: Measured Variables for CIA and PIA ternary diagram presentation

SAMPLE	CIA	PIA	K <sub>2</sub> O/Na <sub>2</sub> O	Al <sub>2</sub> O <sub>3</sub> /Na <sub>2</sub> O	SiO <sub>2</sub> /Al <sub>2</sub> O <sub>3</sub>	Fe <sub>2</sub> O <sub>3</sub> /K <sub>2</sub> O	Al <sub>2</sub> O <sub>3</sub> /SiO <sub>2</sub>	CaO* +NaO	Fe <sub>2</sub> O <sub>3</sub> * +MgO
FBI-101	69.05	96.24	25.33	59.50	25.80	1.85	0.04	0.08	2.85
FBI-102	63.55	94.51	26.00	47.50	50.68	0.60	0.02	0.05	0.64
FBI-103	66.59	95.73	24.00	50.17	31.36	0.49	0.03	0.07	0.74
FBI-104	65.63	94.30	22.13	44.88	25.77	1.07	0.04	0.11	1.93
FBI-105	76.97	98.34	39.83	138.67	10.40	0.64	0.10	0.10	1.69
FBI-106A	65.21	95.87	30.50	59.50	19.29	0.51	0.05	0.10	1.30
FBI-106B	64.77	95.80	35.71	68.29	18.85	0.98	0.05	0.10	2.51
FBI-107	80.77	95.71	8.50	42.00	117.26	2.94	0.01	0.03	0.53
FBI-108	62.50	66.67	1.00	5.00	1000.00	25.50	0.00	0.04	0.52
FBI-109A	63.41	94.87	30.50	55.17	28.16	0.86	0.04	0.08	1.62
FBI-109B	63.24	95.38	35.00	62.50	24.21	0.80	0.04	0.08	1.73
FAN-201	66.38	95.31	22.60	47.00	39.96	1.42	0.03	0.06	1.65
FAN-202	61.84	95.93	44.25	73.75	31.49	0.71	0.03	0.05	1.30
FAN-203	61.45	94.39	38.50	63.75	36.39	0.75	0.03	0.06	1.20
FAN-204	61.05	94.52	31.57	51.29	25.60	0.81	0.04	0.08	1.84
FAN-205	63.50	96.38	42.00	75.25	31.26	0.85	0.03	0.05	1.46
FAP-301	62.31	88.77	28.71	52.43	25.10	0.81	0.04	0.21	1.73
FAP-302	70.37	97.75	52.25	128.25	16.80	1.40	0.06	0.07	3.01
FAP-303	64.34	89.64	49.40	99.60	17.59	0.94	0.06	0.29	2.40
FAS-302	77.34	98.26	44.00	157.00	58.85	8.80	0.02	0.02	3.89

$$CIA = [Al_2O_3 / (Al_2O_3 + CaO^* + Na_2O + K_2O)] * 100 \quad PIA = [(100 * (Al_2O_3 - K_2O)) / (Al_2O_3 + CaO + Na_2O - K_2O)]$$

### 4.3.2 Trace Element Geochemistry

Presented in table 4.4 are trace element concentrations of the Anyaboni Formation sandstones. Table 4.4 shows that most of the samples are rich in Ba and Zr. Ba ranges from 54.4 ppm to 1030 ppm with average of 360.46 ppm and Zr ranges from 52 ppm to 1125 ppm with average of 160.85 ppm. The other Large Ion Lithophile Elements (LILEs); Rb ranges from 14.2 ppm to 75.9 ppm, Cs ranges from 0.79 ppm to 1.93 ppm, and Sr ranges from 7.6 ppm to 97.2 ppm (Table 4.4). The High Field Strength Elements (HFSEs) are characterized by concentrations varying as follows; Hf ranges from 1.3 ppm to 25.8 ppm, Ta ranges from

0.1ppm to 4.5 ppm, Nb ranges from 0.8ppm to 53.4 ppm, Th ranges from 1.33ppm to 33.3 ppm, U ranges from 0.36ppm to 4.73ppm (Table 4.4). Presented in Table 4.5 are trace element ratios of Rb/Sr, Zr/Hf and Th/U for the Anyaboni Formation sandstones. Table 4.5 shows Th/U value ranging from 2.52 to 9.55 with average of 5.55, Rb/Sr value varies from 0.09 to 2.59 with average of 1.66, Zr/Hf value ranges from 34.38 to 42.31 with average of 37.55, La/Th value ranges from 1.68 to 4.82 with average of 3.04, Cr/Th value ranges from 1.61 to 6.73 with average of 3.77 and La/Cr value ranges from 0.37 to 1.96 with average of 0.92 (Table 4.5).

Table 4.4: Trace element concentrations in ppm for Anyaboni Formation sandstones, trace elements data determined by ICP-OES (ALS Mineral, South Africa)

SAMPLE	Cs	Rb	Ba	Th	U	Nb	Ta	Sr	Zr	Hf	Y
FBI-101	0.81	45.30	261.00	4.38	0.76	2.30	0.20	24.00	95.00	2.50	10.40
FBI-102	0.79	31.10	201.00	2.47	0.37	1.10	0.10	18.70	53.00	1.50	6.90
FBI-103	0.86	42.40	237.00	2.19	0.36	1.20	0.10	19.00	55.00	1.60	6.20
FBI-104	1.17	52.60	1030.00	4.37	1.41	5.10	0.40	59.40	110.00	2.90	13.70
FBI-105	1.93	75.90	229.00	8.46	1.64	6.80	0.50	46.70	267.00	7.40	27.20
FBI-106A	1.40	71.50	426.00	6.30	0.66	3.20	0.20	35.50	97.00	2.80	11.70
FBI-106B	1.30	72.50	774.00	4.66	1.07	4.20	0.30	48.30	137.00	3.30	10.30
FBI-107	0.75	6.80	40.20	1.33	0.46	1.10	0.10	10.10	52.00	1.50	6.90
FBI-108	0.87	1.00	73.00	1.41	0.39	0.80	0.10	11.60	55.00	1.30	3.90
FBI-109A	1.44	54.50	324.00	6.21	0.73	5.80	0.50	25.40	131.00	3.40	9.20
FBI-109B	1.43	62.00	358.00	3.42	0.55	2.10	0.20	23.90	76.00	2.20	8.60
FAN-201	1.46	36.70	182.50	4.18	0.66	3.30	0.20	15.60	121.00	3.20	8.00
FAN-202	1.55	51.30	328.00	4.21	0.58	2.40	0.20	23.00	69.00	1.80	7.60
FAN-203	1.56	45.20	316.00	3.62	0.72	3.20	0.20	21.30	76.00	2.00	7.40
FAN-204	1.72	65.30	435.00	4.22	0.72	2.40	0.10	28.10	83.00	2.20	8.70
FAN-205	1.46	54.20	323.00	3.55	0.58	1.60	0.10	22.30	72.00	2.00	7.20
FAP-301	1.91	66.10	558.00	5.37	1.50	8.00	0.70	75.30	215.00	5.50	8.60
FAP-302	1.50	61.70	565.00	33.30	4.73	53.40	4.50	97.20	1125.00	25.80	49.70
FAP-303	1.74	72.30	494.00	9.08	3.60	10.20	1.00	66.10	259.00	6.80	14.60
FAS-302	1.28	14.20	54.40	2.97	0.55	1.70	0.10	7.60	69.00	2.00	4.90

Table 4.5: Ranges and averages of elemental ratios of the Anyaboni Formation Sandstones

Elemental Ratio	Range	Average
Rb/Sr	0.09 – 2.59	1.66
Zr/Hf	34.38 – 42.31	37.55
Th/U	2.52 – 9.55	5.55
La/Th	1.68-4.82	3.04
Cr/Th	1.61-6.73	3.77
La/Cr	0.37-1.96	0.92

### 4.3.3 Rare Earth Elements Studies

Table 4.6 shows REE concentrations (in ppm) of the Anyaboni Formation sandstones. From Table 4.6, La varies from 6.2ppm to 79.1ppm with average of 15.39ppm, Ce varies from 13ppm to 172.5ppm with average of 33.66ppm, Pr varies from 1.5ppm to 19.9ppm with average of 3.80ppm, Nd varies from 5.2ppm to 79.5ppm with average of 14.87ppm, Sm varies from 1.12ppm to 16.45ppm with average of 3ppm, Eu varies from 0.21ppm to 2.53ppm with average of 0.55ppm, Gd varies from 0.92ppm to 13.05ppm with average of 2.60ppm, Tb varies from 0.16ppm to 1.91ppm with average of 0.39ppm, Dy varies from 0.86ppm to 10.6ppm with average of 2.39ppm, Ho varies from 0.15ppm to 1.95ppm with average of 0.44ppm, Er varies from 0.57ppm to 5.97ppm with average of 1.36ppm, Tm varies from 0.09ppm to 0.92ppm with average of 0.21ppm, Yb varies from 0.39ppm to 5.98ppm with average of 1.28ppm and Lu varies from 0.09ppm to 0.28ppm with average of 0.19ppm.

Presented in table 4.7 are the ranges and averages of elemental ratios of the Anyaboni Formation sandstones as compared to chondrite and Upper continental crust. Table 4.7 shows that La/Yb ratio ranges from 6.54 to 12.51 with an average value of 8.80 for the samples

compared to chondrite. LREE enrichment as reflected by  $(La/Sm)_N$  ratio ranges from 3.08 to 5.98 with average value of 3.67 for chondrite normalization.  $(Tb/Yb)_N$  indicates HREE enrichment and ranges from 0.77 to 1.99 with average value of 1.38 for normalized samples by chondrite. This suggests that the samples are relatively enriched in LREE than HREE. The magnitude of  $Eu/Eu^*$  range from 0.53 to 0.71 with an average of 0.62 for chondrite normalized sandstones (Table 4.7). According to Cullers (1994 and 2000), the europium anomaly suggests a felsic source.  $\Sigma LREE$  ranges from 92.04 to 1209.81 with an average value of 235.71 and  $\Sigma HREE$  ranges from 25.48 to 269.29 with an average value of 59.49 (Table 4.7). Hence,  $\Sigma LREE/\Sigma HREE$  ratio ranges from 2.80 to 4.86 with an average of 3.82. This confirms the relatively high enrichment of LREE to that of HREE in the samples from the study area. Cullers (1994) suggest that the source is more likely to be that of felsic source.

The compared analyzed Anyaboni Formation sandstones to the Upper Continental Crust indicate that  $La/Yb$  ratio ranges from 0.7 to 1.34 with average value of 0.94 (Table 4.7). The europium anomaly shows a slight variation and ranges from 0.81 to 1.03 with an average of 0.95. This range of values is significant for felsic derived sediment source. LREE enrichment indicated by  $(La/Sm)_N$  ratio ranges from 0.72 to 1.39 with average value of 0.85 as shown in table 4.9. HREE enrichment of the samples expressed by  $(Tb/Yb)_N$  ranges from 0.61 to 1.47 and has an average value of 1.08. It can be inferred that HREE enrichment in the samples are higher than that of LREE.  $\Sigma LREE$  ranges from 1.68 to 21.16 with average of 4.14 and  $\Sigma HREE$  ranges from 1.52 to 19.18 with average of 4.25.  $\Sigma LREE/\Sigma HREE$  ratio ranges from 0.76 to 1.17 with an average of 0.93; lower values are recorded for UCC-normalized REEs than chondrite-normalised REEs.

Table 4.6: Rare Earth Elements (REEs in ppm) of the Anyaboni Formation sandstones

SAMPLE	La	Ce	Pr	Nd	Sm	Eu	Gd	Tb	Dy	Ho	Er	Tm	Yb	Lu
FBI-101	12.50	26.00	2.81	11.20	2.23	0.42	2.00	0.35	2.17	0.41	1.27	0.22	1.23	0.18
FBI-102	9.60	20.30	2.25	8.30	1.72	0.33	1.54	0.19	1.48	0.25	0.77	0.15	0.59	0.09
FBI-103	8.30	18.10	1.87	7.60	1.46	0.29	1.19	0.19	1.22	0.21	0.79	0.10	0.77	0.13
FBI-104	19.60	39.20	4.79	18.70	3.91	0.83	3.79	0.52	2.86	0.50	1.58	0.24	1.31	0.20
FBI-105	37.90	78.80	9.65	40.20	7.61	1.48	7.28	1.06	6.52	1.10	3.26	0.45	2.45	0.34
FBI-106A	19.10	43.30	4.54	18.40	4.00	0.66	2.80	0.39	2.63	0.43	1.34	0.23	1.25	0.19
FBI-106B	11.30	21.20	2.34	8.00	1.22	0.30	1.53	0.24	1.79	0.42	1.22	0.21	1.24	0.20
FBI-107	6.20	13.00	1.50	5.20	1.12	0.22	1.36	0.20	1.22	0.24	0.67	0.10	0.60	0.08
FBI-108	6.80	14.60	1.73	6.70	1.40	0.26	1.04	0.16	0.86	0.15	0.41	0.09	0.39	0.07
FBI-109A	14.30	29.70	3.29	12.60	2.35	0.44	1.99	0.31	1.84	0.35	1.18	0.16	0.99	0.15
FBI-109B	10.00	20.40	2.40	9.10	1.99	0.39	1.69	0.25	1.96	0.32	0.99	0.14	0.89	0.13
FAN-201	10.10	20.40	2.29	9.10	1.93	0.32	1.50	0.29	1.56	0.31	0.94	0.16	0.95	0.15
FAN-202	9.60	21.60	2.26	8.40	1.60	0.31	1.62	0.25	1.47	0.30	0.90	0.15	0.88	0.13
FAN-203	9.60	22.10	2.23	8.60	1.89	0.42	1.74	0.30	1.51	0.30	0.82	0.14	0.83	0.10
FAN-204	11.60	24.60	2.79	10.20	2.07	0.43	1.87	0.32	1.71	0.34	0.97	0.16	0.91	0.14
FAN-205	9.20	19.40	2.14	8.00	1.49	0.28	1.43	0.19	1.59	0.30	0.83	0.12	0.92	0.12
FAP-301	9.00	17.80	1.95	7.00	1.40	0.24	0.97	0.16	1.25	0.28	0.94	0.16	0.95	0.18
FAP-302	79.10	172.50	19.90	79.50	16.45	2.53	13.05	1.91	10.60	1.95	5.97	0.92	5.98	0.88
FAP-303	17.30	34.40	3.56	13.90	3.10	0.55	2.73	0.44	2.58	0.54	1.87	0.29	1.86	0.28
FAS-302	7.40	15.70	1.76	6.60	1.14	0.21	0.92	0.16	0.95	0.19	0.57	0.09	0.61	0.09

Table 4.7: Ranges and averages of elemental ratios of the Anyaboni Formation Sandstones

Elemental Ratio	Chondrite		Upper Continental Crust	
	Range	Average	Range	Average
La/Yb	6.54-12.51	8.80	0.7-1.34	0.94
(La/Sm) <sub>N</sub>	3.08-5.98	3.67	0.72-1.39	0.85
(Tb/Yb) <sub>N</sub>	0.77-1.99	1.38	0.61-1.47	1.08
(Gd/Yb) <sub>N</sub>	0.85-2.46	1.62	0.59-1.72	1.14
Eu/Eu*	0.53-0.71	0.62	0.81-1.03	0.92
Ce/Ce*	0.01-0.15	0.08	0.25-1.40	0.55
Sm/Nd	0.15-0.22	0.20	0.88-1.29	1.16
ΣLREE	92.04-1209.81	235.71	1.68-21.16	4.14
ΣHREE	25.48-269.29	59.49	1.52-19.18	4.25
ΣLREE/ΣHREE	2.80-4.86	3.82	0.76-1.17	0.93

\*Subscript N denotes Chondrite or Upper continental crust normalized values. Normalization factors are from Sun and McDonough 1989 (for Chondrite); Taylor and McLennan, 1985 (for Upper continental crust)

## 4.4 STATISTICAL AND GEOSTATISTICAL ANALYSIS

### 4.4.1 Statistical Summaries

Presented in table 4.8 are trace element concentrations (in ppm) for U, Th, Zr and V of the Anyaboni Formation sandstones. Table 4.8 shows that the Anyaboni Formation sandstones have a wide range of U (0.36ppm - 4.73ppm), Th (1.33ppm - 33.3ppm), Zr (52ppm – 1125ppm) and V (5ppm-27ppm). Table 4.9 gives the summary statistics of U, Th, Zr and V concentrations of the Anyaboni Formation sandstones with averages of 1.10ppm, 5.79ppm, 160.85ppm and 10.35 respectively. The concentrations of U, Th, Zr and V show significant amount of variability especially Zr. Their variability is indicated by variance as 1.27, 46.03, 55714.77 and 32.45 for U, Th, Zr and V respectively. The variance is ranked as  $U < V < Th < Zr$ . The variability is also shown by the coefficient of variation as 1.02, 1.17, 1.47 and 0.55 for U, Th, Zr and V respectively.

Figure 4.9 gives a histogram representation indicating the frequency distribution of U, Th, Zr and V concentrations in the Anyaboni Formation sandstones. Figure 4.9 indicates that U, Th, Zr and V are skewed to the left. According to McCluskey and Lalkhen (2007), it can be inferred that the distribution of the dataset is not normal and requires to be transformed. From table 4.9, the skewness associated with U, Th, Zr and V are as follows; 2.14, 3.29, 3.38 and 1.28. Presented in table 4.10 is the summary statistics of log transformed data for U, Th, Zr and V concentrations from the Anyaboni Formation sandstones. From table 4.10, the transformed concentration values of U ranges from -0.44 to 0.67 with average of -0.09; Th ranges from 0.12 to 1.52 with an average value of 0.63; Zr ranges from 1.72 to 3.05 with an average of 2.04 and V ranges from 0.70 to 1.43 with average of 0.96, indicating a minimum variation compared to the initial dataset. The degree of variation in the Th, Zr and V

concentrations is reflected by their different coefficient of variation as follows; 0.48, 0.16 and 0.23 for Th, Zr and V respectively. This can be ranked as Th>V>Zr.

Presented in figure 4.10 is a scatter diagram for Th, Zr and V against U concentration of the Anyaboni Formation sandstones. The scatter diagrams suggest there is a positive linear relationship between Th, Zr and V against U concentration for the Anyaboni Formation sandstones (Bewick et al., 2003). Table 4.11 shows the summary correlations and regression analysis of Th, Zr and V concentrations in the Anyaboni Formation sandstones. From Table 4.11 an increasing trend between U and of Th, Zr and V is observed. The Pearson correlation and Spearman's rho coefficients are high for Th (0.876; 0.906), Zr (0.881; 0.931) and V (0.91; 0.913). This suggests that the elements are good pathfinder elements for uranium. From table 4.13, the regression analysis shows that Th, Zr and V accounts for 76.8%, 77.5% and 83.3% of the variation associated with uranium respectively in the Anyaboni Formation sandstones (Bewick et al., 2003). This suggests that V is most suitable for finding U in the study area, followed by Th and Zr.

Table 4.8: Trace element concentrations (in ppm) for U, Th, Zr and V of the Anyaboni Formation

SAMPLE	Th	U	Zr	V
FBI-101	4.38	0.76	95	10
FBI-102	2.47	0.37	53	5
FBI-103	2.19	0.36	55	5
FBI-104	4.37	1.41	110	13
FBI-105	8.46	1.64	267	14
FBI-106A	6.30	0.66	97	6
FBI-106B	4.66	1.07	137	15
FBI-107	1.33	0.46	52	5
FBI-108	1.41	0.39	55	5
FBI-109A	6.21	0.73	131	8
FBI-109B	3.42	0.55	76	6
FAN-201	4.18	0.66	121	12
FAN-202	4.21	0.58	69	8
FAN-203	3.62	0.72	76	10
FAN-204	4.22	0.72	83	13
FAN-205	3.55	0.58	72	9
FAP-301	5.37	1.50	215	11
FAP-302	33.30	4.73	1125	27
FAP-303	9.08	3.60	259	20
FAS-302	2.97	0.55	69	5

Table 4.9: Summary statistics of the variables studied

Element	Mean	Variance	COV	SD	Minimum	Maximum	Skewness	Kurtosis
U_ppm	1.10	1.27	1.02	1.12	0.36	4.73	2.14	6.68
Th_ppm	5.79	46.03	1.17	6.78	1.33	33.30	3.29	13.56
Zr_ppm	160.85	55714.77	1.47	236.04	52.00	1125.00	3.38	13.94
V_ppm	10.35	32.45	0.55	5.70	5.00	27.00	1.28	4.33

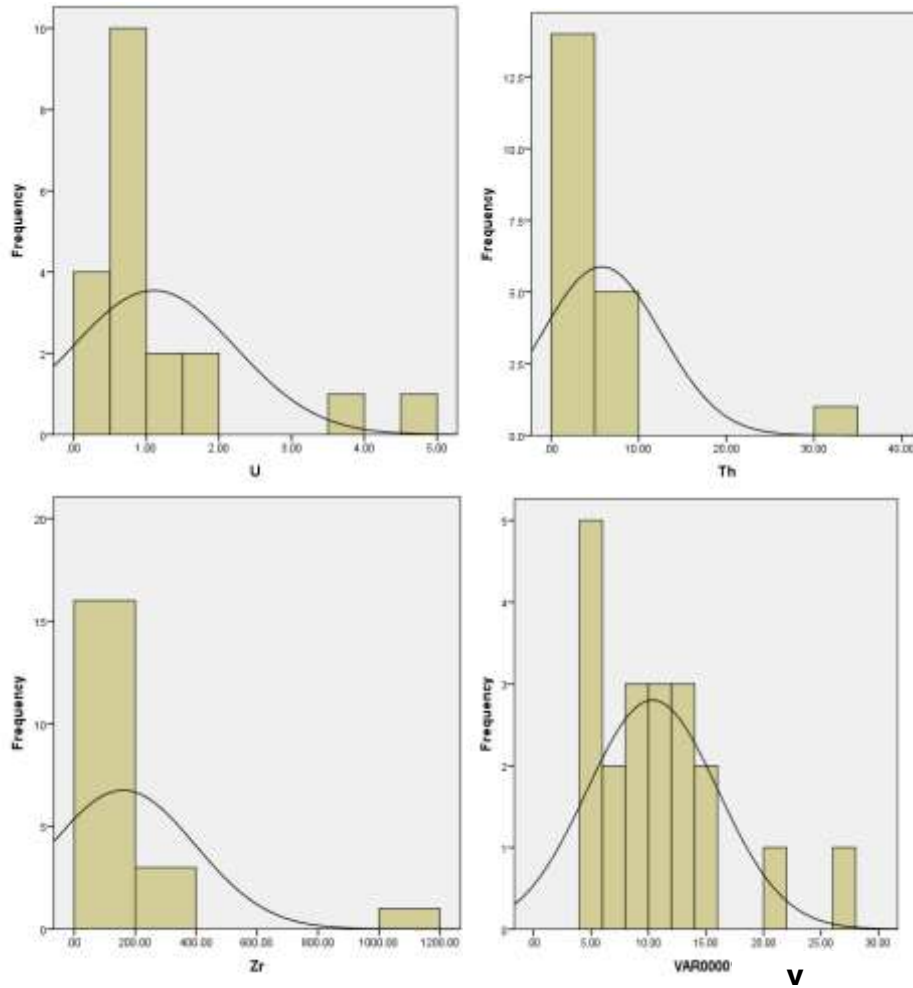


Figure 4.11: Histogram representation indicating the frequency distribution of U, Th, Zr and V concentrations in the Anyaboni Formation sandstones.

Table 4.10: Summary statistics of log transformed data for U, Th, Zr and V concentrations from the Anyaboni Formation sandstones

Element	Mean	COV	Variance	SD	Minimum	Maximum
Log_U	-0.09	N/A	0.09	0.31	-0.44	0.67
Log_Th	0.63	0.48	0.09	0.30	0.12	1.52
Log_Zr	2.04	0.16	0.10	0.32	1.72	3.05
Log_V	0.96	0.23	0.05	0.22	0.70	1.43

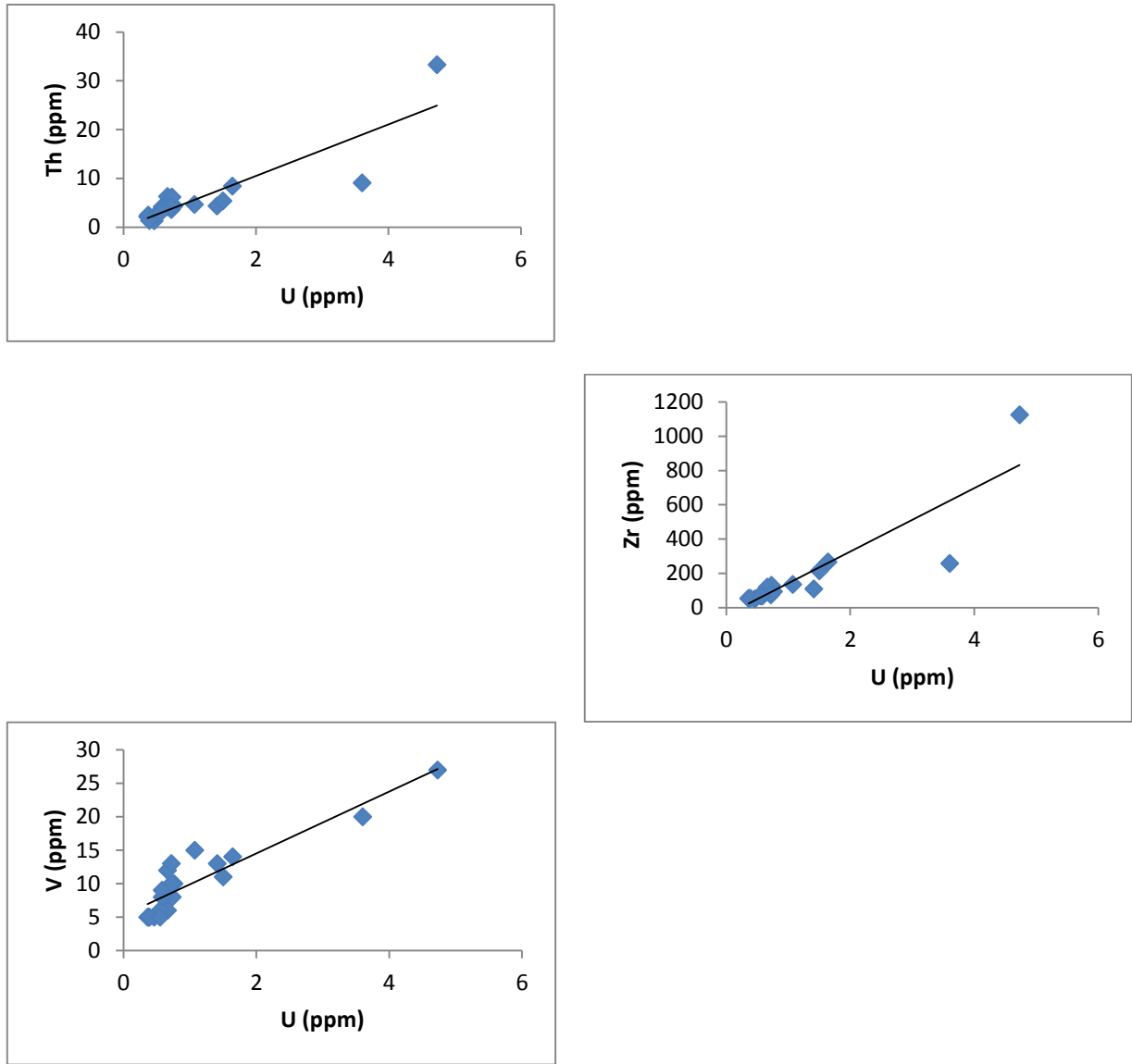


Figure 4.12: Scatter diagram for Th, Zr and V against U concentration of the Anyaboni Formation sandstones

Table 4.11: Summary correlations and regression analysis of Th, Zr and V

Element	Pearson Correlation	Spearman's rho	Regression ( $R^2$ )
Th_ppm	0.876	0.906	0.768
Zr_ppm	0.881	0.931	0.775
V_ppm	0.910	0.913	0.833

#### 4.4.2 Experimental Semivariogram for U, Th, Zr and V concentrations

Presented in figure 4.13, 4.14, 4.15 and 4.16 are experimental semivariograms fitted with spherical model for U, Th, Zr and V concentrations in the Anyaboni Formation sandstones respectively. Figure 4.13 gives nugget effect of 0.02 for U concentration in the Anyaboni Formation sandstones. Bohling (2005) indicates the nugget effect is the variability in data at small separation distances. The sill of the spatial variation is about 0.07 and U concentration distribution of the Anyaboni Formation sandstones has a spatial dependence ratio of 22% (Table 4.12). According to Paz-Ferreiro et al. (2010), it can be inferred that the degree of spatial continuity is low. From figure 4.12, the range after which there is spatial variation in the concentration of U in the study area is about 1000m (Figure 4.13).

The nugget effect expressed by experimental semivariogram for Th concentration in the study area is 0.01 (Figure 4.14). This small distance of separation as indicated by the nugget effect is by far the smallest value obtained. The sill of the Th concentration variation is 0.12 with the spatial dependence ratio of the distribution as 8% (Table 4.12). This implies that the degree of spatial continuity is low. The range (distance) after which there is no spatial variation in the concentration of Th is 1486.96m. The nugget effect obtained by the concentration of Zr in the study area is 0.03 (Figure 4.15). The sill from the experimental semivariogram is 0.09 and the spatial dependence ratio from the concentration of Zr in the study area is 25%. The distance after which there is spatial variation for Zr concentration in the study area is 1760m. Experimental semivariogram for the concentration of V in the study area yielded a nugget effect of 0.018 and the sill obtained from the semivariogram is 0.032 (Figure 4.16). The spatial dependence ratio for the concentration of V is 36% and this

represents by far the highest dependence ratio obtained for the variables studied in the study area. The range is 1100m

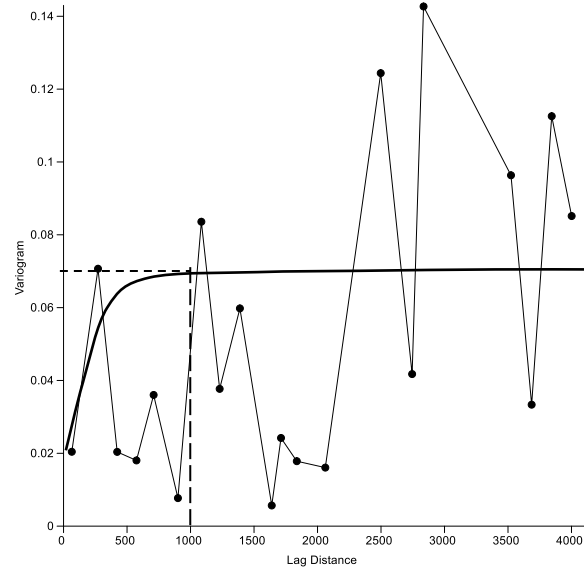


Figure 4.13: Experimental semivariogram fitted with a spherical model for U concentration in the Anyaboni Formation sandstones

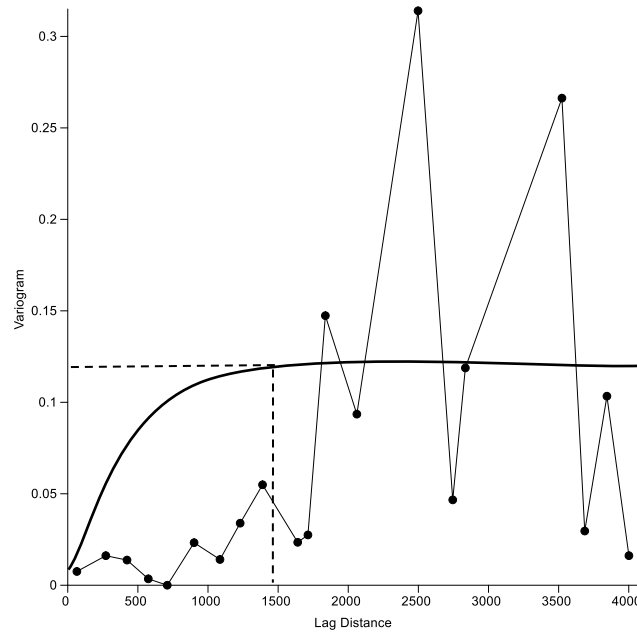


Figure 4.14: Experimental semivariogram fitted with a spherical model for Th concentration in the Anyaboni Formation sandstones area.

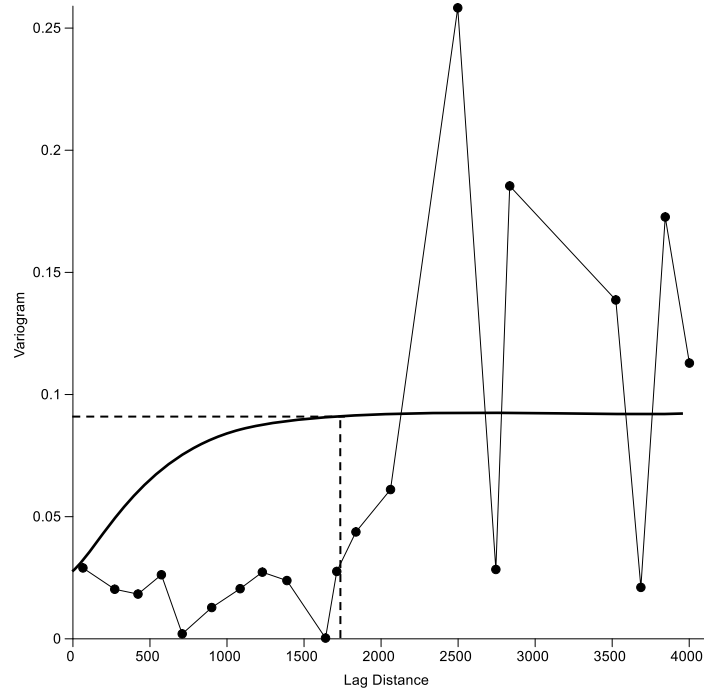


Figure 4.15: Experimental semivariogram fitted with a spherical model for Zr concentration in the Anyaboni Formation sandstones

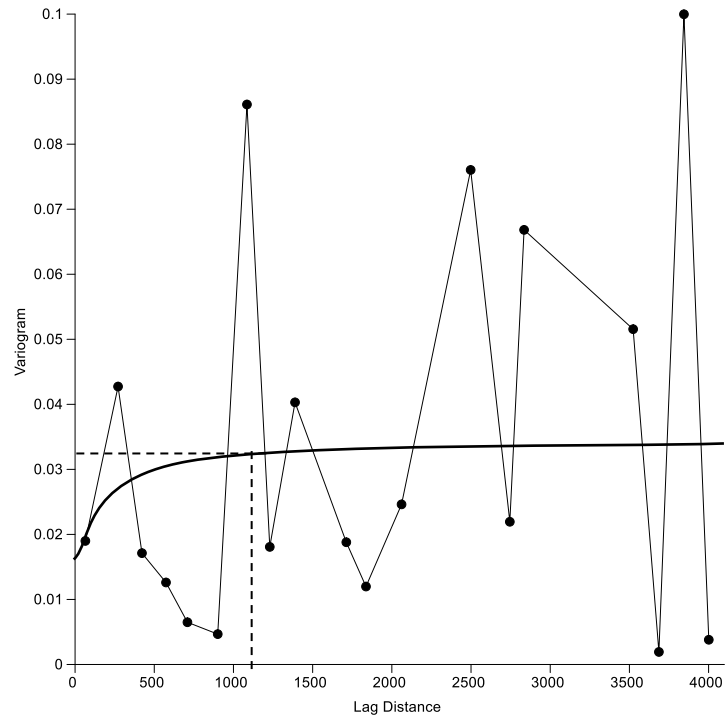


Figure 4.16: Experimental semivariogram fitted with a spherical model for V concentration in the Anyaboni Formation sandstones area.

Table 4.12: Fitted semivariograms of models with their parameters

Element	$C_0$	C	$C_0 / (C_0 + C)$	a (meters)
U_ppm	0.02	0.07	0.22	1000.00
Th_ppm	0.01	0.12	0.08	1486.96
Zr_ppm	0.03	0.09	0.25	1760.00
V_ppm	0.018	0.032	0.36	1100.00

#### 4.4.3 Geochemical Maps for U, Th, Zr and V concentrations

Presented in figure 4.17, 4.18, 4.19, and 4.120 are geochemical maps for U, Th, Zr and V concentration of the Anyaboni Formation sandstones. The geochemical map derived for U concentration in the Anyaboni Formation sandstones indicates that uranium is relatively dominant in the southern portion (Figure 4.17). This geographical area relates to Apimsu locality and towards Anyaboni. These areas are marked by feldspathic sandstones.

The central and the northern portions are characterised by lower concentrations of uranium (4.17). However, the NW corner area is marked by relatively moderate concentration of uranium. These areas coincide with Bisa and Asesewa localities where portions were marked by quartz sandstones (Figure 4.17). This suggests the linkage between uranium mineralisation/concentrations and the feldspathic sandstones rather than quartz sandstones.

From figure 4.18, Th concentration of the Anyaboni Formation sandstones is characterized by relatively high concentrations at the southern portion. However, the krig map indicates that the concentration increases towards the SW corner of the study area (Figure 4.18). The central portion shows moderate concentrations of Th. Characterizing the northern portion is relatively low concentrations of Th. The characteristics exhibited by Th concentration in the

study area follows a similar pattern as U concentration in the study area. Th serves as a good trace element for uranium.

Figure 4.19 shows low concentrations of Zr observed in the NW portion whereas the central portion shows moderate concentrations of Zr. The southern part also is associated with relatively high concentration of Zr (Figure 4.19). This suggests that Zr concentration in the study area follows a similar pattern as that of U. This reveals that Zr can be used as an indicator element for U identification in the area. Figure 4.20 presents V concentration of the Anyaboni Formation to be high at the southern portion of the study area, moderate at the central portion and low at the northern portion. However, some portions in the NW corner is characterised by moderate concentration of V (Figure 4.20). This also follows a similar geochemical pattern as that of the other variables studied.

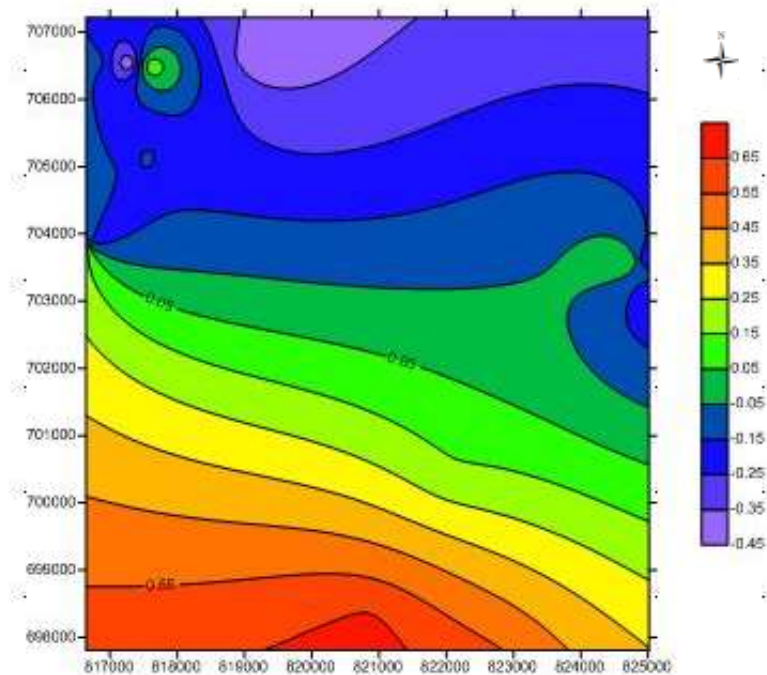


Figure 4.17: Geochemical map for U concentration in the Anyaboni Formation sandstones using kriging

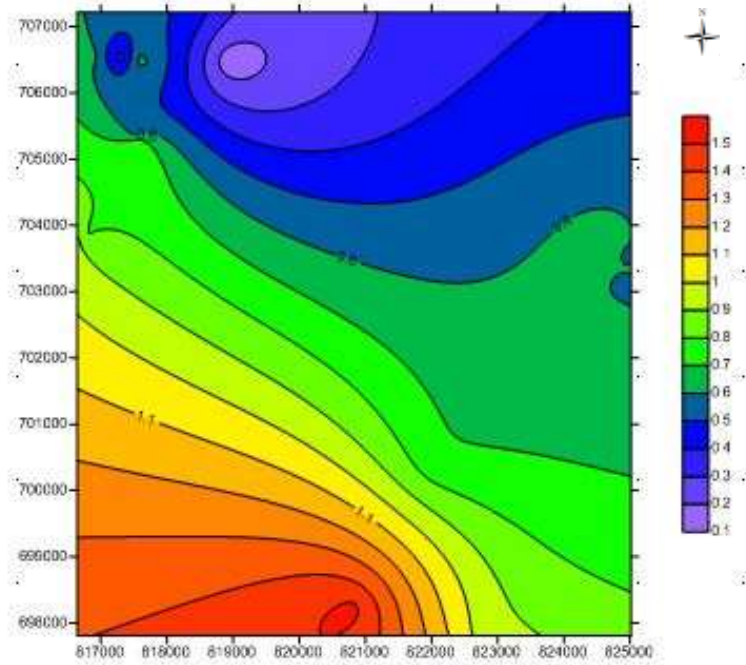


Figure 4.18: Geochemical map for Th concentration in the Anyaboni Formation sandstones using Kriging

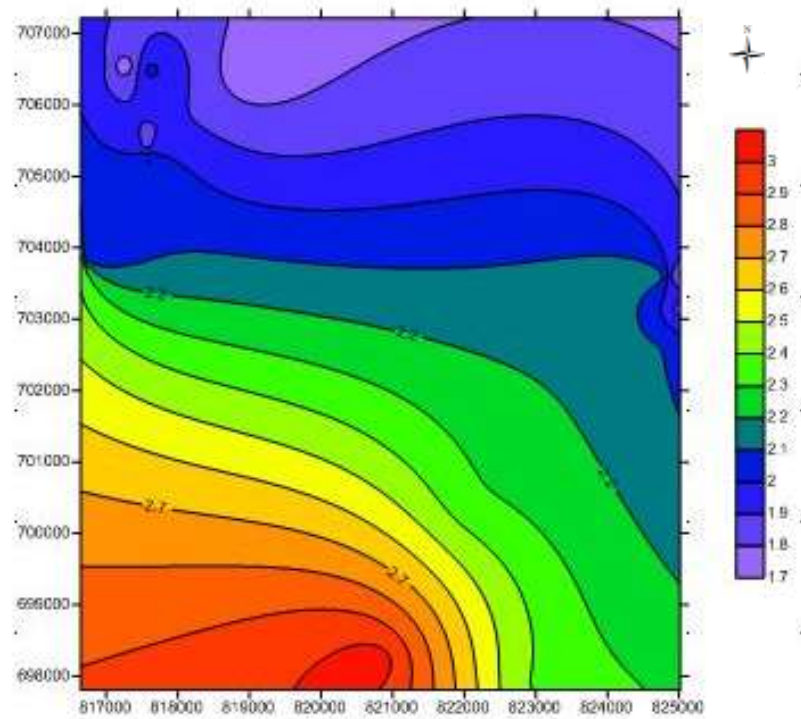


Figure 4.19: Geochemical map for Zr concentration in Anyaboni Formation sandstones using Kriging

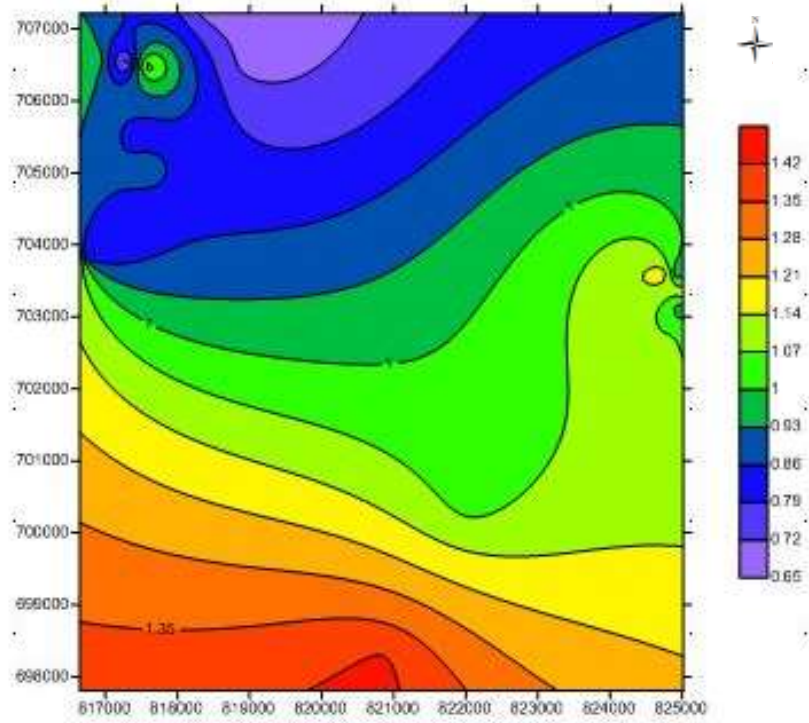


Figure 4.20: Geochemical map for V concentration in the Anyaboni Formation sandstones using Kriging

## CHAPTER FIVE

### DISCUSSION

#### 5.1 SANDSTONE CLASSIFICATION

From the ternary plot (figure 5.1), the samples plotted close to quartz apex which means that the samples are mainly quartz arenites. According to Folk 1974, the plot suggests that the framework grains of the samples are dominantly quartz. Boggs (2009) suggests that quartz arenites emanate from multiple recycling of quartz grains, generally as sedimentary source rocks and less regularly as first-cycle deposits derived from primary crystalline or metamorphic rocks. From figure 5.2, Pettijohn et al. (1972) classification diagram chemically defines the sandstones as arkose, subarkose, sublitharenite and quartz arenite. The classification diagram indicates the dominant sandstone type to be subarkose. This suggests that quartz is the most abundant minerals and feldspar is the second most abundance (Boggs, 2009).

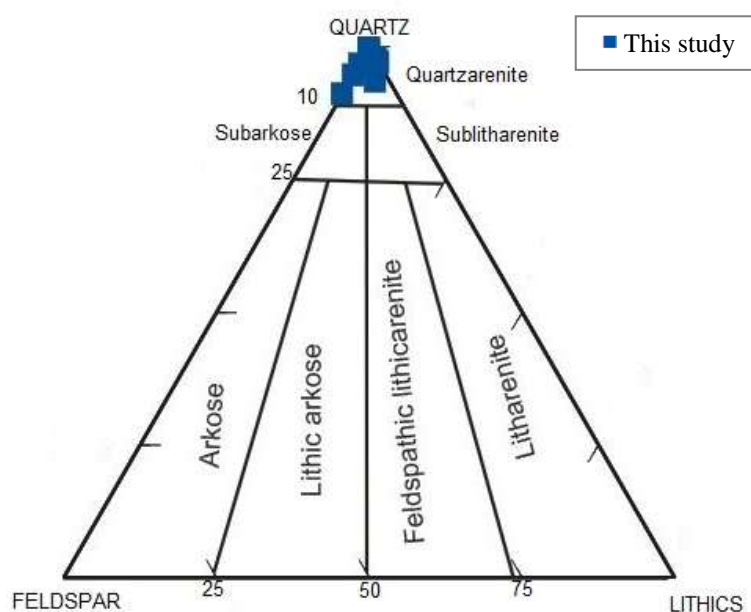


Figure 5.1: QFL diagram for sandstone classification of the samples from the study area modified after Folk, 1974

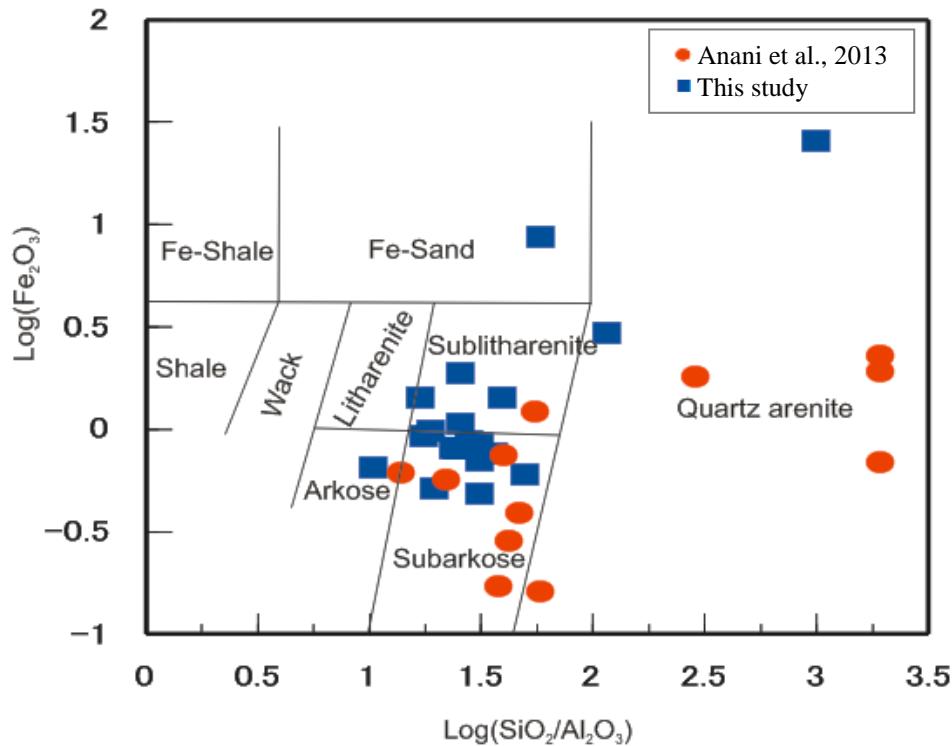


Figure 5.2: Chemical classification of sandstones from the study area based on  $\text{Log}(\text{SiO}_2/\text{Al}_2\text{O}_3)$  versus  $\text{Log}(\text{Fe}_2\text{O}_3/\text{K}_2\text{O})$  diagram of Pettijohn et al. (1972)

## 5.2.LITHOLOGY OF THE PARENT ROCK

From figure 5.3, the QFL ternary diagram for the source rock effect on the composition of the sandstone samples from the study plots close to the quartz apex. The QFL ternary diagram of Suttner et al. (1981) indicates a metamorphic parent rock lithology in a humid climate. The predominance of quartz in the sandstones couples with the source rock indicated by the ternary plot (figure 5.3) suggests that the sandstones were derived largely from granites/gneisses with some inputs from metasediments. This also indicates that the source from which the sandstones in the basin were derived is characterized by some degree of metamorphism. The discrimination function diagram of Roser and Korsch (1986) in figure

5.4 suggests that the Anyaboni sandstones are derived from quartzose sedimentary provenance. This source represents recycled mature polycyclic quartzose detritus of mature continental provenance (Rahman and Suzuki, 2007). The derivation of the sediments could be from a highly weathered granite/gneiss terrain and/or a pre-existing sedimentary terrane.

Figure 5.5 shows provenance discrimination diagrams of Floyd and Leveridge (1987) and Hayashi et al. (1997). Source rock La/Th-Hf discrimination diagram for the Anyaboni sandstones plots predominantly in a felsic source field (Floyd and Leveridge, 1987). The provenance discrimination diagram of Hayashi et al. (1997) plots the samples in a felsic source field (figure 5.6). This indicates that the probable source of Anyaboni Formation sandstones is from granites. To infer the provenance, the different discrimination diagrams suggests that the Anyaboni sandstones are derived from recycled sedimentary origin with some felsic source contribution.

From figure 5.7 A, the trace elements in general are enriched with respect to the chondrite normalized diagram. Conversely, figure 5.7 B shows that the samples are generally depleted in the trace elements with respect to the Upper continental crust normalized diagram. According to Feng and Kerrich (1990), the high-field-strength elements (HFSE) such as Zr, Nb, Hf, Y, and Th are preferentially partitioned into melts during crystallization and anatexis and as a result, these elements are enriched in felsic rather than mafic sources.

The sandstones of the Anyaboni Formation have concentrations of ferromagnesian elements (i.e., Fe, Mg, V, Cr) especially Mg which are lower than the upper continental crust (UCC) indicating the absence of mafic rocks in their source area (Figure 5.8). On the contrary, the concentrations of HFSE such as Zr, Hf and Ta which are generally enriched in felsic rocks relative to mafic rocks except for Ta do not show considerable enrichment or depletion

relative to the upper continental crust (Figure 5.8). It can be inferred that the sandstones of the Anyaboni Formation are derived from a felsic source of the upper continental crust.

The analyzed Anyaboni Formation sandstones are characterized by REE values relatively higher than that of the chondrite (Figure 5.9). The samples are relatively enriched in LREE than HREE. Culler (1994) suggests that this reflects a derivation from mainly felsic and not basic source. The compared analyzed samples from the study area to the Upper Continental Crust indicates that 90% of the samples have REE characteristics/slope is above the horizontal line ( $La/Lu=1.0$ ). This reflects a general depletion of LREE and HREE enrichment relative to UCC standard for normalization. It can be inferred that HREE enrichment in the samples are higher than that of LREE.

The europium anomaly shows a slight variation and ranges from 0.81 to 1.03 with an average of 0.95. This indicates that the substitution of  $Eu^{2+}$  for Ca in plagioclase is minimal as compared to that of the chondrite-normalised REE. This range of values is significant for felsic derived sediment source.

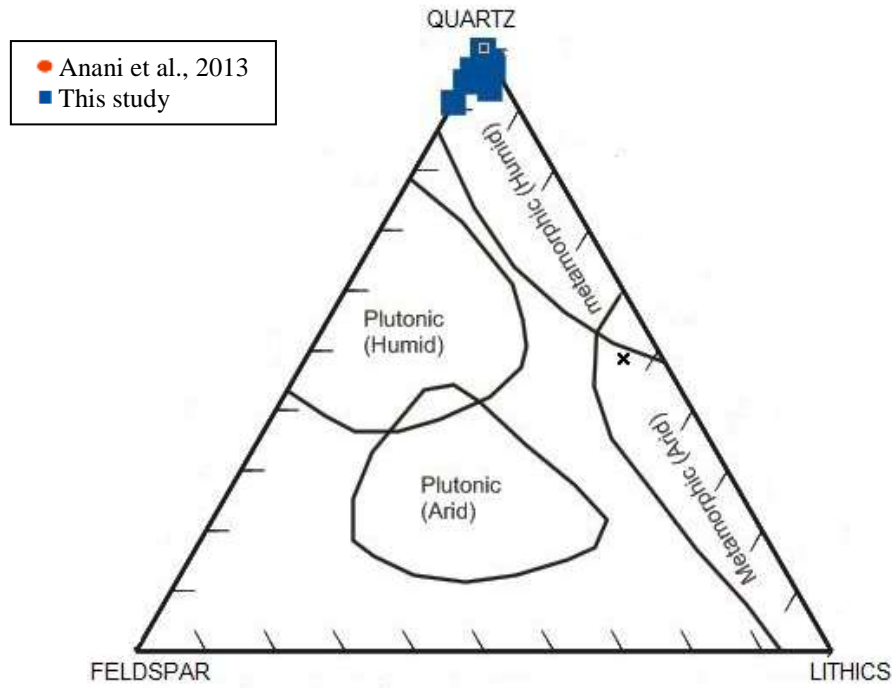


Figure 5.3: The effect of source rock on the composition of the sandstones using Suttner et al., 1981

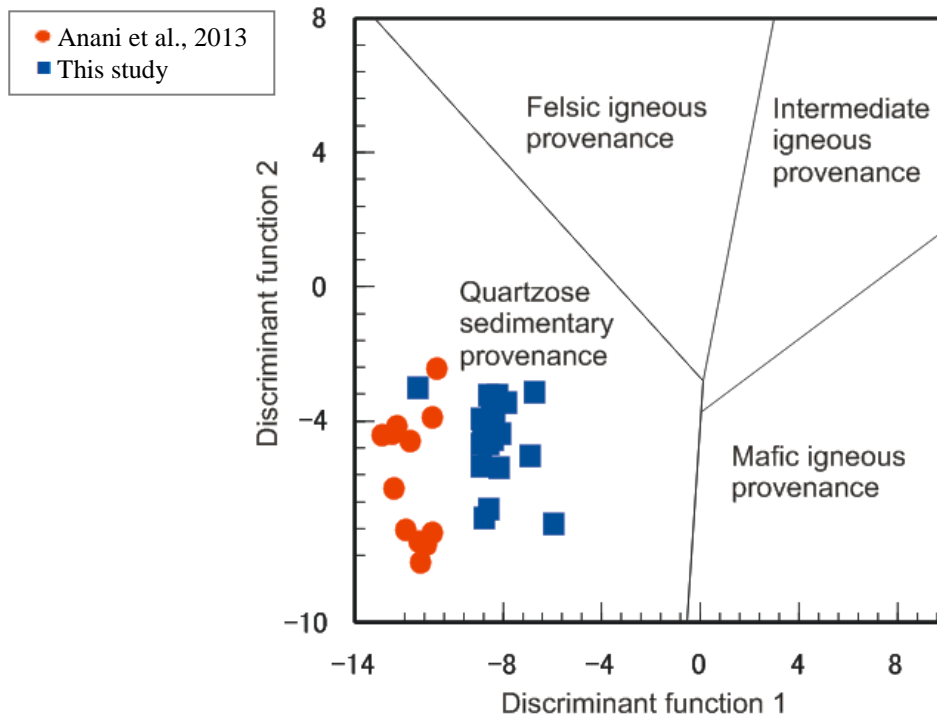


Figure 5.4: Provenance discriminant function diagram using major elements in sandstones from Anyaboni and surrounding areas after Roser and Korsch (1986)

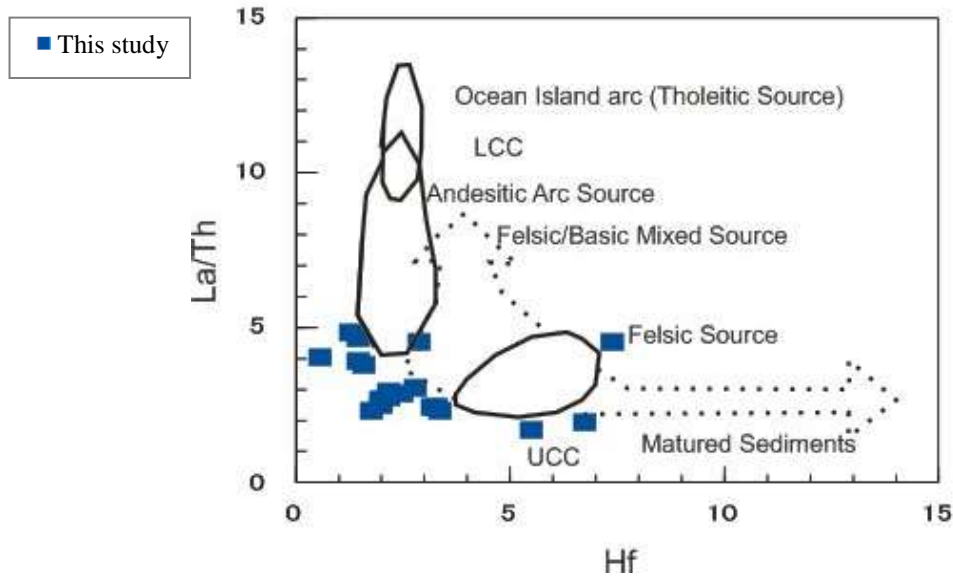


Figure 5.5: Source rock La/Th-Hf discrimination diagram for the sandstone samples from the study area; modified after Floyd and Leveridge, 1987

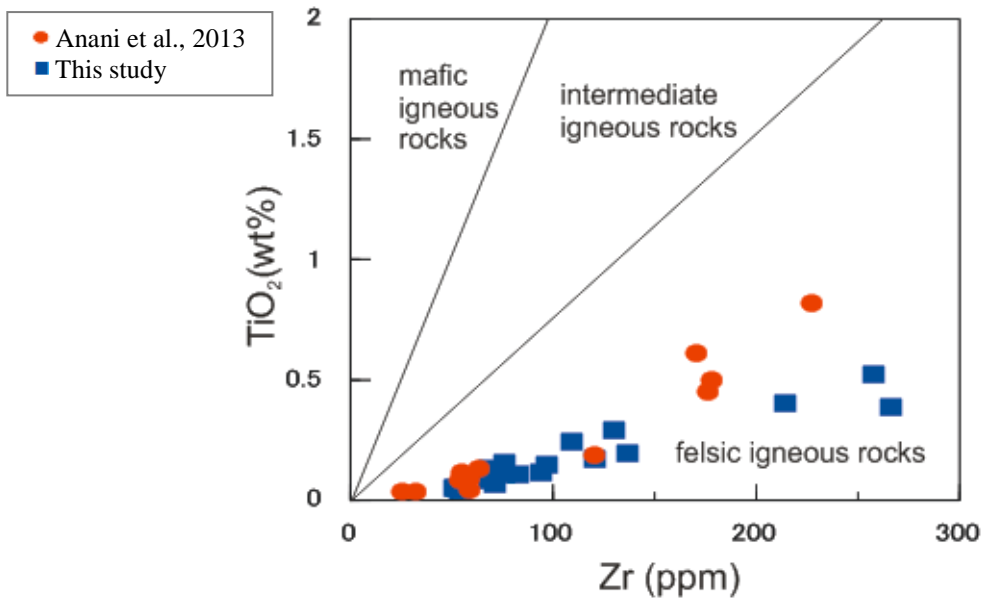


Figure 5.6: Provenance discrimination diagram using TiO<sub>2</sub> (wt %) versus Zr (ppm) with fields from Hayashi et al., 1997

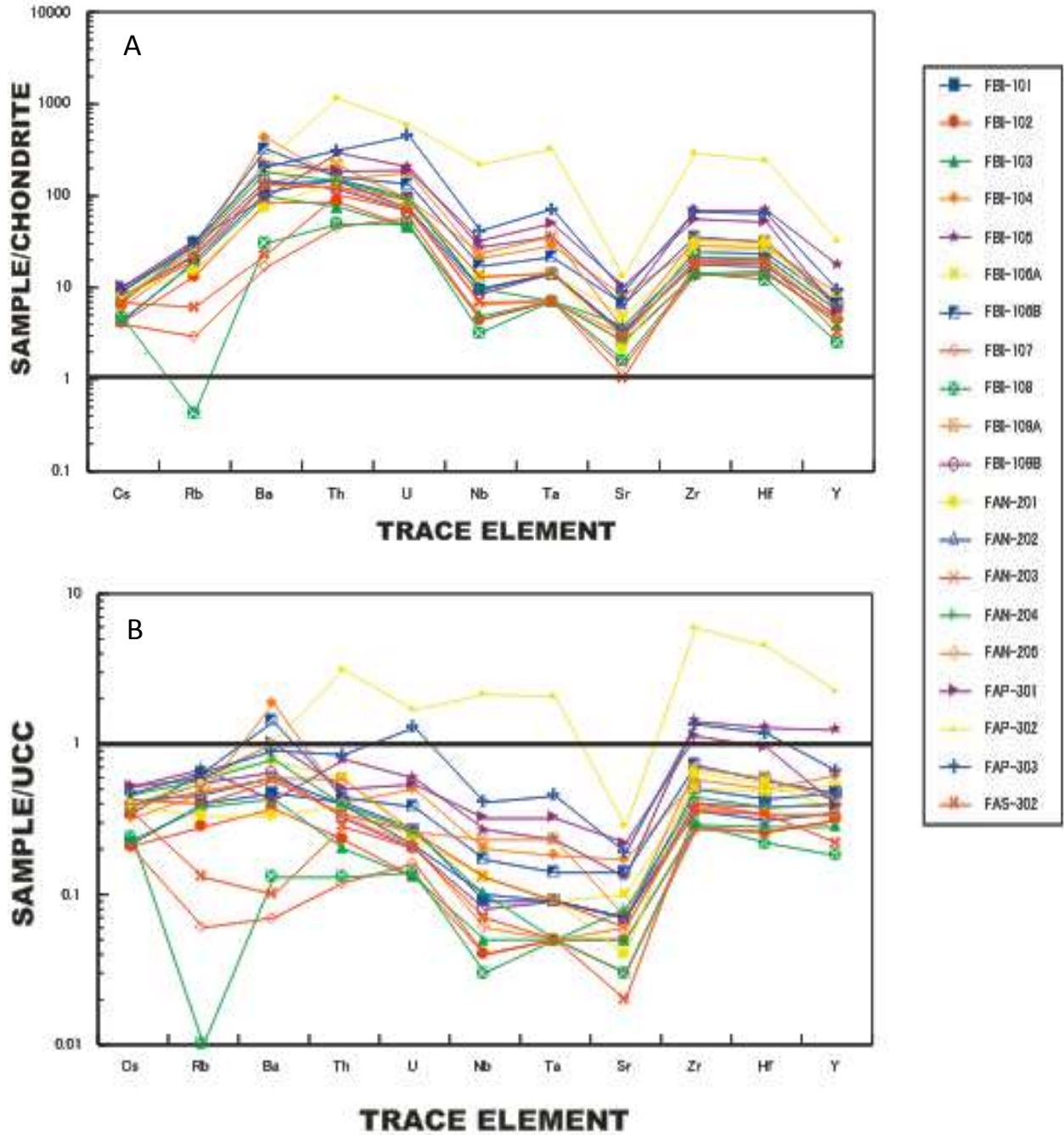


Figure 5.7: (A) Chondrite-normalized trace element diagram (B) Upper Continental Crust-normalized patterns for Anyaboni Formation sandstone samples. Normalization factors from Sun and McDonough 1989 (for A); Taylor and McLennan, 1985 (for B)

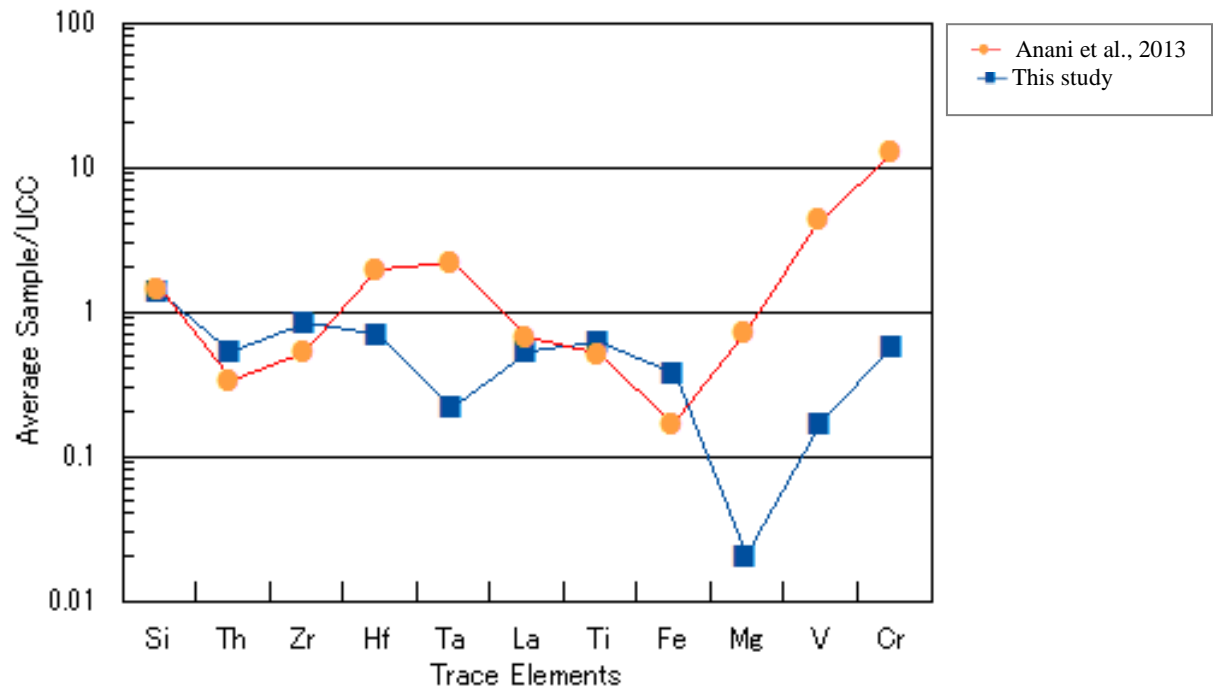


Figure 5.8: Upper Continental Crust-normalized patterns for Anyaboni Formation sandstone samples. Normalization factors from Taylor and McLennan, 1985

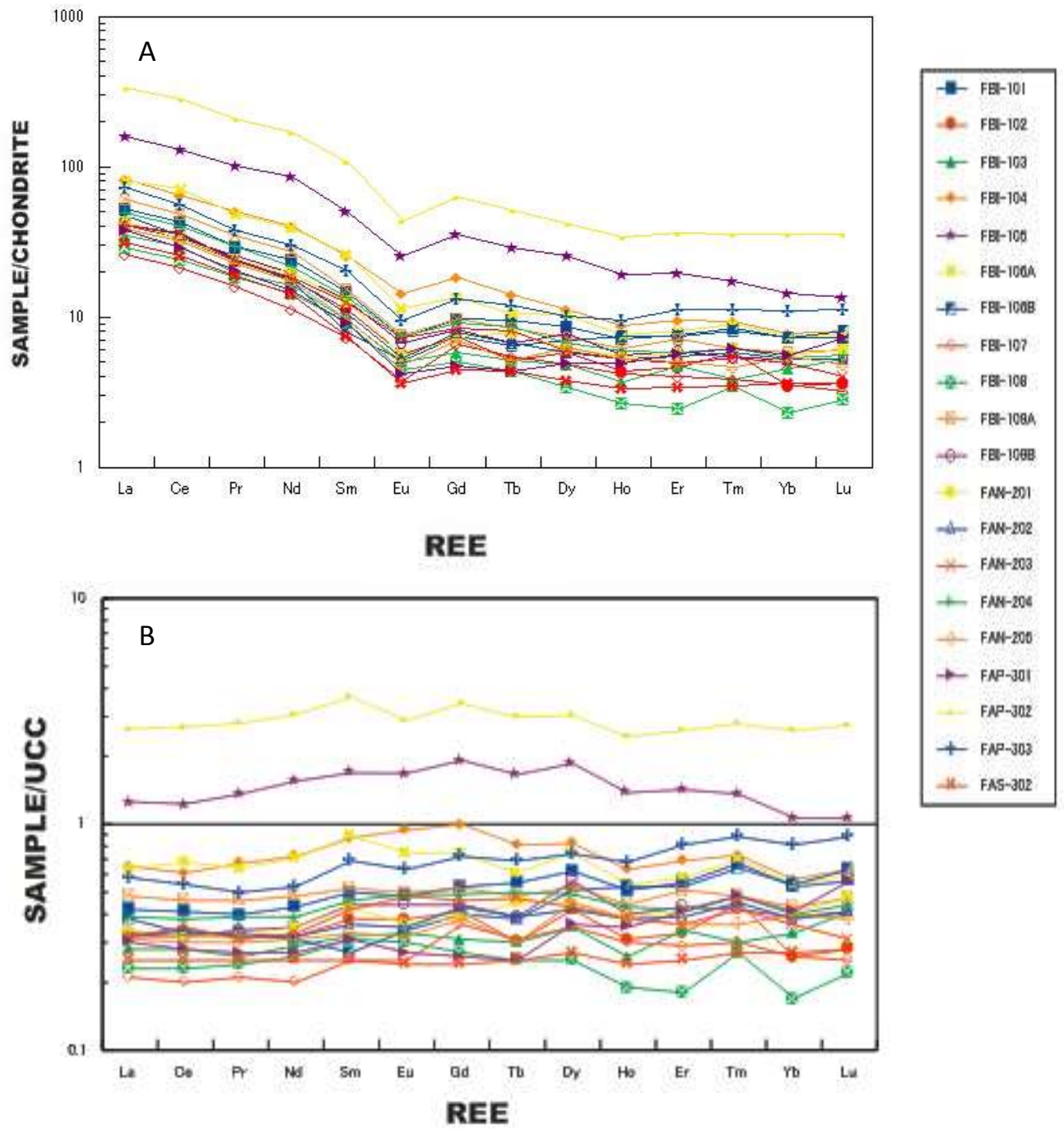


Figure 5.9: (A) Chondrite-normalized REE diagram (B) Upper continental crust-normalized REE diagram  
 Normalization factors from Sun and McDonough 1989(for A) and Taylor and McLennan, 1985 (for B)

### 5.3 TECTONIC SETTING

Presented in figure 5.10 is a provenance and tectonic setting discrimination diagram based on quartz (Q), feldspar (F) and rock fragment (L) in the sandstone samples. To interpret the tectonic discrimination source field, the Anyaboni Formation sandstones were plotted on the QFL ternary diagram of Dickson et al. (1983). The sandstone samples plotted in craton interior or recycled orogenic tectonic settings (Figure 5.10). According to Dickson and Suczek (1979) and Dickson et al. (1983), such craton type reflects matured sandstones derived from a relatively low-lying granitoid or gneissic sources supplemented by recycled sediments from associated platform or passive margin. Dickson et al. (1983), relates the recycled sediment sources to sedimentary strata and subordinate volcanic rocks.

The tectonic discrimination diagram of Roser and Korsch (1986) and Bhatia (1983), suggests that the Anyaboni formation sandstones fall exclusively in the field of passive tectonic margin (figure 5.11, 5.12 and 5.13). According to Roser and Korsch (1986), such a setting relates to largely quartz rich sandstones derived from plate interior or stable continental areas and were deposited in a passive continental margin. Passive margin sandstone types are generally enriched in  $\text{SiO}_2$  and depleted in  $\text{Na}_2\text{O}$ ,  $\text{CaO}$  and  $\text{TiO}_2$ . Bhatia and Crook, 1986 propose that materials from passive margin tectonic setting, may be formed from rifted continental margins with the sediment supply from collision orogens (for matured sediments) and the materials are probably associated with fluvial deposits or deep-sea fan sequences.

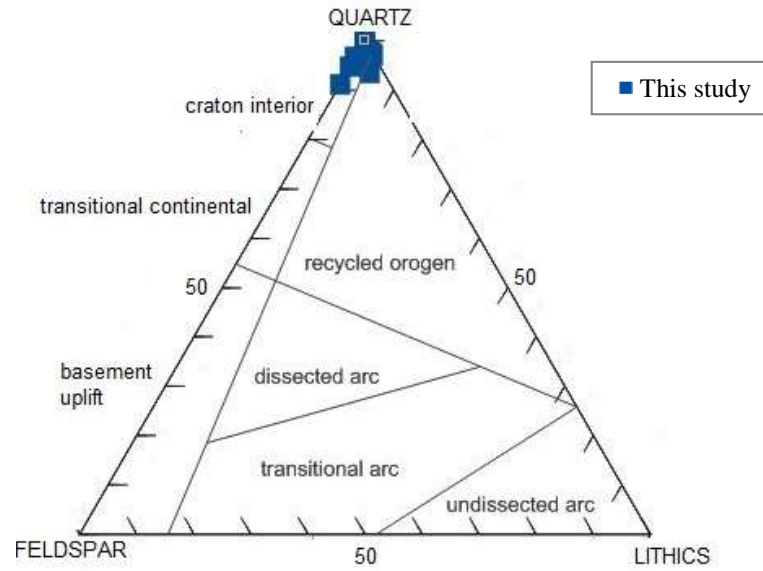


Figure 5.9: QFL ternary diagram showing the provenance and plate tectonic setting of the samples from the study area: using the petrography of the sandstones (after Dickson et al., 1983).

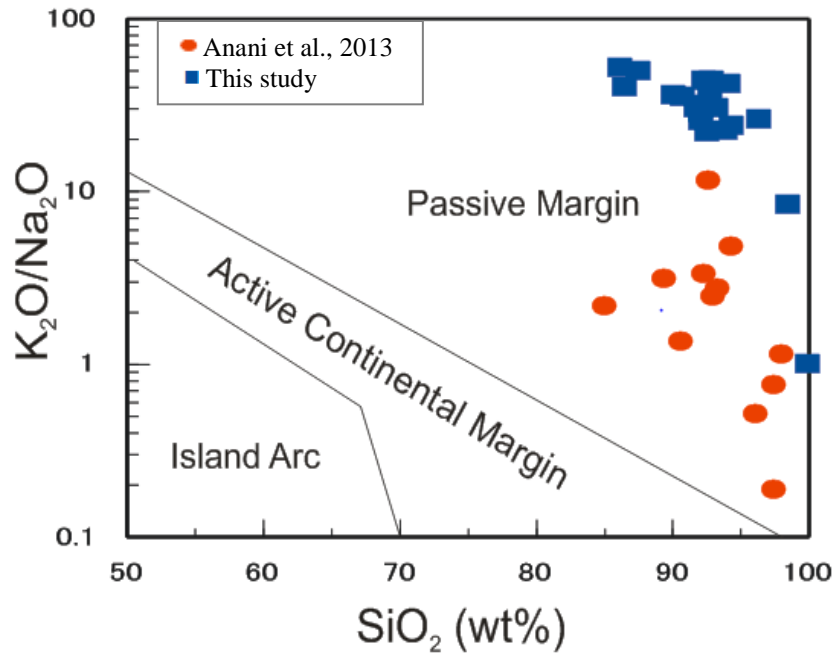


Figure 5.10: Log ( $\text{K}_2\text{O}/\text{Na}_2\text{O}$ ) versus  $\text{SiO}_2$  tectonic setting discrimination diagram of Roser and Korsch (1986) showing the location of the studied samples.

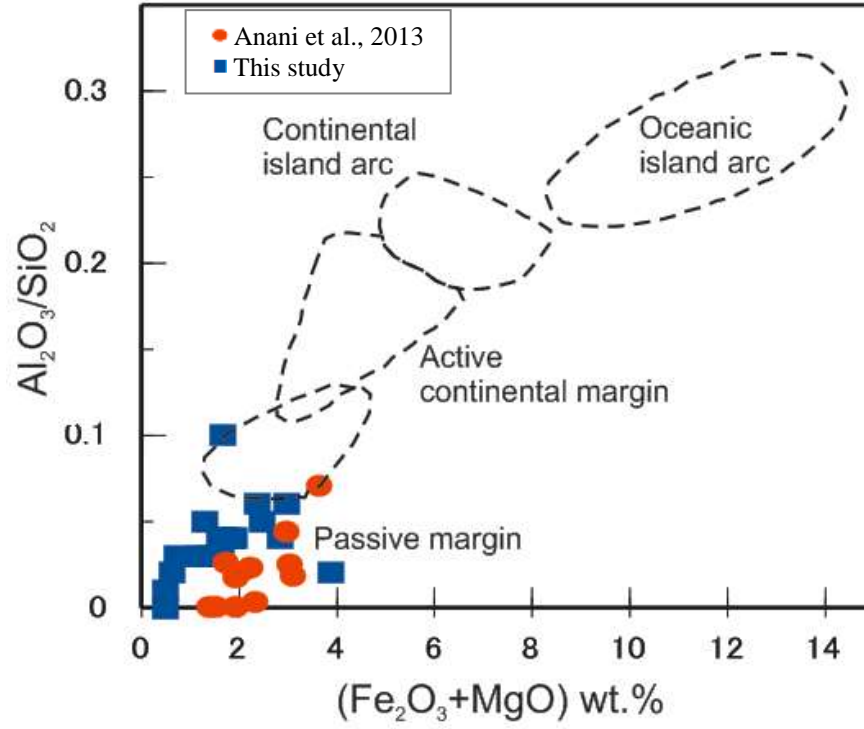


Figure 5.11: Bivariate plots of  $\text{Al}_2\text{O}_3/\text{SiO}_2$  versus  $\text{Fe}_2\text{O}_3 + \text{MgO}$  after Bhatia, 1983

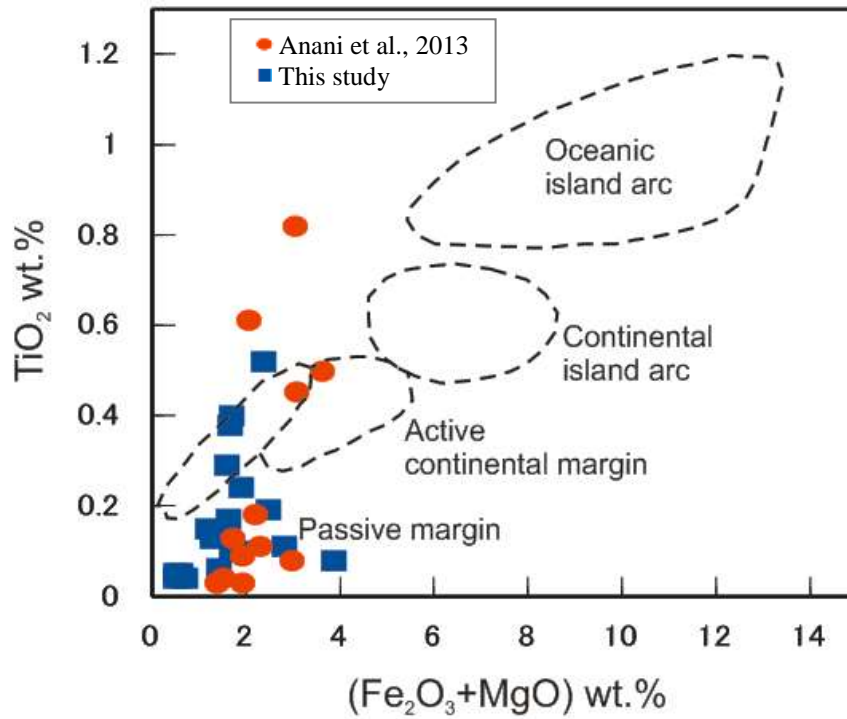


Figure 5.12: Bivariate plots of  $\text{TiO}_2$  versus  $\text{Fe}_2\text{O}_3 + \text{MgO}$  after Bhatia, 1983

#### 5.4 PALEOCLIMATE

Petrographic evidence of the Anyaboni formation sandstones reveals that the sandstones are generally characterised by low percentage of unstable minerals (feldspars), dominance of monocrystalline quartz (figure 4.9) and the alteration of feldspar grains (figure 4.6 and 4.7). Pettijohn et al. (1972) and Boggs (2009) suggest that the source area relates to a warm humid climate with moderate/intense chemical weathering. Figure 5.14 shows a log-ratio plot with weathering indices (1-4) based on climate and relief. From figure 5.14, the Anyaboni Formation sandstones plot in the field with weathering index of 4. Weltje et al. (1998), suggests that recycling and sedimentation occurred in low-relief and humid climatic conditions. From Laird (1972), the sediments plotted in such field are mainly derived from deeply-weathered granitic-gneiss terrain, which are quartz sandstones and poor in feldspar and rock fragments.

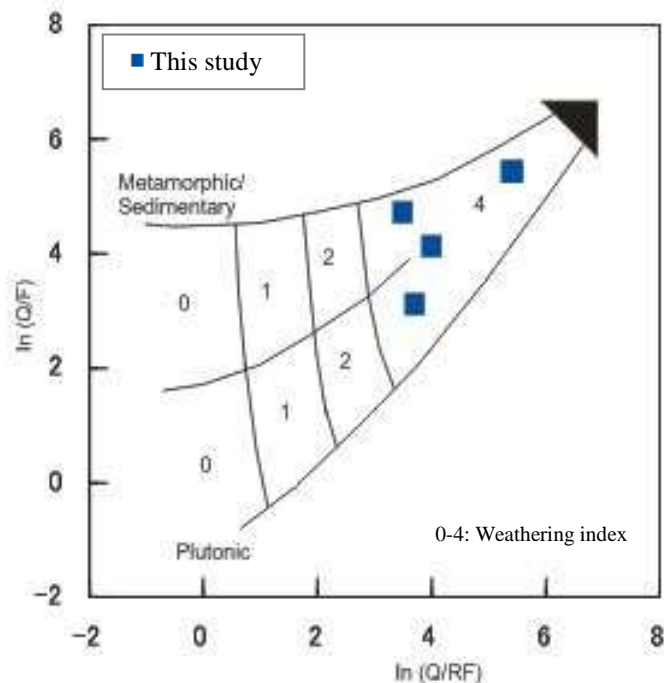


Figure 5.13: Log-ratio plot after Weltje et al. (1998). Q; Quartz, F; Feldspar, RF; Rock fragment Fields 1–4 refer to the semi-quantitative weathering indices defined on the basis of relief and climate as indicated in the table 5.1

Table 5.1: Semi-quantitative weathering indices defined on the basis of relief and climate (after Weltje, et al., 1998)

Semi-quantitative weathering index	Physiography (Relief)		
	High	Moderate	Low
	(Mountains)	(Hills)	(Plains)
	0	1	2
<b>C</b> (Semi) Arid	0	0	0
<b>l</b> Temperate (Sub-humid)	1	0	2
<b>i</b> Tropical (Humid)	2	0	4
<b>m</b>			
<b>a</b>			
<b>t</b>			
<b>e</b>			

## 5.5 SOURCE AREA WEATHERING

Nesbitt and Young (1982) propose that alteration of rocks during weathering results in depletion of alkalis and alkaline earth elements and preferential enrichment in  $Al_2O_3$ . The weathering effect on the sandstones can be obtained by chemical index of alteration (CIA) and plagioclase index of alteration (PIA) (Nesbitt and Young, 1982). The sandstones are characterized by CIA values of 61.05 (minimum), 80.77 (maximum) and an average of 66.51 (Table 4.3). Osae et al. (2006) suggests that the variation reflects moderate to high degrees of weathering.

From Figure 5.15 and 5.17, the sandstone samples plot further away from the feldspars (plagioclase) and closer to smectite, which is a secondary product formed from chemical

weathering. Nesbitt et al. (1997) suggest that the sandstones are likely to have been either derived from recycled materials or more aggressive weathering have occurred to result in the derived sediments depleted in feldspars and residually enriched in quartz.

According to McLennan et al. (1993) and Rahman and Suzuki (2007), Th/U in sedimentary rocks is of interest, as weathering and recycling typically result in loss of U, leading to an elevation in the Th/U ratio. McLennan et al. (1993) suggests that the Th/U ratio in most upper crustal rocks is typically between 3.5 and 4. Hence, sedimentary rocks with Th/U values higher than 4.0 may indicate intense weathering in source areas or sediment recycling. The Th/U ratios in the Anyaboni Formation sandstones range from 2.52 to 9.55, with an average value of 5.55 (Table 4.7), indicating the derivation of these sediments from recycling of the crust.

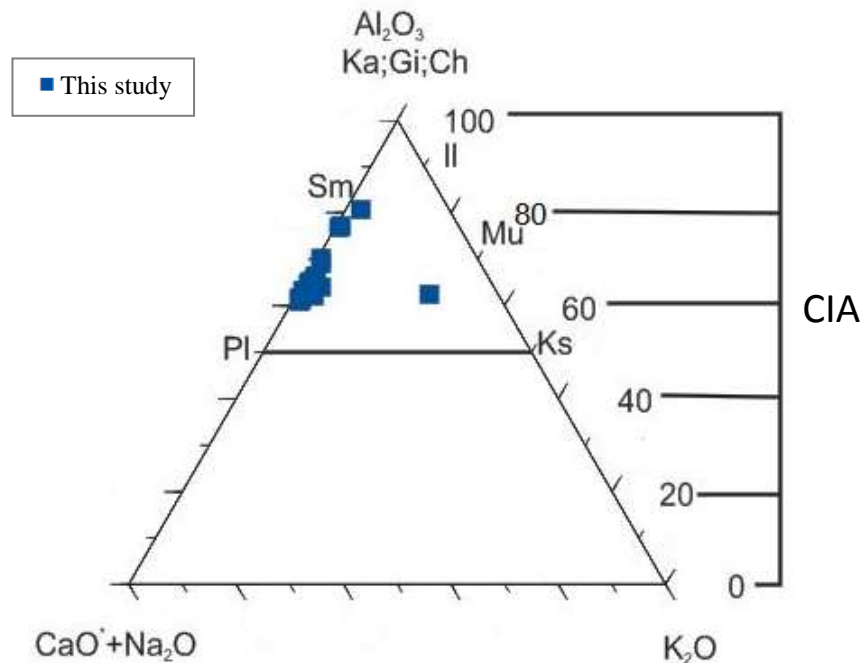


Figure 5.14: Source area weathering characteristics represented on  $\text{Al}_2\text{O}_3$ -( $\text{CaO}^*+\text{Na}_2\text{O}$ )- $\text{K}_2\text{O}$  diagram. The diagrams represent the field of idealized minerals: Pl; Plagioclase, Ks; K-feldspars, Il; Illite, Mu; Muscovite, Sm; Smectite, Ka; Kaolinite, Gi; Gibbsite, Ch; Chlorite

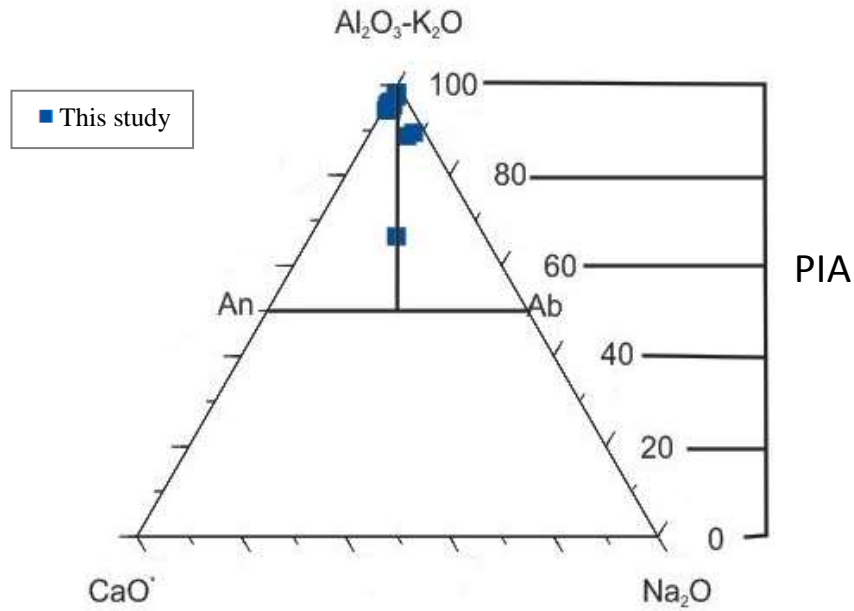


Figure 5.15: Source area weathering characteristics represented on  $(Al_2O_3-K_2O)$ - $CaO$ - $Na_2O$  ternary diagram (Modified after Nesbitt and Young, 1984). The diagrams represent the field of idealized minerals: An; Anortite, Ab; Albite

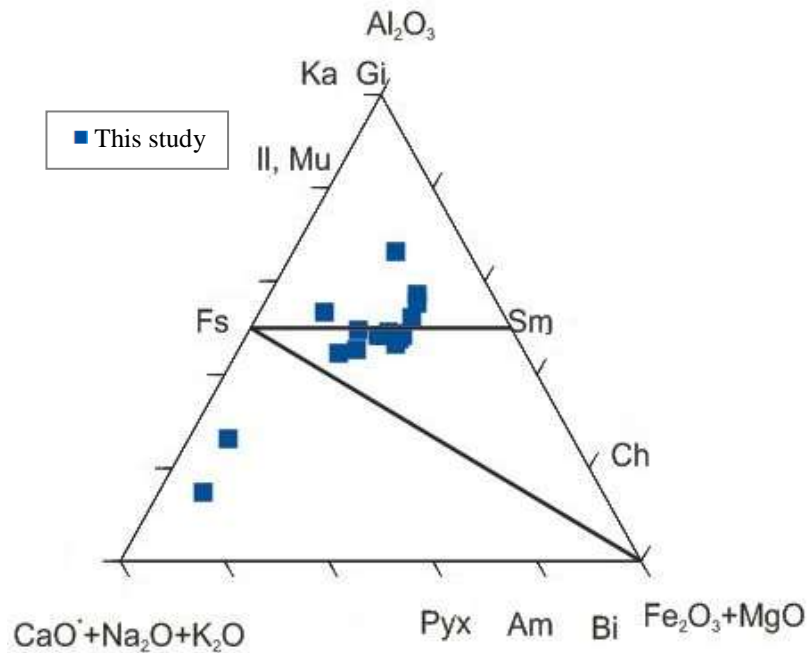


Figure 5.16: Source area weathering characteristics represented on  $Al_2O_3$ - $(CaO^*+Na_2O+K_2O)$ - $(Fe_2O_3+MgO)$  ternary diagram (Modified after Nesbitt and Young, 1984). The diagrams represent the field of idealized minerals: II; Illite, Mu; Muscovite, Sm; Smectite, Ka; Kaolinite, Gi; Gibbsite, Ch; Chlorite, Fs; Feldspars, Pyx; Pyroxene, Am; Amphibole and Bi; Biotite

## **5.6 URANIUM MINERALIZATION POTENTIAL IN THE BASIN**

The study area is generally characterised by low concentrations of uranium. However, the other elements studied; Th, Zr and V may serve as good indicators for uranium tracing in the study area. The positive linearly increasing trend of Th, Zr and V concentrations with uranium concentration from the scatter diagram derived for the Anyaboni Formation sandstones serves as an evidence for this deduction.

The experimental semivariogram derived for the variables studied in the study area indicated that uranium characterization varies with space (location). However, the variation is limited with distance. U, Th, Zr and V concentrations show no variation after 1000m, 1291.67m, 1760m and 916.67m respectively. The use of Th, Zr and V as trace elements for U in the study can be ranked as Zr, Th and V in order of suitability (based on the spatial variation)

The geochemical map generated for U, Th, Zr and V concentrations indicated that higher concentrations of the elements are associated with the southern portion, moderate concentrations are associated with the central portion and lower concentrations are associated with the northern portion of the study area. Hence, revealing an increasing trend from the southwest to the northeast.

## CHAPTER FIVE

### CONCLUSION AND RECOMMENDATION

#### 5.1 CONCLUSION

Significant contribution deduced from this study relates much to provenance, tectonic setting, paleoweathering and paleoclimate conditions of the source rock environment of the Anyaboni Formation of the Voltaian basin. Uranium characterization in the study area can also be inferred from this study.

1. Petrographic evidence suggests that the sandstones of the study are mainly quartz arenite with craton interior or quartzose recycled tectonic setting with a metamorphic (and humid paleoclimate) source rock; associated with sedimentation occurring in a low (plain) relief.
2. Major oxide interpretation indicated sandstones as dominantly subarkose with some sublitharenite, quartz arenite and arkose. The geochemical data shows the rocks are from a felsic/intermediate source and suggested passive margin tectonic setting.
3. It recognize paleoweathering condition of the source environment to be moderate to high from the CIA and PIA values
4. The Spider diagrams indicated sediments were derived from a felsic source composition.
5. Based on the petrographic and geochemical characteristics, the underlying basement rock, Birimian Supergroup (characterised by metavolcanic and metasedimentary rocks) and Tarkwaian Supergroup are the likely sources of the Anyaboni Formation.

6. Uranium concentration has been found to be low in the Anyaboni Formation sandstones. However, there is a strong positive correlation between U and Th, Zr and V concentrations and can serve as pathfinders for U in the area.

## **5.2 RECOMMENDATION**

Preliminary geochemical results from the Anyaboni rocks of the Voltaian Supergroup are not encouraging therefore, further studies with emphasis on soil, water bodies are to be carried out. Geochemical studies are to be conducted at potential areas such as Dahomeyan formation.

## REFERENCES

- Abouchami, W., Boher, M., Michard, A., and Albarede, F. (1990) A major 2.1 Ga old event of mafic magmatism in West Africa: an early stage of crustal accretion. *J. Geophys. Res.* 95, 17605–17629.
- Adamek, P.(1976) Raw materials prospection Report to the Government of Ghana, International Atomic Energy Agency, Technical Assistance Report No. 1143, 27pp
- Affaton, P., 1990. Le bassin des Volta (Afrique de l'Ouest): une marge passive, d'âge protérozoïque supérieur, tectonisée au Panafrican (600±50 Ma). Editions ORSTOM, Collection Etudes et Thèses, Paris, 500 pp.
- Affaton, P., Sougy, J., and Trompette R. (1980)The tectono-stratigraphic relationships between the upper Precambrian and lower Paleozoic Volta Basin and the pan-African Dahomeyide orogenic belt (West Africa). *American Journal of Science*, 280(3), 224-248.
- Ako, J.A., Wellmann, P., 1985. The margin of the West African craton: the Voltaian Basin. *Journal of the Geological Society London* 142, 625–632.
- Anani, C.(1999) Sandstone petrology and provenance of the Neoproterozoic Voltaian Group in the southeastern Voltaian Basin, Ghana. *Sediment. Geol.* 128, 83–98.
- Anani, C., Moradeyo M., Atta-Peters, D., Kutu, J., Asiedu, D. and Boamah, D.(2013) Geochemistry and provenance of sandstones from Anyaboni and surrounding areas in the voltaian basin, Ghana. *International Research Journal of Geology and Mining (IRJGM)* (2276-6618) Vol. 3(6) pp. 206-212

Annan-Yorke, R., (1971). Geology of the Voltaian Basin (summary of current ideas). In: Cudjoe, J.E. (Ed.), Special Bulletin for Oil Exploration. Geological Survey Department, Accra, Ghana, p. 29.

Barfod, G.H., Vervoort, J.D., Montanez, I.P., Riebold, S., 2004. Lu–Hf geochronology of phosphates in ancient sediments. 13th Goldschmidt Conference, Copenhagen. *Geochimica et Cosmochimica Acta*, Abstract Volume, vol. 68, p. A336.

Beer, K.E. and Taylor J. (1953) The radioactivity of placer concentrates from the Gold Coast, Geological Survey and Museum, Atomic Energy Division, ReportNo.135.

Bewick, V., Cheek, L., & Ball, J. (2003). Statistics review 7: Correlation and regression. *Critical Care*, 7(6), 451

Bhatia M R. (1983) Plate tectonics and geochemical composition of sandstones; *J. Geol.* 91 611–627.

Bhatia, M.R. and Crook, K.A.W. (1986) Trace element characteristics of greywackes and tectonic setting discrimination of sedimentary basins. *Contrib. Mineral. Petrol.* 92, 181–193.

Blaise J. R.(2014). Uranium geology exploration and resources in Africa

Boggs Jr. S. (2009) Principles of sedimentology and stratigraphy. Prentice Hall, 4<sup>th</sup> ed., 688pp

Boher, M., Abouchami, W., Michard, A., Albarede, F., and Arndt, N. T. (1992) Crustal growth in West Africa at 2.1 Ga. *Journal of Geophysical Research: Solid Earth* (1978–2012), 97(B1), 345-369.

Bohling, G. (2005) Introduction to geostatistics and variogram analysis. Kansas geological survey, 20p

Carney, J.N., Jordan, C.J., Thomas, C.W., Condon, D.J., Kemp, S.J. and Duodo, J.A. (2010) Lithostratigraphy, sedimentation and evolution of the Volta Basin in Ghana. *Precambrian Research* 183, 701–724.

Clauer, N. (1976) Isotope Geochemistry of sedimentary environments of Strontium: Application geochronology of coverage Craton Quest – Afriqain. Universite Louis Pasteur of Strasbourg Institute of Geology

Couëffé, R. and Vecoli, M. (2011) New sedimentological and biostratigraphic data in the Kwahu Group (Meso-to Neo-Proterozoic), southern margin of the Volta Basin, Ghana: Stratigraphic constraints and implications on regional lithostratigraphic correlations. *Precambrian Research*, 189(1), 155-175.

Cullers R.L. (1994) The controls on the major and trace element variation of shales, siltstones and sandstones of Pennsylvanian–Permian age from uplifted blocks in Colorado to platform sediment in Kansas, USA; *Geochim.Cosmochim. Acta* 22 4955–4972.

Cullers, R. L. and Podkovyrov, V. N. (2000) Geochemistry of the Mesoproterozoic Lakhanda shales in southeastern Yakutia, Russia: Implications for mineralogical and provenance control, and recycling. *Precamb. Res.* 104, 77–93.

Cuney, M. (2009) The extreme diversity of uranium deposits. *Miner. Deposita*, 44, 3–9.

Dahlkamp F.J. (1993) Uranium ore deposits. Springer, Berlin, p 460

Dickinson W.R. and Suczek C.A. (1979) Plate tectonics and sandstone compositions; Am. Assoc. Pet. Geol. Bull. 63 2164–2182.

Dickinson W.R., Beard L.S., Brakenridge G.R., Erjavee J.R., Ferguson R.C. and Inman K.F.(1983) Provenance of North American Phanerozoic sandstones in relation to plate tectonic setting; Geol. Soc. Amer. Bull. 94 222–235.

Dickinson, W. R. (1985). Interpreting provenance relations from detrital modes of sandstones. Provenance of Arenites (Zuffa, G. G., ed.), 333–361, Advanced Study Institute Series 148,NATO.

Dickson, K.B. and Benneh, G. (1992) A new geography of Ghana. England: Longman.

Duodu, J. A. (2009) Geological Map of Ghana 1: 1 000000 Geological Survey Department

Feng, R., & Kerrich, R. (1990). Geochemistry of fine-grained clastic sediments in the Archaean Abitibi greenstone belt, Canada: implications for provenance and tectonic setting. *Geochimica et Cosmochimica Acta*, 54(4), 1061-1081.

Floyd, P.A. and Leveridge, B.E. (1987) Tectonic environment of the Devonian Gramscatho basin, south Cornwall: framework mode and geochemical evidence from turbiditic sandstones. *Journal of the Geological Society*, 144(4), 531-542.

Folk, R.L.(1974)*Petrology of Sedimentary Rocks*.2<sup>nd</sup>ed., Hemphill Publishing Co., Austin, Texas.182 pp

Guelpa, J.P. and Vogel, W. (1982) International Uranium Resources Evaluation Project (IUREP) orientation phase mission report: Ghana. Draft. International Atomic Energy Agency, Vienna (Austria).

Gupta, M. and Singh, S. (2003) Greening of the Internet. In Proceedings of the 2003 conference on Applications, technologies, architectures, and protocols for computer communications (pp. 19-26). ACM.

Hayashi, K., Fujisawa, H., Holland, H.D. and Ohmoto, H. (1997) Geochemistry of ~1.9Ga Sedimentary rocks from northeastern Labrador, Canada. *Geochimica Cosmochimica Acta* Vol. 61, pp. 4115-4137.

International Atomic Energy Agency (1976) Recognition and evaluation of uraniumiferous areas

Jordan, C.J., Carney, J.N., Thomas, C.W., McDonnell, P., 2008. Application of remote sensing and field mapping to a revision of the geology of the Volta Basin. In: Kalsbeek, F. (Ed.), *The Voltaian Basin, Ghana. The Voltaian Basin, Ghana. Workshop and Excursion, March 10–17, 2008, Abstract Volume*. Geological Survey of Denmark and Greenland (GEUS), Copenhagen, pp. 87–90.

Jordan, C.J., Carney, J.N., Thomas, C.W., McDonnell, P., Turner, P., McManus, K., McEvoy, F.M., 2009. *Ghana Airborne Geophysics Project: BGS Final Report*. British Geological Survey Commissioned Report, CR/09/02. 325 pp. (Available electronically by application to the Director, Ghana Geological Survey Department, Accra)

Kalsbeek, F. and Frei, R. (2010) Geochemistry of Precambrian sedimentary rocks used to solve stratigraphical problems: an example from the Neoproterozoic Volta Basin, Ghana. *Precambrian Research* 176, 65–76.

Kalsbeek, F., Frei, D. and Affaton, P. (2008) Constraints on provenance, stratigraphic correlation and structural context of the Volta basin, Ghana, from detrital zircon geochronology: an Amazonian connection? *Sedimentary Geology* 212, 86–95.

Kesse, G.O., (1985) *The Mineral and Rock Resources of Ghana*. A.A. Balkema, Boston, 610pp

Laird MG (1972). Sedimentology of Greenland Group in the Paparoa Range, West Coast, South Island, New Zealand. *J Geol Geophys* 15: 372–393.

Langmuir, D. (1978) Uranium solution–mineral equilibria at low temperatures with applications to sedimentary ore deposits. *Geochim Cosmochim Acta* 42:547–569

McCluskey, A., and Lalkhen, A. G. (2007). Statistics II: Central tendency and spread of data. *Continuing Education in Anaesthesia, Critical Care & Pain*, 7(4), 127-130.

McLennan SM, Taylor SR, McCulloch MT, Maynard JB (1990). Geochemical and Nd-Sr isotopic composition of deep-sea turbidites: crustal evolution and plate tectonic associations. *Geochim Cosmochim Acta* 54: 2015–2050.

McLennan, S.M., Hemming, S., McDaniel, D.K. and Hanson, G.N. (1993) Geochemical approaches to sedimentation, provenance and tectonics, in Johnson, M.J., Basu, A. (eds.): *Geological Society of America, Special Papers* 285, 21–40.

McLennan, S.M., Taylor, S.R. and Eriksson, K.A. (1983) Geochemistry of Archaean shales from Pilbara Supergroup, Western Australia; *Geochim. Cosmochim. Acta* 74 1211–1222.

Nesbitt HW, Fedo CM, Young GM (1997). Quartz and feldspar stability, steady and non-steady-state weathering, and petrogenesis of siliciclastic sands and muds. *J Geol* 105: 173–192.

Nesbitt, H.W.M. and Young, G.M.(1982) Early Proterozoic climates and plate motions inferred from major element chemistry of lunites. *Nature* 299, 715–717.

Nininger, R.D. (Ed.). 1956. Exploration for nuclear raw materials (Vol. 2). Van Nostrand. Pp 1-3

Obaje, N. G. (2009). *Geology and mineral resources of Nigeria* (Vol. 120). Springer.

Osaе S, Asiedu DK, Banoeng-Yakubo B, Koeberl C, Dampare SB(2006). Provenance and tectonic setting of Late Proterozoic Buem sandstones of southeastern Ghana: Evidence from geochemistry and detrital modes. *J Asian Earth Sci* 44: 85–96.

Paz-Ferreiro, J., Vázquez, E. V., and Vieira, S. R. (2010). Geostatistical analysis of a geochemical dataset. *Bragantia*, 69, 121-129.

Pettijohn F.J., Potter, P.E. and Siever, R.(1972)*Sand and Sandstone* (Berlin: Springer-Verlag), 241 p.

Pettijohn FJ, Potter PE, Siever R (1987). *Sand and Sandstones*. 2<sup>nd</sup>ed. New York, NY, USA: Springer-Verlag.

Porter, S.M., Knoll, A.H., Affaton, P., (2004). Chemostratigraphy of Neoproterozoic cap carbonates from the Volta Basin, West Africa. *Precambrian Research* 130, 99–112

Rahman, M. J. J., & Suzuki, S. (2007). Geochemistry of sandstones from the Miocene Surma Group, Bengal Basin, Bangladesh: Implications for Provenance, tectonic setting and weathering. *Geochemical Journal*, 41(6), 415-428.

Roser B.P. and Korsch R.J. (1988) Provenance signatures of sandstone mudstone suites determined using discrimination function analysis of major element data. *Chem. Geol* 67: 119–139.

Roser B.P. and Korsch R.J. (1986) Determination of tectonic setting of sandstone-mudstone suites using SiO<sub>2</sub> content and K<sub>2</sub>O/Na<sub>2</sub>O ratio; *J. Geol.* 94(5) 635–650.

Sun, S.S. and McDonough, W.F.(1989) Chemical and isotopic systematics of oceanic basalts: implications for mantle composition and processes. Geological Society, London, Special Publications, 42(1), 313-345.

Suttner, L.J., Basu, A., and Mack, G.H., 1981. Climate and the origin of quartz arenites. *Journal of Sedimentary Research*, 51(4)

Taylor, S.R. and McLennan, S.M. (1985). *The continental crust: Its composition and evolution*; Blackwell Scientific Publications, 312 p.

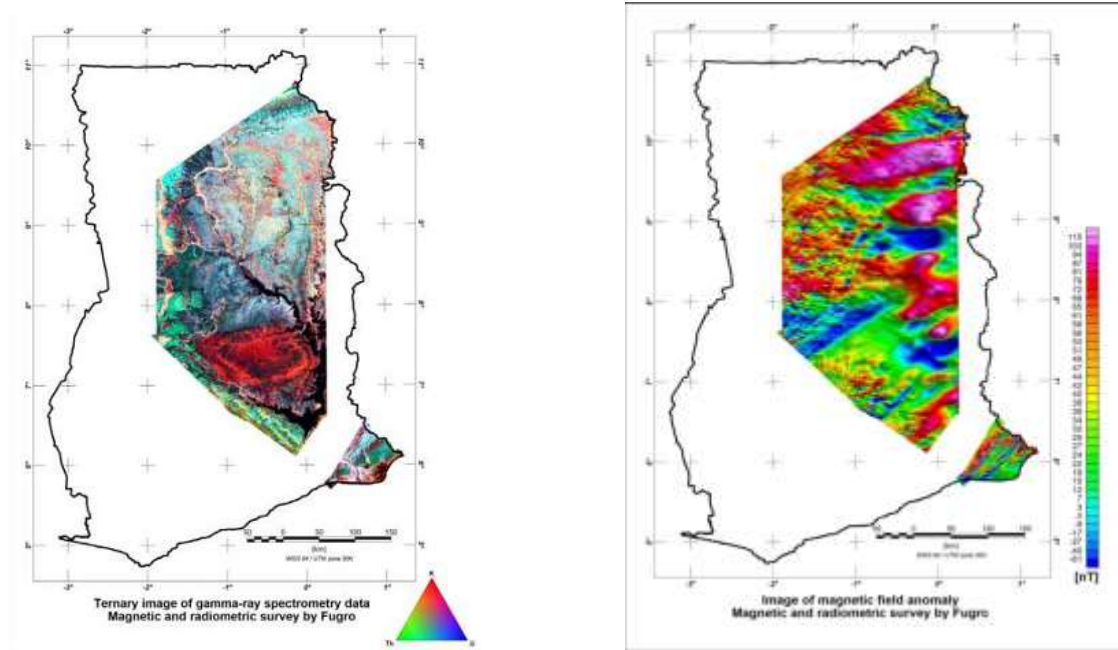
Trompette, R. (1994) *Geology of Western Gondwana (2000–500 Ma), Pan-African–Brasiliano Aggregation of South America and Africa*. Balkema, Rotterdam. 350 pp.

Uranerzbergbau GmbH Co., KG. (1972) The prospecting for uranium and thorium in the Republic of Ghana, June, 1968 to June, 1971. Final report (Unpublished)

Weltje G.J. Meijer X.D. and De Boer P.L. (1998) Stratigraphic inversion of siliciclastic basin fills: a note on the distinction between supply signals resulting from tectonic and climatic forcing. *Basin Res*10: 129–153.

World nuclear association (2010) Geology of uranium deposits: [www.world-nuclear.org/info/Nuclear-Fuel-Cycle/Uranium-Resources/Geology-of-Uranium-Deposits/](http://www.world-nuclear.org/info/Nuclear-Fuel-Cycle/Uranium-Resources/Geology-of-Uranium-Deposits/) (accessed December, 2014)

APPENDIX



GAMMA-RAY SPECTROMETRY

MAGNETIC FIELD ANOMALY

Figure A: Airborne geophysical survey of the Volta River Basin and Keta Basin, Ghana (Jordan et al., 2008)

